UNIVERSITY OF
LINCOLN

A unified neural model explaining optimal multi-guidance coordination in insect navigation

Xuelong Sun

Doctor of Philosophy

2021

School of Computer Science

University of Lincoln

A unified neural model explaining optimal multi-guidance coordination in insect navigation

Xuelong Sun

School of Computer Science

University of Lincoln

A thesis submitted in partial fulfilment of the requirements of the University of Lincoln for the degree of Doctor of Philosophy

Supervisors

Professor Shigang Yue

Doctor Michael Mangan

Doctor Vassilis Cutsuridis

May 2021

Abstract

The robust navigation of insects arises from the coordinated action of concurrently functioning and interacting guidance systems. Computational models of specific brain regions can account for isolated behaviours such as path integration or route following, but the neural mechanisms by which their outputs are coordinated remains unknown. In this work, a functional modelling approach was taken to identify and model the elemental guidance subsystems required by homing insects. Then we produced realistic adaptive behaviours by integrating different guidance's outputs in a biologically constrained unified model mapped onto identified neural circuits. Homing paths are quantitatively and qualitatively compared with real ant data in a series of simulation studies replicating key infield experiments.

Our analysis reveals that insects require independent visual homing and route following capabilities which we show can be realised by encoding panoramic skylines in the frequency domain, using image processing circuits in the optic lobe and learning pathways through the Mushroom Bodies (MB) and Anterior Optic Tubercle (AOTU) to Bulb (BU) respectively before converging in the Central Complex (CX) steering circuit.

Further, we demonstrate that a ring attractor network inspired by firing patterns recorded in the CX can optimally integrate the outputs of path integration and visual homing systems guiding simulated ants back to their familiar route, and a simple non-linear weighting function driven by the output of the MB provides a context-dependent switch allowing route following strategies to dominate and the learned route retraced back to the nest when familiar terrain is encountered.

The resultant unified model of insect navigation reproduces behavioural data from a series of cue conflict experiments in realistic animal environments and offers testable

hypotheses of where and how insects process visual cues, utilise the different information that they provide and coordinate their outputs to achieve the adaptive behaviours observed in the wild. These results forward the case for a distributed architecture of the insect navigational toolkit.

This unified model then be further validated by modelling the olfactory navigation of flies and ants. With simple adaptions of the sensory inputs, this model reproduces the main characteristics of the observed behavioural data, further demonstrating the useful role played by *sensory-processing* $\rightarrow$ *CX* $\rightarrow$ *motor* pathway in generating context-dependent coordination behaviours. In addition, this model help to complete the unified model of insect navigation by adding the olfactory cues that is one of the most crucial cues for insects.

Declaration

I, Xuelong Sun, declare that this thesis describes an original research carried out on my own. It has not been previously submitted to any university for the award of any degree. Where I have quoted from the work of others, the source is always given.

XUELONG SUN

Acknowledgements

Four years of studying for my PhD is not easy and sometimes very stressful. But thanks to the help from many people around me, the whole journey has been thoroughly enjoyable and meaningful and will always be the experience with my great cherishing.

Firstly, a great thanks to my first supervisor Prof Shigang Yue who is always so supportive, considerate and patient. He has provided me with great inspirations for not only my studies but also my life. Then a huge thanks to my second supervisor Dr Michael Mangan who has spent plenty of time and effort. I could not be luckier to have such a brilliant advisor from whom I have learnt a lot. Thanks to his constant encouragement and excellent guidance that have helped me a lot in improving my research skills, academic writing and solidly pushing forward my studies. Also, I want to thank Dr Vassilis Cutsuridis's kind help.

I am grateful to the fantastic colleagues and friends in the Computation Intelligence Lab (CIL) of the University of Lincoln, who have offered valuable help and enlightening discussions. Particular thanks to Jiannan Zhao and Tian Liu, who have also been my great roommates. Accompanying and encouraging each other appear to be very important during hard times. All the previous and current members of CIL hugely enhanced my experience, and this thesis would not have been completed without the help from them.

I would also like to thank the EU FP7 projects HAZCEPT (318907) and EU Horizon 2020 project STEP2DYNA (691154), and ULTRACEPT (778602). The secondments supported by these projects greatly enriched my PhD experience. During the secondment at Tsinghua University and Guangzhou University, my communication skills have been improved, and my horizons have been broadened by having meaning-

ful communications with excellent colleagues there.

Then, sincere thanks to my best friends Youkang Wu, Yiwen Yang and those I play word-guessing game with. They are so lovely and supportive and encouraged me a lot when I am down.

I would like to thank the support of my families who continually stand on my side and appreciate my efforts. Finally, from the bottom of my heart, I want to say thanks to Wenli Fu, who helped me through the most challenging time. Thank you for your constant patience, understanding and pep talks that supported me to walk through this rough journey.

List of Selected Publications

[1] **Sun X**, Yue S, Mangan M. "A decentralised neural model explaining optimal integration of navigational strategies in insects" in *eLife Science* 2020: 9:e54026, doi:10.7554/eLife.54026.

[2] **Sun X**, Mangan M, Yue S. "An analysis of a ring attractor model for cue integration" in *Conference on Biomimetic and Biohybrid Systems.*(***Living Machine***) Springer, Cham, 2018: 459-470, doi:10.1007/978-3-319-95972-6_49.

[3] **Sun X**, T. Liu, C. Hu, Q. Fu and S. Yue. "ColCOSΦ: "A Multiple Pheromone Communication System for Swarm Robotics and Social Insects Research," in *2019 IEEE 4th International Conference on Advanced Robotics and Mechatronics **(ICARM)*** 2019, doi: 10.1109/ICARM.2019.8833989.

[4] paper planned to submit to eLife:
Sun X, Mangan M, Yue S. "Modelling odour/wind navigation in fly and ants" in *eLife Science*.

Contents

List of Figures

List of Abbreviations

AL	antenna lobe
AMMC	antennal mechanosensory and motor center
ANN	artificial neural network
AOTU	anterior optic tubercle
APN	AMMC projection neuron
BU	bulb
CX	central complex
CBL	central body lower
CBU	central body upper
DRA	dorsal rim area
DRME	dorsal rim medulla
EB	ellipsoid body
FB	fan-shape body
GA	gall
GUI	graphical user interface
KC	Kenyon cell
LAL	lateral accessory lobe
MB	mushroom body
MBON	mushroom body output neuron
MLE	maximum likelihood estimation
NO	noduli
OL	optic lobe
OH	olfactory homing
PB	protocerebral bridge
PN	projection neuron
POL	polarisation-sensitive
PI	path integration
RA	ring attractor
RF	route following
RMS	root mean square
SMP	superior medial protocerebrum
UAV	unmanned aerial vehicle
UI	user interface
UW	upwind
VN	visual navigation
VH	visual homing
WPN	wedge project neurons
WTA	winner take all
ZM	Zernike moments

Chapter 1

Introduction

1.1 Background and Motivation

Navigation, a skill shared by almost all the animals living in the land, water or sky, endows creatures with the vital ability to reach the desired location. Although navigation can be defined with different levels of universality (from simple stimuli-response as Simon's ants [25] to ability with map-like cognition [26], [27]), here to cover a wide range of orientation behaviours have been observed in insect (potentially includes both the 'taxon' and 'locale' navigation defined in rodents [28]), navigation is defined as: the movement from one place to another driven by specific guidance. Under this definition, animal navigation comes in many forms and shapes (see Figure 1.1), for instances, in a large scale (thousands of miles), regular *migration* from and to a breeding site [29] (like birds, butterflies and fishes), or within a relatively shorter distance, returning home after foraging (also termed *homing*, like ants and bees). Solving navigation problems is so crucial and universal in living organisms that nature has provided elegant solutions, bringing great inspirations for studies aiming to unravel neural mechanisms underpinning navigation and solving robotic navigation problems respectively. The latter field even gets momentum recently with the emergence of self-driving cars and UAVs.

Among the animal navigators, insects are one of the most interesting classes, not only because insects have fascinated researchers by their unrivalled ability of solving many complex navigation problems [30], [31], but also the brain size of insects are rel-

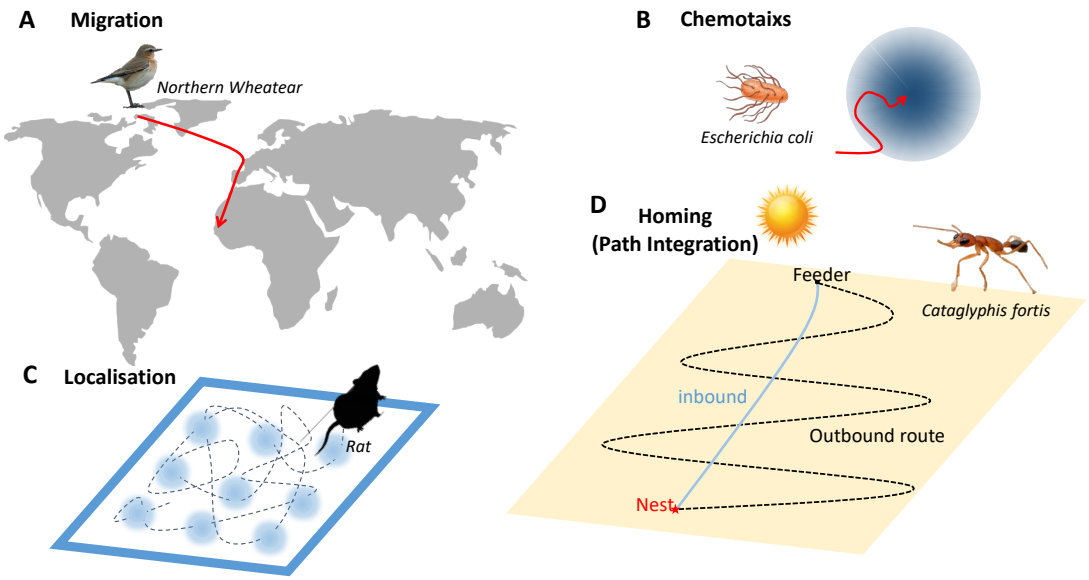

Figure 1.1: **The examples of animal navigation.** (**A**) Birds' (*Northern Wheatear*) migrates from Alaskan to Africa [1]. Picture of bird is taken by Phil Gower shared via Birdshare. (**B**) Chemotaxis behaviour of bacterial [2]. Picture of bacterial is adapted from dreamstime. (**C**) Navigation trajectories of rat overlapped with the firing rate of grid cells in the entorhinal cortex [3]. (**D**) Desert ants homing using path integration (for reviews see [4]).

atively tiny with less than one million neurons [32], [33] compared to vertebrates and humans with about 100 billion neurons [34]. As being such an ideal studying model, insect navigation has been intensively studied for more than a century [35]. Numerous behavioural studies have unveiled the rich repertoire of the insect navigation system, and evidence suggests that different central foraging insects (like ants and bees) apply similar navigation strategies using analogous environment cues despite their differing environments. Taking this evidence together leads to an insect navigation toolkit presented by Wehner [36], of which the most fundamental are path integration (PI) and visual navigation (VN). PI continuously tracks the distance and direction travelled to provide a global vector pointing to the start point (home vector), while VN provides the visual reference that can be compared with the current view to generate a homing signal (will be introduced in more details in Chapter 2).

Although insect navigation behaviours have been increasingly well understood and conceptually or mathematically modelled, the neural basis underlying this has not yet been known until some important findings of the insect brain, especially the central complex (CX) and mushroom body (MB), were published very recently. Nevertheless,

there is still a long way to go to get the whole picture of insect navigation, where the specific navigation behaviour is mapped to the corresponding neural circuit that can conduct this kind of navigation computation. From the current point of view, the well-known insect navigation behaviours and the increasing knowledge of neural circuit together provide a great opportunity for researchers in the field of computational modelling to build a biology constrained model that can explain the navigation behaviours and make further testable predictions for both the behavioural studies and neurobiological studies. Therefore, in this thesis, as motivated by the above facts, a unified computation model is developed aiming to bridge the following main three gaps in the understanding of insect navigation:

- Evidence has shown that insects can optimally integrate multiple guidance systems when navigating, but a biologically plausible neural model has yet been developed to explain how this can happen in the insect brain.
- Current VN models can only account for parts of the visual navigation behaviours that have been observed in insects. Is there a unified way to bio-plausibly model the visual navigation behaviours? And if so, how does VN interact with other navigation subsystems in a biologically plausible way, e.g. PI?
- Could the unified model and coordination mechanism developed above be a general framework to explain all navigation-related behaviours at the level of neurons, such as odour/wind navigation?

1.2 Methodology

1.2.1 Why Insect Navigation?

Understanding the intelligence of animals is one of the major goals in biology. The complex behavioural repertoire involving flexible integrating of multiple modalities and small brain with limited neurons make insect navigation an ideal synthesis for studies of animal intelligence and cognition [37], [38]. By studying how complex

navigation behaviours can be generated in the insect brain, we may unravel the fundamental mechanisms for navigation and even provide inspirations for studies concerning more complex behaviour in higher-order animals, as navigation in insects already covers most of the basic parts of cognitive mechanisms like learning, working memory, decision-making, etc [31], [32].

1.2.2 Why Computational Model?

Computational modelling, as it literally means, referring the use of computers to simulate and study complex systems that are impractical or impossible to do direct mathematical analysis. As a complementary approach of traditional techniques (i.e., experimental and theoretical) to understand biology systems, computational models are playing increasing roles due to its apparent advantages [39], [40]: first, with a reasonable computational model established, conducting different experiments in varied settings can be simply implemented by just adjusting different parameters in the model and simulation environment. Furthermore, during the whole process of simulation, all the variables and states can be easily manipulated and monitored as needed. By doing these simulations, one can test the hypothesis, provide novel insights, make testable predictions that can guide future experimental design, do sensitivity analyse, etc. Second, computational models can judge if a specific mechanism is sufficient to explain observed phenomena where theoretical analysis can hardly tell. Although it is challenging to build a *reasonable* computational model, results derived from computational model simulation can make significant contributions to science advances as long as the model is based on plausible hypothesis, like the finite element method in physics and engineering [41], the model in cell-cell interactions [40], [42], etc.

In the field of insect navigation, computational modelling also plays an important role and has already made some significant contributions. For instance, the classic snapshot model provided the insight that continuous comparing the current view with a stored snapshot taken at the goal is sufficient for generating insect-like visual navigation [14]. More recently, a computation model of PI presented in [43] heuristically represents the current heading signal as a sinusoidal activity pattern of an array of neu-

rons, and then the speed signal determines the rate at which the activity is accumulated. This mechanism is astonishingly close to the very recently published biologically constrained model [10]. The idea that representing a directional signal by an array of neurons as a sinusoidal activation profile is also very enlightening because this facilitates the computation in navigation involving many vector operations [44] and indeed offers an explanation as to why the neurons in CX are arranged in a column format [10], [13], [45]. Finally, the idea of comparing the current heading with the memory to generate steering command via a left-/right-shifted mechanism also interprets the neural anatomy in the CX [10], [13].

In summary, computational models have many advantages and collaborating with experimental biology could be highly fruitful ([10] is a good example), which also provides the primary motivation for this thesis.

1.2.3 Biological Constraints

As introduced in Chapter 1.2.2, a good computational model aiming to explain a biology system should base on reasonable assumptions, constructed at a suitable abstraction level and provides testable predictions [40]. As the model in this dissertation is developed with the biological constraints to verify if the proposed mechanism is sufficient to produce observed insect navigation behaviours in a proof-of-concept way. Hence the performances of the model are tested by comparing them with the behavioural data from real insects instead of the actual neural spikes. The loop from neuron to behaviour could not be closed by merely reproducing neural activities [46], but reproducing the natural behaviour using the biologically constrained model at least proves that the proposed mechanism is sufficient for generating such behaviours, which is indeed the desired outcome this thesis aims to achieve.

To summarise how we use the biological data in this thesis:

- **Anatomy and physiology:** models are constrained to the known anatomical and physiological evidence, but if there is no exiting data rational hypothesis will be made based on the investigation of the mechanism that an insect may exploit.

- **Ethology:** simulation results of the computational model are bench-marked by

the comparison of homing routes and heading directions with the data from behavioural studies of real insects in biologically realistic environments.

It should be noted that the biological data used in this thesis comes from different species of insects, i.e., behavioural data mainly comes from desert ants while anatomical and physiological data is from studies of fruit flies, locusts and honeybees. However, the logical rationality of using biological data across species will be addressed or discussed via homologous inference. As this thesis mainly focuses on the modelling of homing behaviour of insects, i.e., returning home after foraging or exploring, other navigation behaviours like the long-distance migration, pheromone-based swarm collectively strategies are beyond the scope of this study. Simulations are limited to the 2D flat ground (i.e., no pitch and roll).

1.3 Thesis Outline

This thesis is divided into five main chapters:

Chapter 2 surveys the large body of the insect navigation study including the ethological studies of the famous insect navigator- desert ant, the neurobiological studies of the insect brain underpinning the navigation behaviours and also computational models looking to explain the function of neural circuity of the insect brain and interpreting observed navigational behaviours.

In Chapter 3, a unified model that can account for both the visual homing and route following behaviour in insect navigation is developed. Based on the frequency encoded visual information, this model can reproduce the primary visual navigation data from real insects and thus fills the gap in understanding how insect may use different visual navigation strategies in different visual contexts to navigate.

In Chapter 4, a biology-plausible neural model is presented to realise the optimal integration of competing directional cues. Based on the classical ring attractor model, simulation results suggest that this neural network can combine cues according to their certainty but converges on the most certain cue if cues have larger conflicts. This result is reminiscent of the biological results from mammals' heading direction systems.

Therefore RA can be the candidate for optimally integrating multiple guidance cues in insects navigation.

Chapter 5 then gives a unified model for insect navigation by combining the visual navigation models and the cue integration model described in the previous two chapters. With another contextual switching circuit added, this unified model reproduces many recent behavioural data from cue-conflict experiments. Required computations are mapped to specific brain regions based on the known neurobiological data, providing testable suggestions for anatomy and physiology studies with emphasis on CX and MB.

Then, in Chapter 6, to further verify the utility and plausibility of the proposed unified model, we adapted the model to replicate the odour navigation both in flies and ants which has not been neurally modelled. Simulation results show that with small input and output adaptions, this model can account for the chemotaxis and odour-gated anemotaxis behaviours, suggesting the sensory experience depended multi-guidance coordination could be a mechanism that is conserved across insects to solve navigation-related tasks.

Finally, Chapter 7 summarises the main contributions of this thesis and the future research topics that could build on this study.

Chapter 2

Literature Review

The great ability of insects navigation has fascinated researchers since at least a century ago (about 19th century) when Fabre found that bees and wasps can return to their nest even after been displaced kilometres away [47]. In recent years, with the aid of rapidly developed technology of animal tracking, neuron observation and computational modelling, researches start to unveil the mystery of insect navigation by enormous observation, analysis and investigation. This in turn brings a rich literature that will be reviewed in this chapter in three sub-parts: first, the ethology research revealing the rich repertoire of insect navigation behaviour. Second, the anatomy and physiology studies of insect brain concerning navigation, which is crucial as they provide direct knowledge of the neural basis underpinning specific navigation tasks; Third, the useful and complementary tool in studying biology system- computation modelling. As insect navigation is a researching field of multi-discipline, knowledge from these three sub-parts cooperate and indeed make up the three-level understanding of insect navigation [46]: behaviour (level3) $\leftrightarrow$ computation (level2) $\leftrightarrow$ neuron (level1), where computation plays a crucial role in bridging the neurons (neural basis) and behaviour (ethology) by modelling the two transitions (from level1 to level2 and from level3 to level2). This reflects the modelling motivation of this thesis.

This review specifically focuses on path integration, visual navigation and their integration while other mechanisms will be briefly introduced, aiming to provide an overview of our current understanding of these navigation behaviours and their neural basis. Finally, based on this knowledge, a summary was drawn to clarify the problems

and challenges that will be addressed in this thesis.

2.1 Ethology- Insect Navigation Behaviours

After Fable's discovery [47], modern research interests of insect navigation firstly started more than a century, when Pièron in 1904 first displaced the ant and found the ant would run straight in a direction as it has not been displaced [48]. Then in the 1920s, Felix Santschi in North Africa found that ant can use the celestial cues to orient [35]. Later in 1949, Karl von Frisch gave an explanation of ant's such ability by revealing the significant fact that honeybee (*Apis mellifera*) can use polarised light as a compass to navigate [49], making honeybee a popular model for studying insect navigation behaviour. However, intensive investigation of insect navigation behaviour did not yet come until Wehner started to focused on how desert ants (*Cataglyphis bicolor*) sensed direction and distance in 1970s [5], which consequently made the desert ant genus *Cataglyphis* gradually become one of the most popular models to study navigation behaviours of insects. And subsequently studies on other types of ants (like *Cataglyphis fortis*, *Cataglyphis nodus*, *Cataglyphis velox* and also *Ocymyrmex* and *Melophorus*) (see Figure 2.1A) have also been conducted, bringing rich literature concerning ethological study of ants navigation. Navigation behaviours have also been observed and investigated in other insects (see Figure 2.1), enriching the ethological data of insect navigation and making the toolkit proposed by Wehner derived from desert ants' navigation behavioural data [36] possible to be extended to other insects. This section will introduce the insect navigation repertoire including path integration, visual homing, route following, systematic search, and odour/wind navigation in detail.

2.1.1 Path Integration

Similar to the early sailors using *dead reckoning* to navigate when travelling on the sea, animals apply path integration to continuously keep track of the distance and direction that has been travelled. This information is integrated to build a vector memory called the *home vector* that can guide the agent directly back not only to the nest but

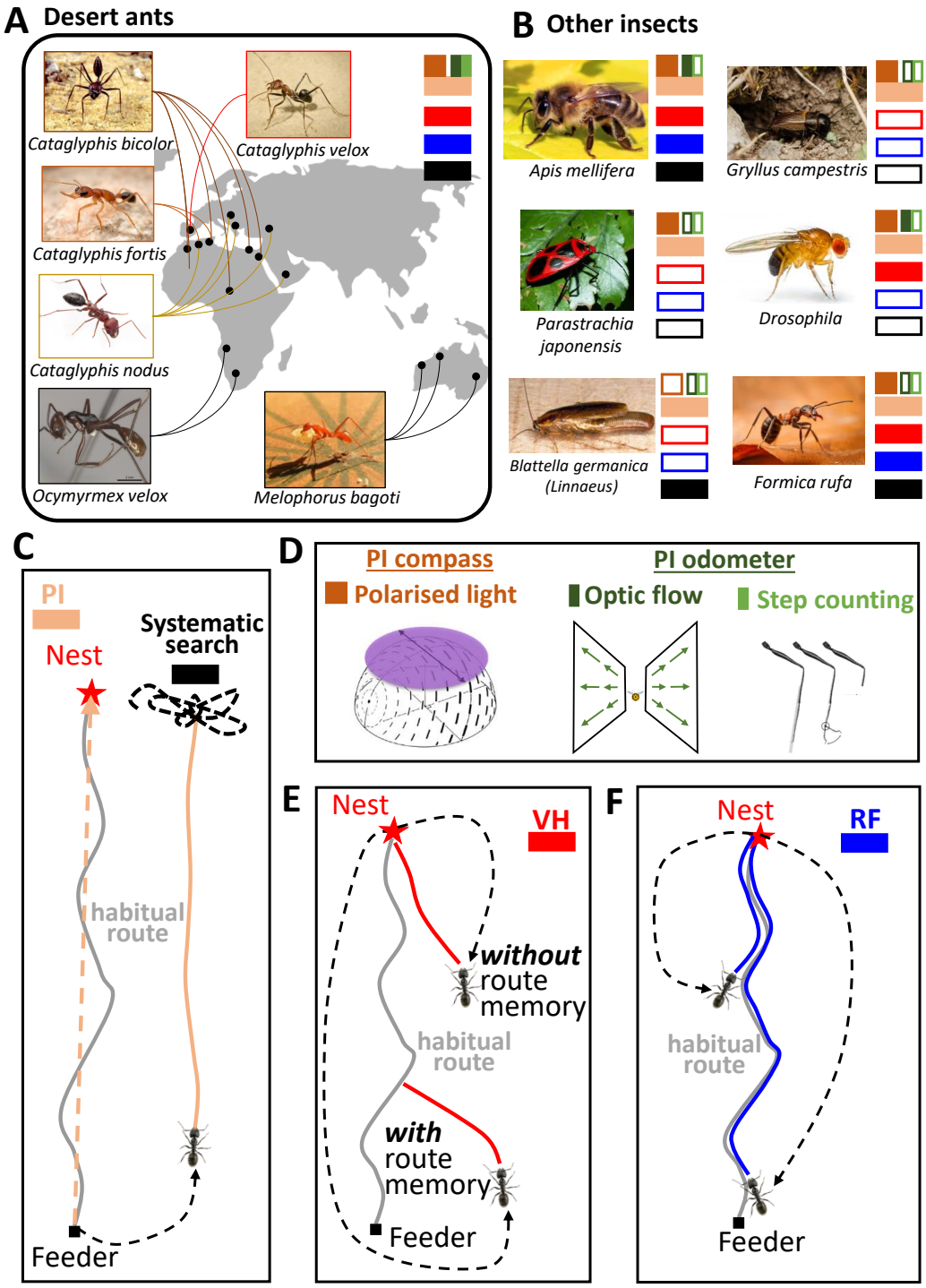

Figure 2.1: **The summary of insect navigation behaviours.** (**A**) Desert ant species and its distribution around the world (data from Antmaps). Pictures of ants: *C. bicolor* from [5]; *C. velox* from Michael Mangan; *C. fortis* from [4]; *O. velox* from AntWiki; *C. nodus* from ants; *M. bagoti* from Antoine Wystrach; (**B**) Other insect species. Pictures of animal: *Apis mellifera* from Cumnor Hill; *Gryllus* from Gilles San Martin; *Drosophila* from Shutterstock; *Blattella* from James Castner; *Formica rufa* from Michal Kukla. (**C**) Path integration (orange line) and systematic search (black line). (**D**) Sensory information required by path integration. (**E**) Visual homing (**F**) Route following. All species are labelled with colour-coded boxes (colour are matched with that in (**C**)-(**F**)), where filled box means evidence has been found in that specie's performing certain navigation behaviour.

the previously visited food sites. One can confirm that an animal has a path integrator if after the animal has been displaced to another unfamiliar location, it can travel a certain distance in the direction pointing to the position where the nest should have been [50] [4] (see Figure 2.1C). Many insects have been observed to use this strategy, like in ants [48] [51], honeybees [52] (for a review of path integration in ants and bees see [53]), in shield bugs [54] [55], in crickets [56], in cockroaches [57] and also in fruit flies [58].

To continuously update *home vector*, path integration requires two sources of sensory information: a stable compass tracking the direction and a measurement of the distance travelled (see also Figure 2.1D):

For the compass, since Karl von Frisch [49] first showed that polarised light can served as a directional reference for honeybees, usage of this celestial cue have also been observed in other insects like desert ants [51], monarch butterflies [59], honeybees [60], crickets [61], locust [62] and fruit flies [63]. Taking this cue as the compass is reliable because the polarised light source is located at an infinite distance (or strictly very far away) from the animal so will not change when the animal translates but will vary during rotational motion. Behavioural studies in dung beetles revealed that aside from polarised light other celestial cues such as sun position [64]–[66], spectral and intensity cues [65] in an integrated way with polarised pattern. The Milky Way [67] [68] and the moon position [69] can also be used for orientation. In addition, evidence from insects has also shown the usage of magnetic for navigation [70]–[72] (and for a recent review see [73]), but whether and how this cue contributes to PI remains unclear.

For the odometer measuring the travelled distance, Wittlinger et.al [74] [75] nicely showed that distance estimation in ant is generated by integrating the number of steps. Another mechanism applied by insects to measure distance is called *optic flow* wherein the rate at which the visual information moves across insects' retina when they are travelling in their environment is calculated. This mechanism is usually applied by flying insects like honeybees [76] [77] (where the result of their path integration is obtained by observing the waggling dance that conveys the location (direction and distance) of the food site), sweet bees [10] and moth [78] while walking insects like ants shown to

use both the step counting and optic flow [79] [80] (although ants appeared to ignore the lateral optic flow [81]). Interestingly, when measuring the distance, a functional compass appeared to be needed [82] [83]. To summarise, walking insects like ants apply two mechanisms: *step counting* and *optic flow* while flying insects rely on *optic flow* only, and the celestial compass is necessary for distance estimation.

2.1.2 Visual Navigation

Visual information also plays an important role in insect navigation. Studies have shown that many insects use visual memory to return to a specific place, such as their nest or a regular feeding site. For example, cockroaches can visually learn the locations of the shelters [84], and fruit flies [85] and crickets [86] are able to use visual cues to locate the cool spot within a hot environment. Visual information seems more vital for social hymenopterans (central-place foraging insects) like ants and bees in the context of navigation, and a large part of the behavioural data that supports the use of vision in navigation are in these animals. Given the mechanisms involved in visual navigation, it appeared to be two distinct types- called visual homing and route following (or in [87] termed positional image-match and alignment image-matching respectively). Evidence also showed that ants may select different visual navigation strategies according to their current visual context (i.e, On or Off-route) [18].

2.1.2.1 Visual Homing

As reviewed in [88], the simplest visual navigation mechanism applied by insects is to take visual features as the beacons guiding the agent to pinpoint a specific location, which is the so called *beacon aiming*. Then the more impressive strategy named visual homing is to store the view at the locations of the goal for later image matching. This visual navigation behaviour has been observed in a wide range of insects (for review see [89]), for instance, honeybees [90] [14], wasp [91], ants (desert ant [92] and wood ant [93]) use this to approach the nest or feeding site, or approach the habitual route [94] [18] (see Figure 2.1E). In addition, visual homing can also account for station keeping behaviour in hoverflies [95] and waterstriders [96] (as reviewed in [87]).

2.1.2.2 Route Following

Another way of using visual information to navigation is to recall an appropriate view memory at a certain location, and then realign the current view with the recalled view to compute a turn angle so that the agent can recapitulate its habitual direction (see Figure 2.1F). This is the so called route following that allows insects fast and robustly travelling between a rewarded food site and the nest. Evidences of insects' possessing this behaviour have been found in desert ant (*Cataglyphis* [97] [98] [99] and *Melophorus* [100]), wood ants [101] [102] and bees [103]. These visual routes are stored as long-term memories that can last for the entire lifetime of ants [104].

2.1.3 Olfactory Navigation

As we may have experienced how annoying the mosquitoes are when we are enjoying the summer evening. Like other insects, mosquitoes use olfactory cues to localise the 'food', i.e., they are attracted by carbon dioxide exhaled by us and living animals [105]. Likewise, examples of insects use olfactory cues for navigation are widely existed across different insect species in different states (larvae or adult), among which the most classical one is the ants use pheromone trails to recruit foragers to a food site [106] [107]. Another mechanism of using olfactory has been intensively studied is the chemotaxis behaviour of *Drosophila* larva [108] [109]. Other examples could be found in pheromone plume tracking of moth [110], homing route memorising in desert ants [111], etc. Further, olfactory navigation usually involves the wind shaping the spatiotemporal distribution of the odour concentration. Thus when navigation, insects also sensed the wind direction and take both the perceived odour and wind direction into account to make navigational decisions. Like the odour-gated upwind following behaviours observed in ants [112] [113] [21] and flies [114]. Evidence also suggested more sophisticated mechanisms that combing olfactory cue with other cues like vision to navigate (for review see [115]).

2.1.4 Systematic Search

When all other guidance systems are not available (e.g., naive ants in a visually unfamiliar environment without forming home vector), insects will perform the systematic search as the last resort to find familiar terrain. During the search, the animal loops in directions while frequently returning to the starting point and then start a new and larger searching loop [116] [117]. As a rudimentary behaviour, many insects have been observed to apply systematic search when they 'get lost', for instance, in desert ant (*Cataglyphis* [116] [118], *Melophorus* [119]), desert isopod and cockroach [118], honeybees [120], etc. However, whether a separated system is needed to realise systematic search is still unclear because systematic search could be regarded as the spontaneous result of path integration memory's repeatedly accumulating and releasing near the zero-state [10], [27]. Maybe there is also no need for the insects to detect 'lost' as the searching behaviour can also be driven by the motor-control system (e.g., modelled by a central pattern generator) when this is no any significant input.

2.1.5 Interactions of Multiple Guidance Systems

As introduced in the previous sections, the fact that insects possess multiple guidance systems (path integration, visual navigation, olfactory navigation and systematic search) for navigation raises the question of how do these subsystems interact with each other? Also as the objective of this thesis is to build a unified model that can account for the multi-guidance coordination, behavioural studies investigating the interactions of different navigation behaviours will act as the benchmark of this study. Data on the integration of navigational strategies are therefore reviewed in this section.

First of all, the basic and natural reason for insects' developing different strategies for navigation may be that they are living in different environments. The best strategy for a specific specie should be indeed suitable for the environment it lives in. For instance, desert ants living in visually barren landscapes like the salt pans rely primarily on PI [51] [121] while ants living in relatively cluttered visual environments only follow PI for half of the home vector distance [50] [122] and can even ignore PI output [123] when released in visually familiar sites. It seems that the degree to which

insect relies on visual cues correlates with the richness of available landmarks [122]. This idea could be extended and generalised to support the hypothesis that the weighting of each guidance system when integrated to steer the animal is determined by the certainty of that cue. This view of optimal cue integration contrasts the idea of *dominance hierarchy* proposed by Karl von Frisch [124] (as cited by [125]) and followed by Cruse et.al [126]. However, behavioural studies have provided more evidence supporting the hypothesis of optimal cue integration rather than the *dominance hierarchy*. These studies were inspired by two predictions that optimally integrating multiple cues can make (for review see [125]):

First, when cues are placed in conflict, an intermediated output should be taken (see Figure 2.2 for the summarised evidence of optimal cue integration in insect navigation behaviour). As in Figure 2.2A, ants *Cataglyphis fortis* were trained to visit the feeder and then return to the nest marked by a landmark, and then were taken to the test filed where the landmark was placed in different distances from the feeder (see the green squares in Figure 2.2A(b) (f)) that is side away from the habitual route. The ants' courses gradually deviated toward the landmark as the home vector was run off. This results suggested that ants weighted the directions from PI and VN according to the state of PI [6]. Similar data have also been found in *Melophorus bagoti* [121] with higher weighting attached to VN. In [7], the state of PI was also manually altered (as shown in Figure 2.2B), ants (*Cataglyphis fortis*) were trained to approach a feeder marked by a landmark through two segments of the route: a straight path with 10m length shaped by a channel and an immediate left-turn after getting out of the channel. When testing, all the trained ants start their foraging trip in the channel but were displaced forward by 0m (iii), 4m (ii) or 8m (i) to format different length of the home vector when they get out of the channel. Foraging trajectories of ants demonstrated that they combine the direction recommended by PI and VN. Similar results have also been observed in *Cataglyphis velox* [8] as shown in Figure 2.2C, ants were trained to foraging and homing in a narrow corridor, and when testing, the trained ants were captured at the positions with different distances from the feeder to alter the length of the home vector, and then were released at the releasing point. The initial headings of

the homing ants were recorded. The results demonstrated that the ants optimally integrate directions from PI and VN. The authors in [8] further showed that the weighting of PI when combined with VN can be estimated by the length of the home vector, i.e., the length of the home vector determines the certainty of PI in the hypothesis of optimal integration. Differs from the above studies where the integration of PI and VN was investigated by altering the length of the home vector (i.e., the certainty of PI), behavioural experiments in [9] was conducted by changing the certainty of visual navigation to explore ants' cue integration behaviour. As shown in Figure 2.2D, zero (without PI memory) and full (with PI memory) vector ants that have been trained in advance (*Melophorus bagoti*) were released at three different releasing points (RP1, RP2 and RP3) with increasing distances from the nest. Zero vector ants released at RP1 and RP2 still have preferred homing orientation but not at RP3. Because, as qualitatively assumed, the VN based on the terrestrial cues becomes less reliable as the distance from the nest increases (quantitative analyses will be addressed in this model, see 3.2.2). However full vector ants released at RP3 still have a significant initial heading preference recommended by PI. At RP2 and RP1, the initial heading orientation appeared to be generated by optimally integrating PI and VN according to their certainty (see Figure 2.2D). In a word, all these data support the hypothesis that PI and VH are optimally integrated and the weighting of PI and VH, when combined, can be determined by the length of the home vector and the visual familiarity respectively.

Second, adding more cues into guidance system brings precision as proven by [127] [128]. Figure 2.2A(a) and (b) show one example of this prediction, whereby the addition of a visual landmark close to the goal produced homing paths that converged more tightly around the habitual route compared to that of no landmark placed at the nest. This has been confirmed again in two species of Australian desert ant [129]. Steck et.al [130] also found that with both the olfactory and visual information available, the searching pattern of *Cataglyphis fortis* will be more concentrated.

The hypothesis that multiple guidance systems operate simultaneously and optimally coordinate the paths of insects to the goal location is the basis of this modelling study.

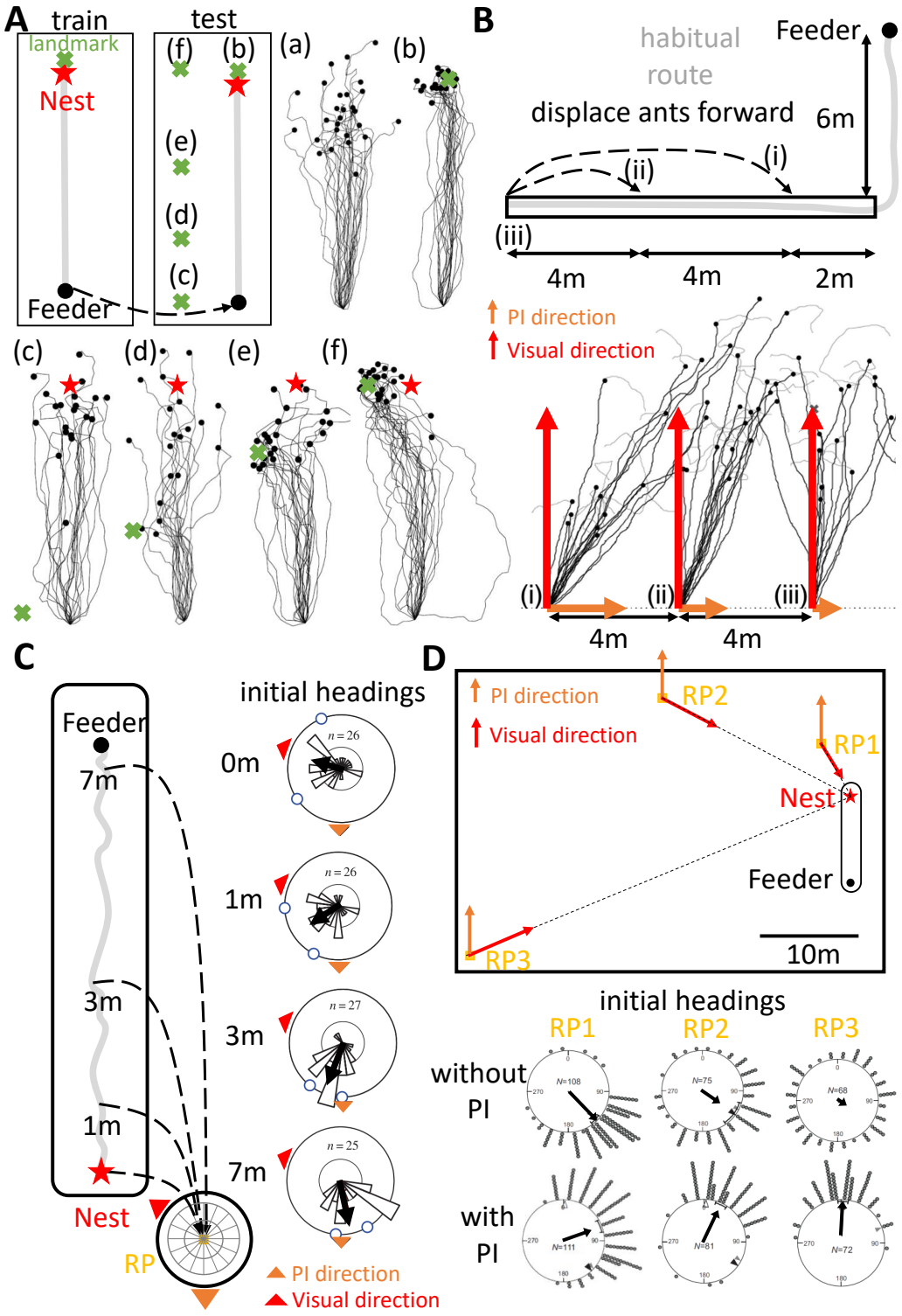

Figure 2.2: **Evidence supporting optimal cue integration of PI and VN in insect navigation.** **(A)** The competition of path integration and landmark. Black curves depict the homing routes of ants and black dots indicate the start of searching. Figure is adapted from [6]. **(B)** Competition between visual cue and path integration. Homing paths are shown in the same way as in **(A)**. Note the compromised direction taken by the ants in (i) and (ii). Figure is adapted from [7]. **(C)** Cue combination of path integration and visual navigation. As the length of home vector increase, the integrated output shifts to the direction PI indicated. Figure is adapted from [8]. **(D)** Cue combination of path integration and visual navigation by varying certainty of visual cues. Figure is adapted from [9].

Note that other formats of multi-guidance interactions (e.g., PI acts as the reference for learning flights of bees [131] and learning walks of ants [132]) are beyond the scope of this study, so will not be discussed in details (but for a recent review introducing many formats of multimodal interactions in insect navigation see [115]).

2.2 Neurobiology- Neural Circuits for Navigation

Unlike the rich understanding of insect navigation behaviours, the evidence and knowledge of the neural substrates underlying these complex navigation behaviours are relatively lacking. But fortunately, now the focus of attention in understanding insect navigation has shifted to the exploration of neural basis [12], together with known data across different insect species, meaningful interpretations and hypothesis can be made to guide future research and modelling. This section will introduce the anatomical and physiological data related to navigation behaviour.

To understand the neural basis of insect navigation, the first step was made in 1967 by Vowels who found that lesions of the tract between optic ganglia and the mushroom body (MB) affect wood ants' performance in T-maze task [133], followed by a similar study on cockroach [134], where cockroach with bilaterally ablated MB lost the visual learning ability to locate a cold spot within a hot environment. And then this experimental scenario was conducted in fruit flies (*Drospohila*), astonishingly revealing the crucial role of CX (central complex, another brain region in insects) instead of MB in visual place learning [85]. These studies suggested that both MB and CX plays a role in insect navigation, and in fact, they are two of the most distinct and intensively studied neuropil related to navigation in the insect brain, thus focus of this review will be attached to the CX and MB that will be introduced in the following two subsections.

2.2.1 Central Complex

As shown in Figure 2.3, the CX originated over 400 million years ago is in the midline of insect central brain. This brain region is conserved across a wide range of insects (locust: [135] [136], fruit fly: [137], dung beetle: [138], cockroach: [139],

bees: [140], moth: [141]) and has changed little over time [142] [143]. The CX has the same substructure across different species, consisting of the fan-shaped body (FB in *Drosophila*, equivalent to central body upper (CBU) in locust/moth/butterfly), ellipsoid body (EB in *Drosophila*, equivalent to central body lower (CBL) in locust/moth/butterfly), protocerebral bridge (PB) and a pair of noduli. The neuroarchitecture of the CX is rather unique that the horizontal layers intersect the 16-18 vertical columns (fruit fly has 18 column in the PB while other insects like the locust has 16, as shown in Figure 2.3C,E) [45] [142] [135] [144] [145] (see also Figure 2.3E). Each column innervated by specific type of column cell existing in sets of 8-9 neurons in each hemisphere [45] [11].

As a crucial part in the central brain of insects, the CX plays many functional roles in different behavioural tasks (for reviews see [146] [147] and [13]). This review will focus on the navigation-related functions of the CX.

2.2.1.1 Heading Direction System

The first evidence revealing that the CX playing a role in navigation is the discovered neural pathway that is sensitive to the polarised-light (for reviews see [148] and [149]). As introduced in Chapter 2.1.1, polarised light is a crucial cue for insect orientation. And specifically, the direction of polarised light is sensed by sets of ommatidia in the dorsal rim area (DRA) of the compound eye. Then the information is processed in the optic lobe and sent to the inner brain area (see the neural pathway of DRME via AOTU to BU and finally targets the CX in Figure 2.3B). [150] has shown that in PB, the POL neuron's tuning correlates with its anatomical position. Similar properties have been directly observed in the CX of *Drosophila*, [151] showing that neurons in the EB of the CX ('wedge' neurons) encode the heading direction combined both the cue from visual and self-motion and this heading representation can be maintained in the darkness. Follow on studies [152] [153] [154] proposed that P-EN ('tile' neurons, also CL2 in other species), P-EG, E-PG ('wedge' neurons, also CL1a in other species) in the CX form a ring attractor network that can continuously update the fly's heading direction by integrating the angular velocity and the visual stimuli. Very

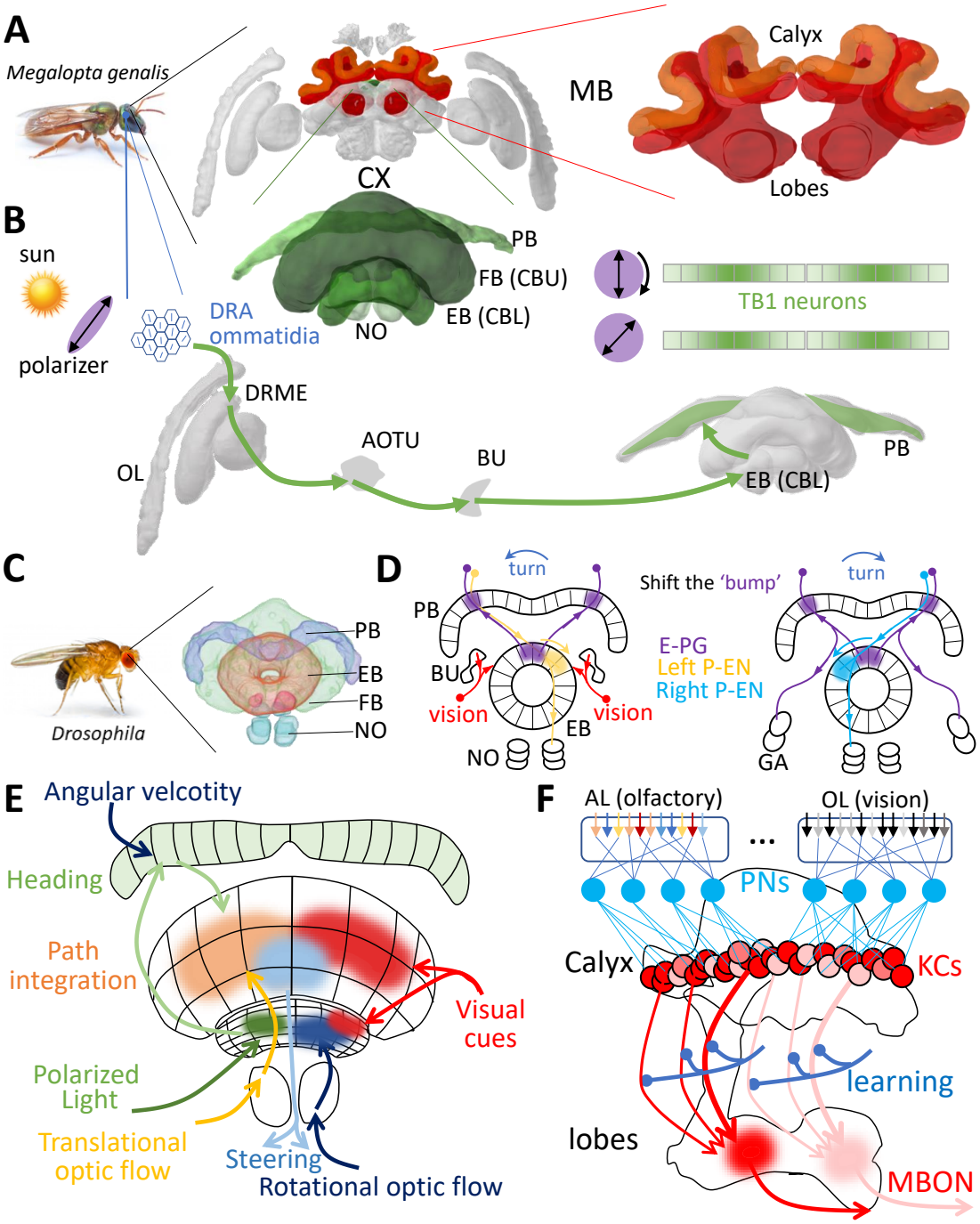

Figure 2.3: **The anatomy and proposed function of CX and MB in insect brain.** **(A)** The CX and MB in sweat bee (*Megalopta genalis*, picture is adapted from [10]). Pictures of brain region (and in **(B)**) are from InsectBrainDatabase. **(B)** The neural pathway of polarised light. **(C)** The CX of *Drosophila*. Picture of fly is from Shutterstock. Picture of brain region is adapted from [11]. **(D)** The schematic diagram of the fruit fly's heading direction system, highlighting how the angular velocity shifts the 'bump' activation in the PB. The visual information is passed through BU to the EB. **(E)**. The summary of the CX's functional role in insect navigation. **(F)** The summary of the MB's valence encoding through reinforcement learning with the visual and olfactory input.

recent studies [155] [156] also reveal how the neural plasticity in the heading direction system transform visual features rapidly to the 'bump' of the activation and how that enables the integration of multiple cues to a single heading representation. Pisokas et.al [157] further demonstrated the commonalities and differences of RA heading direction circuit across species [149] by modelling two different species (fly and locust) based on the known anatomy data.

To summarise, the heading direction system in the CX is a ring attractor network with recurrent excitation, global inhibition and one-slice offset connection enabling 'bump' shifting driven by the rotational movements (see Figure 2.3D). This heading system appeared to be ubiquitous in insects (dung beetle [158], butterfly [159], bees [10] and cockroach [158]) and also in mammalian [160] [161] so may be a conserved circuit for animal to establish a reliable internal heading representation underlying varies navigation behaviours.

2.2.1.2 Candidate for Insect Navigation Centre

Except from the polarised light, vision and proprioceptive cues used in heading direction system, evidences have shown that the CX also receives other processed sensory inputs, like the mechanosensory cue from the wings and antennae [162], the spatial orientation memory [163] and also the action selection [164]. Moreover, the CX also takes part in the locomotion control (for a early review see [165]). This was further proven by the lesion of the CX caused the locomotion failure in *Drosophila* [166] [167]. Recent study on cockroach has greatly push forward the understanding of the CX in locomotion control [168] [169] [170] [171] [172], among which [172] is a milestone which demonstrated that neuron activity in the CX predict and cause specific movements of the cockroach. Taken together, as illustrated in Figure 2.3E, this all make the CX very suitable for navigation computing as navigation per se is a sensory-motor process [12] [13] [173].

2.2.2 The Mushroom Bodies

Researches have also suggested that the pair of neuropils in the insect mid-brain known as the Mushroom bodies also play an important role in navigation. One motivation for Vowels's MB lesion experiment [133] is the early suggestion that MB may be involved in insects' complex cognitive processes [174]. Then direct correlations between the foraging efficiency and size of MB has been reported, which is the reminiscent of the widely existed phenomena that insects with great navigation ability usually have larger MB and more complex structure in the input projecting area (as reviewed in [175]). Then follow on evidences demonstrated that the lifespan volume and structure changes in MB may be due to the increased memory demands related to the navigation tasks in social insects (bees: [176] [177] [178]; ants: [179] [180]; wasps: [181]). Direct evidence have proven the essential role played by the MBs in olfactory memory processing in *Drosophila* (for reviews [182]). Although many studies have reported the larger visual input projected to the MB in insects that rely on visual information for navigation (bees: [183] [184]; ants: [179]; wasps: [185]; beetles: [186]; butterflies: [187] and moth: [188]), not until very recent has direct evidence been published to confirm the role of MB in insects' visual navigation [189] [190] [191].

The MB consists of calyx, pedunculus and lobes ([192], see Figure 2.3A) which is a good example of 'structure determines function' in biology system, as its anatomical architecture is very suitable for storing a large amount of memory patterns. In the context of associative olfactory memory in *Drosophila*, each PN samples a small number of AL glomeruli and innervate a large number of Kenyon cells (KCs) in the calyx. Each KC is innervated by several PNs and then all the KCs converge in parallel to a few MB output neurons (MBONs) [192]. The KC act as a coincidence detector and the whole MB circuitry can be regarded as a valence calculator [193], wherein KCs only response to specific PNs activation patterns and then innervate the MBONs via plastic synapses mediated by the reinforcing signal associated with the specific stimulus (like sugar or electronic shock), leading to an association between specific olfactory pattern and stimulus. This associative learning is still reasonable and effective if the input patterns derived from visual information rather than olfactory [173], wherein the

reinforcing signal provided by the training state and the MBON output indicates the familiarity (valence) of the presented view (see more in Chapter 2.3).

To summarise, as depicted in Figure 2.3F, the MB is a valence calculator that can tell the animal how good is the currently presented stimuli, and this signal can biases the animal's memory-based decision-making like 'should I keep going this direction?' in the context of navigation.

2.3 Modelling- from Neural Circuits to Behaviours

As another important complementary tool to understand insect navigation, computational modelling has an extensive history from the models at the conceptual or algorithmic level to the recent models more constrained by known anatomical and physical data. Computation modelling in insect navigation bridges the gap from the neural data to the behaviour [173] [46], usually bringing meaningful insights impractical to be obtained from direct neuron recordings.

This section will briefly review the modelling works of insect navigation but with particular focus on two recent seminal works (PI model in [10], and RF model in [17]) that this work mainly based on.

2.3.1 Modelling Path Integration

As the most widely existed navigation mechanism among animals, the modelling study of PI started first. Modelling PI is to modelling the updating and reading of the home vector, Jander [194], H. Mittelstaedt and M.L. Mittelstaedt [195] first proposed their PI model, followed by many other PI models ([43] [196] [197] [198] [199] [200]) choosing different reference frames (egocentric vs. geocentric), using different coordination system (static vs. dynamic vectorial basis and Cartesian vs. polar). As reviewed and analysed in [201] [202] [4] and noise-tolerance testing in [203], the most efficient, reliable and natural way to model the insect PI is to update home vector by applying a static-vectorial representation in the Cartesian coordinates (generally, the vector can be projected onto more than two axes) with allocentric distance (speed) and geocen-

tric direction sensing. Based on this idea, the speed in each axis (direction) can be accumulated and then the home vector can be calculated by vector summation. This representation appeared to be biologically plausible as the heading direction cells (see Chapter 2.2.1.1) in an insect are arranged in an array of 8 neurons (corresponded to 8 Cartesian axes) with different direction preferences. Stone et.al [10] further proved this and a PI model constrained by anatomical data that can account for behavioural data was proposed, standing for the state-of-the-art understanding of insect PI system.

In that PI model [10], as illustrated in Figure 2.4A, for updating home vector, the key component is the identified a set of neurons (CPU4) integrating the direction signal at the rate determined by the speed signal and thus the home vector is represented by the neural activities as sorts of population encoding; for reading the home vector, a set of identified steering neurons (CPU1) shifted the home vector (CPU4 neuron activity) to left/right and then the heading direction is subtracted from that left/right-shifted activation respectively to get the activation level of the left/right turning neurons, then these two neurons compete with each other to control the motor. Note that this reading mechanism well interprets the reason for insects using redundant coordinates (8 rather than 2 axes) to encode direction is for the ease of readout to generate motion command. The key contributions of this work fall in: first, a neural mechanism integrating direction and speed signal; second, the steering circuit that can neurally compares the current heading and desired heading (in the PI context, the memory of home vector) to generate ideal motion command (see Figure 2.4B).

2.3.2 Modelling Visual Navigation

To discern the ability of insects to visually return to a place of particular interest (a feeding site, a nest or a cold spot, etc.), modelling studies try to unravel the basic information contained in a view from the insect's perspective that can be used for navigation. For VH (as introduced in Chapter 2.1.2, visual navigation of insects includes two kinds of strategies: VH and RF), the first attempt was made by Cartwright and Collett [14] [15] where the home vector is calculated based on the comparison between the features (e.g, the angular position and size of landmarks) extracted from the current

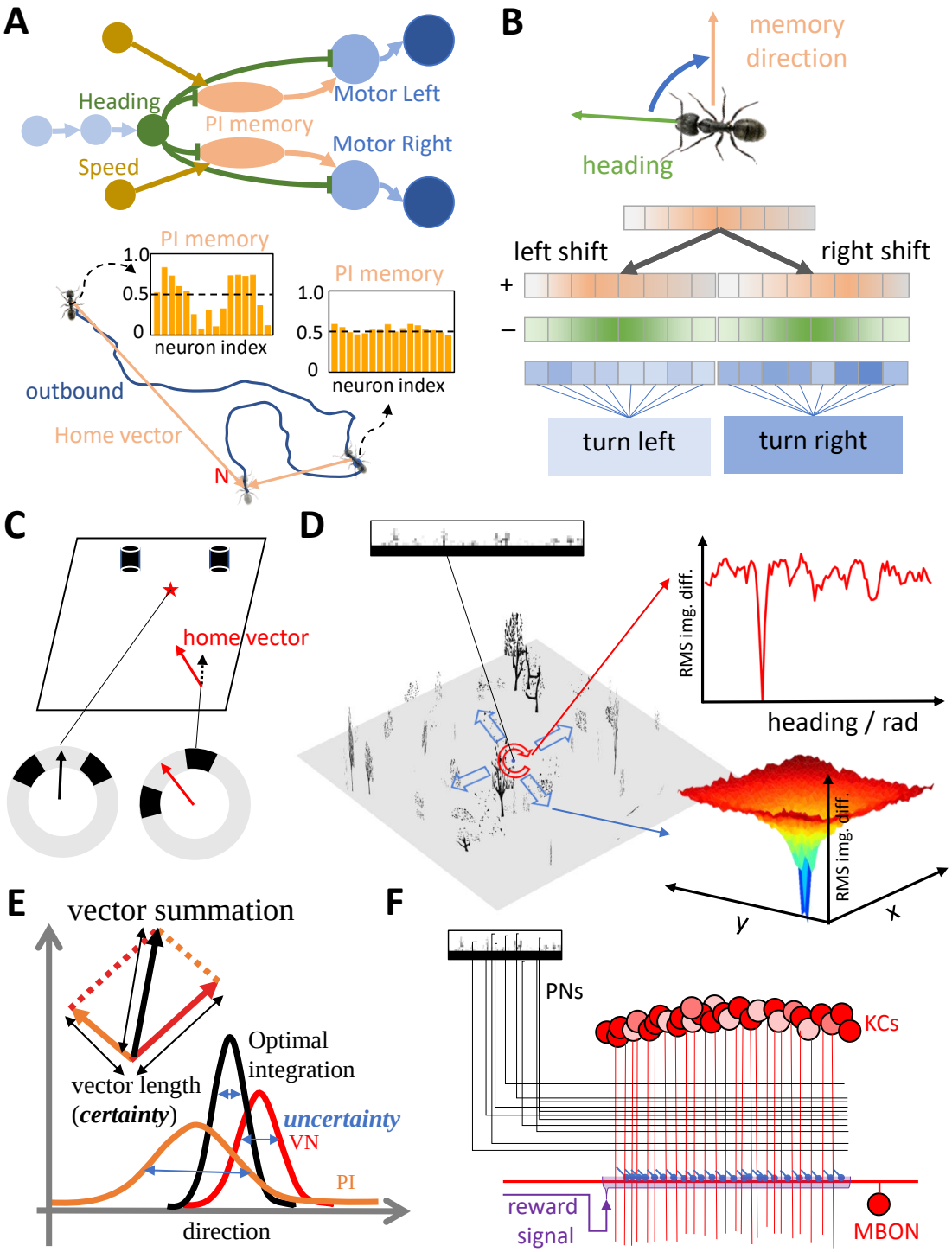

Figure 2.4: **The summary of recent model of PI, VH and their optimal integration.** **(A)** The PI model from [10]). Upper part is the schematic diagram of the PI model where the PI memory integrating the heading and the speed signal. Lower part is a example outbound and the PI memories are shown for two sampled locations. **(B)** The steering circuit comparing the memory direction and the current direction to generate a turning signal [10] [12] [13]. **(C)** The 'snapshot model' of VH that calculates the home vector by salient features in the view [14] [15]. **(D)** The RMS image difference of between images sampled (1) across locations with fixed heading, (2) at fixed location with different headings and the reference image. The simulated 3D world and a example view is also shown. **(E)**. The illustration of optimal cue integration method proposed by [7] [16]. **(F)** The MB model [17] for RF.

view and the 'snapshot' taken at the goal place (the so-called 'snapshot model', see Figure 2.4C). Follow on studies have shown that extracting features is not essential, as the pixel-wise difference between the panoramic reference image and the image sampled at other locations increase monotonically with the distance from the location where the reference image was taken [204] (see Figure 2.4D), then homing can be realised by gradient descent. Other algorithms also make use of different image processing ways to calculate a home vector to drove homing behaviour like global optic flow [205] (for review see [206]) and other approaches [207] [208] [209] [210] [211] [212] [213], for a comparative study of different visual homing models for reproducing crickets' visual homing data see [214]. Recently Stone et. al [215] strikingly demonstrated that frequency encoding of the panoramic view can also realise robust visual homing.

Unlike the VH, all the models will successfully guide the agent homing to the goal by using just one reference image, for modelling of RF wherein the agent can retrieve a habitual route (see Chapter 2.1.2.2) meaning to first store multiple views and when homing recall the appropriate view at the appropriate locations along the route. Early models took inspirations from the observation of the ants' characterised behaviour called learning walks during which the views are suggested to be learnt [216]. Müller and Wehner [217] found that when departing the nest desert ants will walk spirally around the nest and at some points stop and turn back whilst facing the nest entrance. Similar behaviour was also found previously in wood ants [218] that at some discrete locations, ants fixated the feeder marked by a salient landmark and when walking to the feeder significant changing of heading was observed as if the ant try to align the landmarks edges in the field of view to match that of the views stored at the fixating point. Based on these suggestions, models with the hypothesis that multiple views are stored in sequence and will be appropriately retrieved during route following are proposed [88] [101] [94]. However, it was proved difficult to use multiple views [219] and it may be not plausible for insects to store multiple images. Thus Baddeley et al. [220] built a neural network trained with the views experienced along a training route obviating the need for sequentially storing and retrieving multiple images. When homing, at each step, the simulated ants scan the visual world to choose the most familiar direction

assessed by the trained neural network to go forward. Results showed that this model can account for many properties of RF behaviour in insects. Based on this model, the following study [221] further proved that RF behaviour can be guided by a holistic memory by training the network with more biologically realistic views mimicking the real ants learning walks in [218] [94]. Using a unified visual familiarity along to guide the animal to the goal not only produces RF behaviour but in some scenario can operate for VH-like behaviour driving ants from novel locations to the goal [222] [223]. Baddeley et al.'s model [220] provided the first explanation of RF in insect navigation within a visually complex environment, while Ardin et al. [17] first bio-plausibly mapped this computation to an insect brain region-MB (for details of MB see Chapter 2.2.2) and shed light on how the visual familiarity can be encoded in a neural circuit to produce RF behaviour in ants and bees [224]. As depicted in Figure 2.4F, inspired by the *Drosophlia*'s olfactory learning, this MB model was trained with the images along the habitual route to tuning the connecting strength from the KCs to MBON triggered by the rewarding signal. Thus as introduced in Chapter 2.2.2, the output of the MB can assess the familiarity of the current view presented. The homing process is just the same as that of Baddeley et al.'s model [220] with continuously scanning and then going forward to the most familiar direction.

2.3.3 Modelling Olfactory Navigation

Unlike PI and VN that biologically constrained model has been proposed, for other mechanisms like the olfactory navigation, currently fewer neural models have been published including modelling the MB to do olfactory learning in *Drosophila* [225] and olfactory searching algorithms across species (for review see [226]). Also, some abstracted sensory-motor models explaining chemotaxis behaviour of *Drosophila* larvae [227] [228] [229] [230]. Based on the observed chained casting and surging reflex, some mathematical models can reproduce main characteristic patterns of plume-tracking of moth [231] [78], flying flies [232] and odour-gated unwind following in walking flies [233] [114]. Indeed, the mechanism underlining the chemotaxis behaviour is somehow similar to that of visual homing. In both scenarios, the agent

senses the strength of the attractive sensory signals (i.e., in chemotaxis, the odour concentration and in VH, the visual familiarity) and then by applying a gradient tracking method the agent can move to the goal location. This similarity allows for the possibility of explaining odour navigation behaviours by using the model of visual navigation, which will be verified in this thesis.

2.3.4 Modelling Systematic Search

Some studies suggested that systematic search is a spontaneous behaviour of PI [203] [10] [27], but mathematical models that can reproduce observed search patterns [116] [118] [234] [235] can also be useful to uncover the mechanical basis of such behaviour. Neural model concerning this behaviour is relatively lacking and further investigation is required to clarify if searching behaviour is a spontaneous result of PI and the motor-control circuit or it is controlled by a specific neural circuit.

2.3.5 Modelling Multi-guidance Coordination

Although in insect navigation, the interaction of the PI and VN have been observed in many behavioural studies (see Chapter 2.1.5), to date, there is no bio-plausible neural model that reveals how this may be implemented in the insect brain. Modelling of these behaviour starts from the classic problem: if insects possess a *cognitive map* [236] [237] [238]? To answer this question, the key point is to verify if the visual-based memory (VM) is linked with the vector (PI) to generated a centralise representation of the world. Although evidence has shown various forms of interaction between VN and PI, a decentralised mechanism [126] [239] [125] seems sufficient to theoretically explain most of the data from insects, especially for the aspects of optimal cue integration [16], arguing that there is no need for insects to have a cognitive map. As this study focus on the modelling of how guidance from PI and VN can be optimally integrated to steer insects in the neuron level, only models aiming for this will be introduced.

Collett [7] first proposed the hypothesis that integrating the direction preferences from PI and VN approximating the Bayesian optimum [240] and demonstrated how the

coordination behaviour can be realised without any centralised control. Based on this a mathematical model was established by [16] to optimally combine the downstream guidance routine outputs via simple vector summation (see Figure 2.4E) and reproduce main behavioural findings in cue-conflict experiments of real insects.

2.4 Summary- Current Gaps in Understanding Insect Navigation

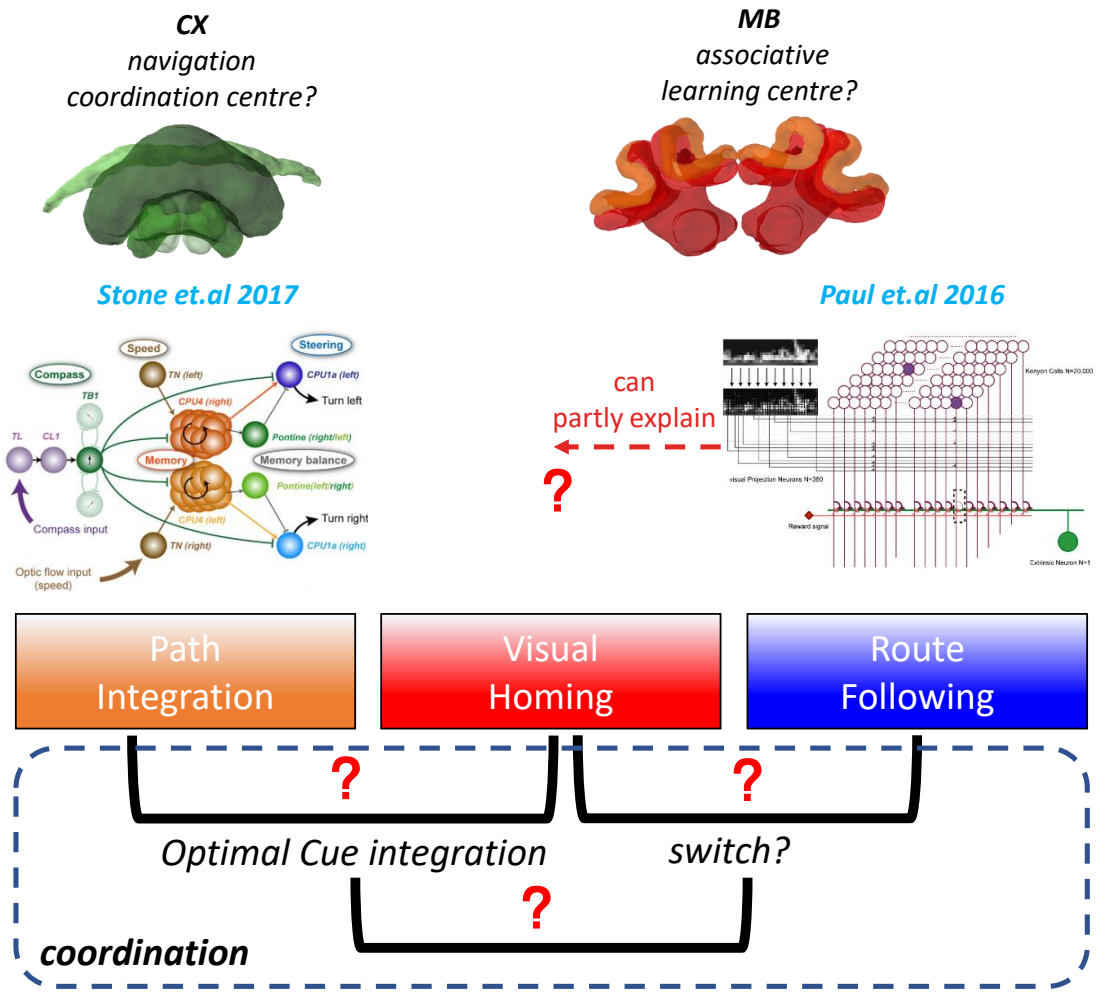

Figure 2.5: **The summary of the current gaps in understanding insect integration.** Red question marks indicate the current gaps.

Putting together the current knowledge of insect navigation from ethology, modelling and neurobiology with emphasis on PI, VN and their integration raises the problems that will be tackled in this thesis. As shown in Figure 2.5, we now have relatively well understanding of PI that is believed to operate in the FB of the CX by

integrating the heading direction from PB and the speed signal from NO [10]. However, although the current MB model [17] can account for the RF and partial aspects of the VH behaviour, a unified neural model for replicating all the observed visual navigation behaviour is still lacking. Another significant gap in understanding insect navigation behaviour is the multi-guidance coordination system. Behavioural studies have shown that insects flexibly and robustly solve navigation tasks by applying optimal cue integration [7] [8] [9] [50] and contextual strategy selecting [18]. However, aside from some mathematical and conceptual models suggesting optimal cue integration can be implemented by *vector summation* [16], and CX may use the output from the MBs to weight cues [241], currently there is no computation model at the neural level that reveals how this coordination can be realised in an insect brain. As described in Chapter 2.2, despite increasing neuroanatomical evidence suggesting that the CX receives sensory inputs and send motor outputs, and thus may coordinate navigation behaviour [146] [242] [13], a computational model explaining how this is achieved by the neural circuitry has yet to be developed. The MBs are believed to be the associative learning centre of insects, but the neural mechanism interpreting how MBs cooperate with the CX to generate contextual behavioural still needs investigation.

Understanding insect navigation is to map the specific behavioural to the corresponding neural circuit and understand the mechanical computation that a neural circuit can conduct. With sensory information, body movements and ecology involved, this is a multi-level problem [46] where a computation modelling can play a useful role to bridge the gap from the neural circuits to the behaviours.

Chapter 3

Modelling Visual Navigation-How Frequency Encoding Allows for Visual Homing and Route Following

Current VN models based on the MB architecture (see Chapter 2.3.2) can replicate RF behaviours whereby insects visually recognise the direction previously travelled at the same (or approximate) position [17] [224], and some studies [222] [221] also showed that this mechanism can also operate for VH-like behaviours (i.e., guide the agent to the goal from a novel location). However, there are still several problems challenge this model, for example, a mental re-alignment process lacking biological interpretation of is required, sometimes it is sensitive and not robust [223], and more importantly, the current MB model cannot account for the behavioural data in [243] [100] [50] [99] [18] where instead of going to the direction predicted by the above model, ants appeared to go directly back to their habitual route from novel locations following a displacement (e.g. after being blown off course by a gust of wind). Furthermore, Wystrach et.al [18] suggested that ants may apply different visual navigation strategies On and Off route. Thus a novel model that can allow for not only the VH and RF behaviours but also the strategy selecting mechanism is needed. This chapter presents a unified model based on the frequency encoding of the visual information to interpret the VH and RF behaviours in insects. The strategy selecting belongs to the multiple guidance coordination system so will be presented in Chapter 5.

3.1 Introduction

As described in Chapter 2.1.2.2, RF is one of the most crucial mechanisms in insect navigation behaviour whereby remembered homing direction can be recalled at appropriate locations when homing, also plays a role in insect navigation; Visual homing (see Chapter 2.1.2.1) is another important guidance according to the behavioural data, whereby foragers derive a homing signal by comparing the difference between current and stored views (for reviews see [89] [87]). Yet, a key gap in our understanding remains. Contemporary VM models based on the MBs can replicate realistic RF behaviours in complex visual environments (ant environments: [244] [17], bee environments: [224]) but do not generalise to visual homing scenarios whereby the animal must return directly to familiar terrain from novel locations (ants: [50], bees: [245], wasps: [246]). Storing multiple nest-facing views before foraging, inspired by observed learning walks in ants [217] [132] and flights in bees and wasps [247] [248], provides a potential solution [222] [221], but simulation studies have found this approach to be brittle due to high probabilities of aligning with the wrong memory causing catastrophic errors [223]. Moreover, ants released perpendicularly to their familiar route do not generally align with their familiar visual direction as predicted by the above algorithms [18], but instead move directly back towards the route [243] [100] [50] [99] [18], which would require a multi-stage mental alignment of views for current models. New computational hypothesis are thus required that can guide insects directly back to their route (often moving perpendicularly to the habitual path), but also allow for the route direction to be recovered (now aligned with the habitual path) upon arrival at familiar surroundings (see Figure 2.1E, F).

3.2 Results

3.2.1 Frequency Encoding Can Serve as the Information Basis for VH and RF

To verify if the frequency encoded vision contains the required information we need to model the visual navigation, the **amplitudes** and *phase* components of frequency coefficients (using Zernike moments, for details see Chapter 3.3.3) are tested across the simulated 3D world (shown in Figure 3.8). Note that the more standard (compared to Zernike moments) Fourier transform could be a choice with some specific preprocessing [215]: the amplitude coefficients of the Fourier transform on the x- and y- changing coordinates traced from the 2D shape of the skyline can be a rotational invariant signature to recognise views. But this method can not work for the view under foliage where the sky does not clearly form a single area, i.e., the outline of the skyline is not a single continuous curve. Another generalised Fourier transform on the sphere called spherical harmonics (SH) can also be used [249] but ZMs in our current settings (the visual environment and the only yaw-rotation involved motion) outperformed SH. Therefore, to be more robust and strong to justify the concept of frequency encoding based visual navigation, Zernike moments was selected.

Figure 3.1 demonstrates that the frequency encoded view contains the information: 1) like the RMS image difference (see Figure 2.4D) increasing monotonically with distance from the referencing locations, that can drive gradient-descent homing without continuous re-alignment. 2) angular cue in the panoramic view for later on compare to get the angular difference and thus drive a turn to replicate the route. This information provides the basis for our VH and RF model.

3.2.2 Mushroom Bodies as Drivers of Visual Homing

For ants to return directly to their familiar route after a sideways displacement (Figure 2.1E) without continuous mental or physical realignment they require access to rotational invariant visual cues. [215] recently demonstrated that binary images of panoramic skylines converted into their frequency components can provide

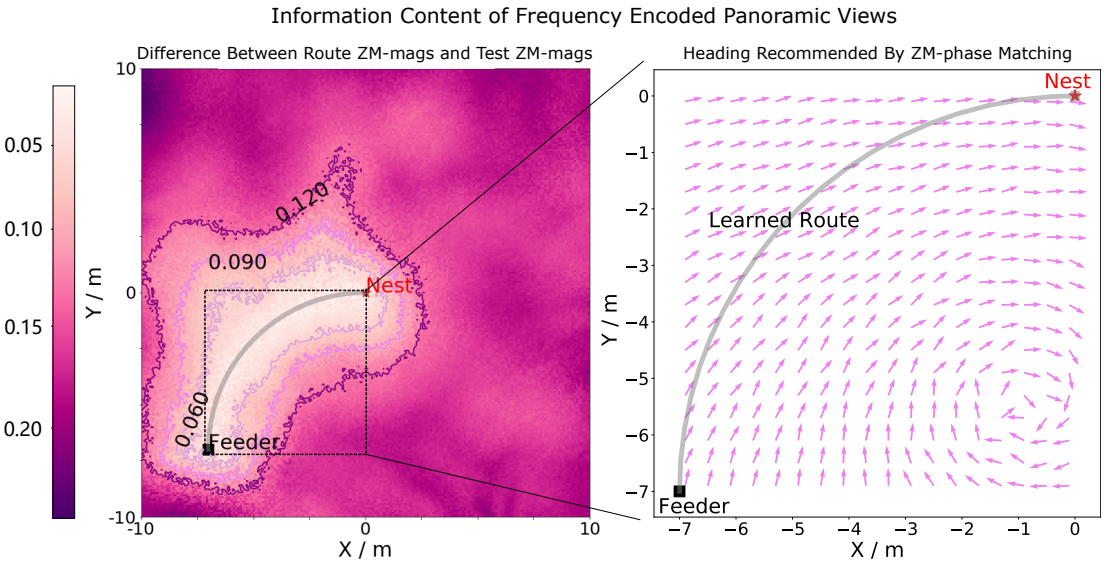

Figure 3.1: **The amplitudes and *phase* information of frequency encoded panoramic view.** Left: heat-map of the minimal difference of the frequency **amplitudes** between the panoramic images sampled at meshed locations across the world with random headings and the locations on the arc-shape habitual route. Right: quiver plot of the directions determined by the angular difference between the frequency encoded view *phase* sampled across the locations with random headings and that of the images sampled on the route.

such a rotationally-invariant encoding of scenes in a compact form (see Chapter 3.3.3 for an introduction to frequency transformations of images). Moreover, they demonstrated that the difference between the rotationally invariant features (the **amplitudes** of the frequency coefficients) between two locations increases monotonically with distance producing an error surface reminiscent of the image difference surfaces reported by [204] (and also see Figure 2.4D) which can guide an agent back to familiar terrain. Here we investigate whether the MB neuropils shown capable of assessing the visual valence of learned rotationally-varying panoramic skylines for RF [17] [224], might instead assess the visual valence of rotationally-invariant properties of views sampled along a familiar route supporting visual homing.

To this end, the intensity sensitive input neurons of [17]'s MB model are replaced with input neurons encoding rotational invariant **amplitudes** (Figure 3.2 left, blue panel). The network is trained along an $11m$ curved route in a simulated world that mimics the training regime of ants in [18] (see Chapter 3.3 and Chapter 3.3.5.1 for details on simulated world, image processing, model architecture and training and test regime).

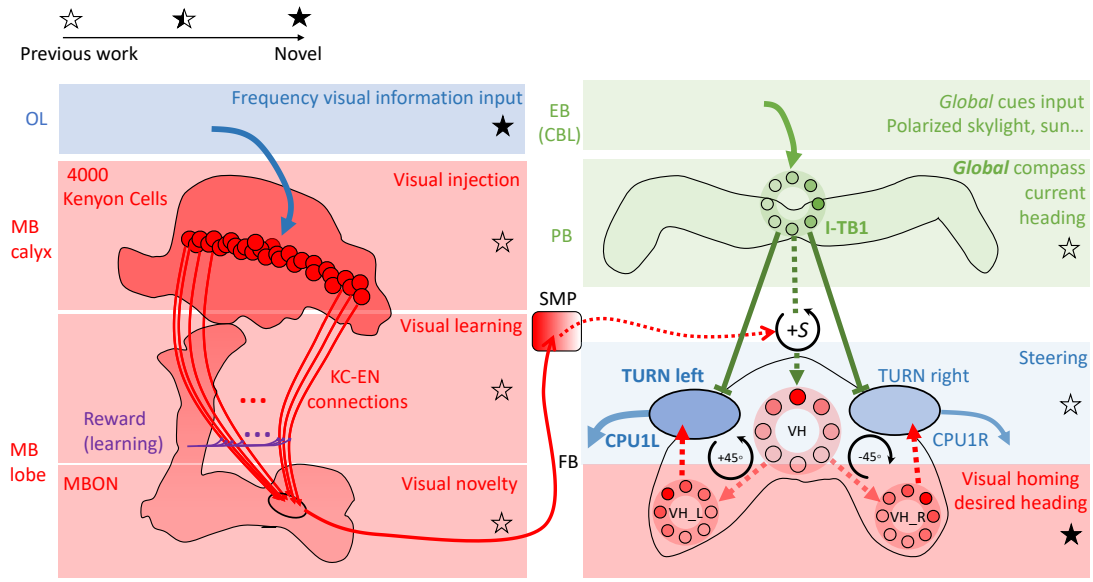

Figure 3.2: **The MB neural model for VH.** Rotational-invariant **amplitudes** are input to the MB calyx which are then projected to the Kenyon cells (KCs) before convergence onto the MB output neuron (MBON) which seeks to memorise the presented data via reinforcement learning based plasticity (for more details see Chapter 3.3.4.2) (MB circuit: left panels). SMP neurons measure positive increases in visual novelty (through input from the MBON) which causes a shift between the current heading (green cells) and desired headings (red cells) in the rings of the CX (SMP pathway between MB and CX: centre panel; CX circuit: right panels). The CX-based steering circuit then computes the relevant turning angle. Example activity profiles are shown for an increase in visual novelty, causing a shift in desired heading and a command to change direction. Each model component in all figures is labelled with a shaded star to indicate what aspects are new versus those incorporated from previous models (see legend in upper left).

After training, the firing rate of the MB output neuron (MBON) when placed at locations across the environment at random orientations reveals a gradient that increases monotonically with distance from the familiar route area, providing a homing signal sufficient for VH independent of the animal's orientation (Figure 3.3C).

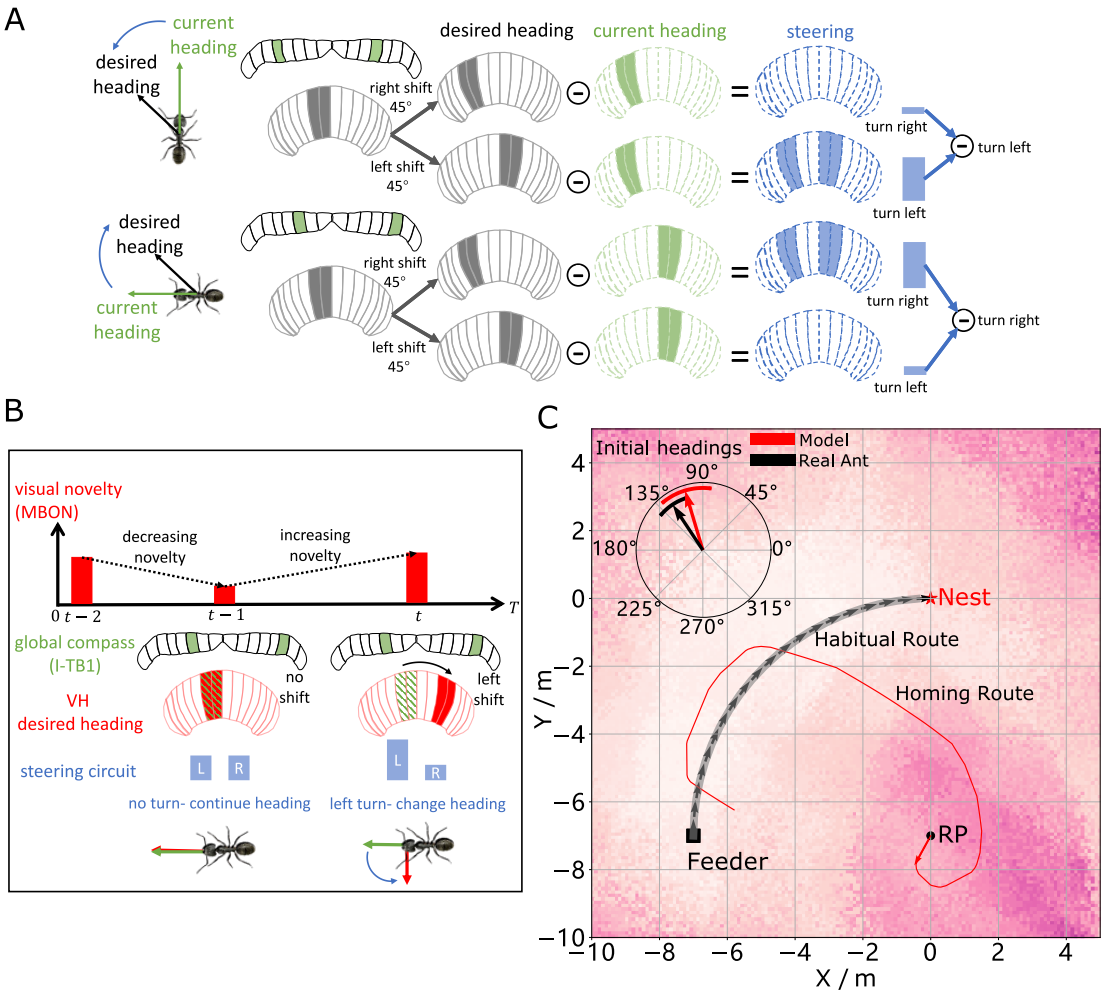

Figure 3.3: **The steering circuit underlying the motor output for VH.** (**A**) Schematic of the steering circuit function. First the summed differences between the impact of 45 °left and right turns on the desired heading and the current heading are computed. By comparing the difference between the resultant activity profiles allows an appropriate steering command to be generated. (**B**) Schematic of the visual homing model. When visual novelty drops ($t-2$ to $t-1$) the desired heading is an unshifted copy of the current heading so the current path is maintained but when the visual novelty increases ($t-1$ to t) the desired heading is shifted from the current heading. (**C**) The firing rate of the MBON sampled across locations at random orientations is depicted by the heat-map showing a clear gradient leading back to the route. The grey curve shows the habitual route along which ants were trained. RP (release point) indicates the position where real ants in [18] were released after capture at the nest (thus zero-vector) and from which simulations were started. The ability of the VH model to generate realistic homing data is shown by the initial paths of simulated ants which closely match those of real ants (see inserted polar plot showing the mean direction and 95% confidential interval), and also the extended exampled path shown (red line). Note that once the agent arrives in the vicinity of the route, it appears to meander due the flattening of visual novelty gradient and the lack of directional information.

Motor output is then generated by connecting the MBON to a steering network recently located in the fan-shaped body (FB/CBU) of the CX that functions by minimising the difference between the animal's current and desired headings [10] (see also

Chapter 2.3.1). [10]'s key insight was that the anatomically observed shifts of activity in the columnar neurons that encode the desired heading in essence simulate 45° turns left and right, and thus by comparing the summed differences between the activity profiles of these predicted headings to the current heading then the appropriate turning command can be computed (see Figure 3.3A). We adopt this circuit as the basis for computing steering commands for all strategies as suggested by [13].

In the proposed VH model the current heading input to the steering circuit uses the same celestial global compass used in [10]'s PI model. Insects track their orientation through head-direction cells [151] whose concurrent firing pattern forms a single bump of activity that shifts around the ring as the animal turns (measured through local visual [152] [154], global visual [150] and proprioceptive [151] cues). Neuroanatomical data [153] [250] [157] supports theoretical predictions [251] [252] that the head-direction system of insects follows a ring attractor (RA) connectivity pattern characterised by local excitatory interconnections between direction selective neurons and global inhibition. In this work, the global compass RA network is not modelled directly but rather we simulate its sinusoidal activity profile in a ring of I-TB1 (locusts and $\Delta 7$ of flies) neurons found in the PB (Figure 3.2 green ring).

A desired heading is then generated by copying the current activity pattern of the global compass neurons to a new neural ring which we speculate could reside in either a distinct subset of I-TB1 neurons [253] or in the FB. Crucially, the copied activity profile also undergoes a leftward shift proportional to any increase in visual novelty (a similar shifting mechanisms has been proposed for the head-direction system [152] [154]) which we propose is measured by neurons in the superior medial protocerebrum (SMP, where the MBONs converged to and has known connections with the CX.) [193] [254] (see Figure 3.2 centre and activity of red rings). The result is a mechanism that recommends changing direction when the agent moves away from familiar terrain (visual novelty increases) but recommends little change to the current heading when the visual novelty is decreasing (see Figure 3.3B for a schematic of the VH mechanism). We note that there is a distinction between a ring network which describes a group of neurons whose pattern of activity forms a circular representation regardless of actual

physical arrangement and RA networks which follow a specific connectivity pattern (all modelled RAs labelled in figures). Taken together the model iteratively refines it's orientation to descend the visual novelty gradient and thus recover familiar terrain (see Figure 3.2 for full model).

Figure 3.3C demonstrates that the proposed network accurately replicates both the directed initial paths as in [18] (see the inserted black arrow, a t-test between the simulation and real data was conducted and no significant difference was found (P=0.764 ¿ 0.05)), and extended homing paths as in [50] observed in ants displaced to novel locations perpendicular to their familiar routes. We note that upon encountering the route the model is unable to distinguish the direction in which to travel and thus meanders back and forth along the familiarity valley, unlike real ants, demonstrating the need for additional route recognition and recovery capabilities.

In addition, the performance of MB's encoding ability then is evaluated by changing the value of highest order of frequency coefficients (thus the number of the coefficients also changed as we use the components from the lowest order to the defined highest one). Results in Figure 3.4 demonstrate that as long as the enough frequency components are used to train MB network, the number of KCs does not have significant effects on the encoding performance, implying that information of the panoramic view should be encoded by at least 81 frequency component without losing the main feature and 1000 KCs is enough for encoding the route memory (here marked by 20 images). Note that the requirement of the number of KCs depends largely on the number of images needed to be remembered by the network (memory capacity).

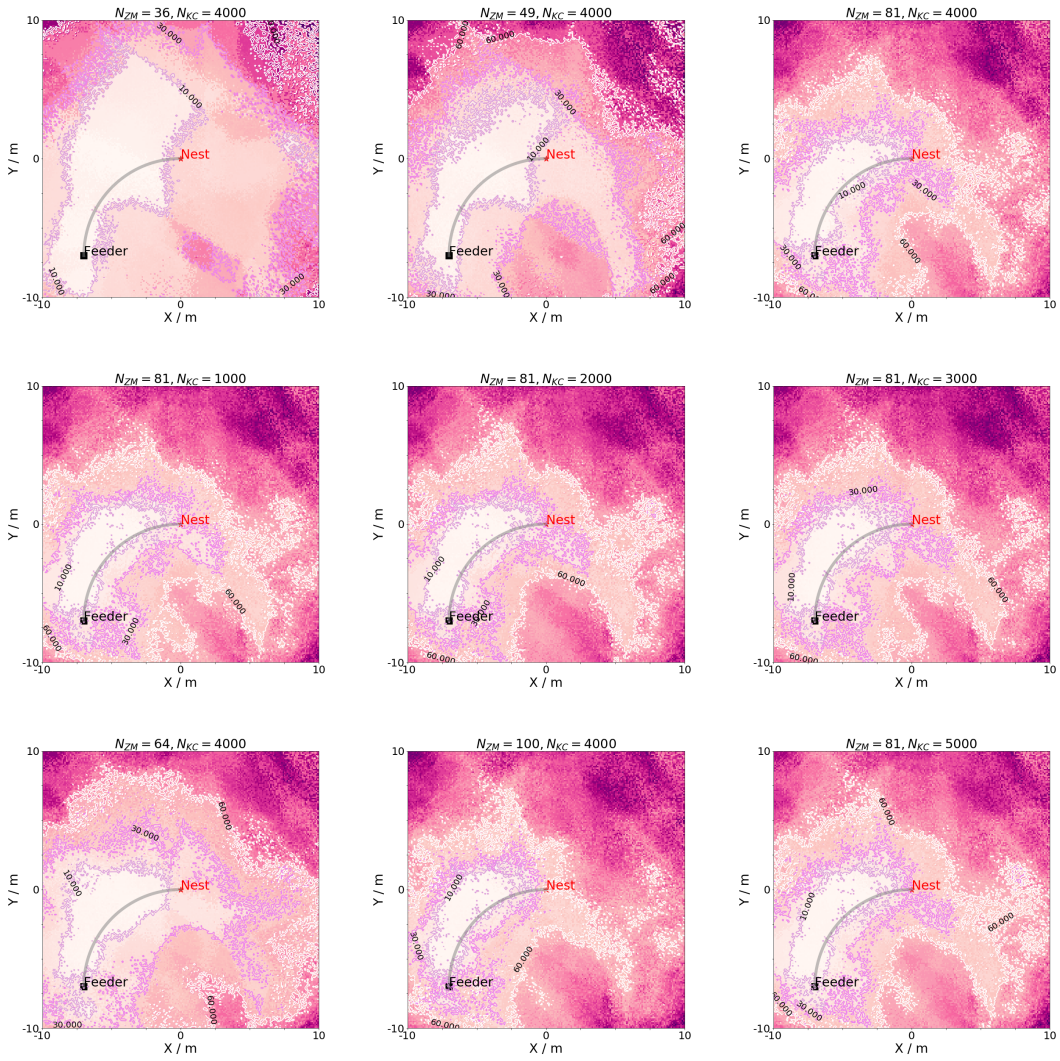

Figure 3.4: **Evaluating MB model for encoding the visual familiarity.** The heatmaps of the visual familiarity measured by the MBON neurons. The first row shows the results of the MB network with 4000 KCs but with various number of frequency components 36, 49 and 81. The second row depicts the results for 81 frequency components with 1000, 2000 and 3000 KCs. Last row lists other results with the parameter from left to right: (64, 4000), (100, 4000), (81, 5000). 1000 KCs is the fewest to guarantee good model performance.

3.2.3 Route Following in the Insect Brain

The model described above can guide insects back to their familiar route area, but lacks the means to recover the route direction upon arrival as observed in homing insects. This is not surprisingly as VH relies upon translationally-varying but rotational-invariant information whereas RF requires rotationally-varying cues. Thus we introduce a new elemental guidance system that makes use of the rotationally-varying *phase* coefficients of the frequency information derived from the panoramic skyline which

tracks the orientation of specific features of the visual surroundings (see Chapter 3.3). Here we ask whether by associating the rotationally invariant **amplitudes** (shown useful for place recognition) with the rotationally-varying *phases* experienced at those locations, insects might recover the familiar route direction.

Neuroanatomical data with which to constrain a model remains sparse and therefore a standard artificial neural network (ANN) architecture is used to investigate the utility of *phase*-based route recovery with biological plausibility discussed in more detail below. A 3-layer ANN was trained to associate the same 81 rotational-invariant **amplitudes** as used in the VH model with the rotational varying *phase* value of single frequency coefficient experienced when travelling along the habitual route which we encode in an 8 neuron-ring (see Fig. 3.5A and Chapter 3.3.4.3 for detailed model description). Thus, when the route is revisited the network should output the orientation that the *phase* converged upon when at the same location previously, which we note is not necessarily aligned with the actual heading of the animal (e.g. it may track the orientation to vertical bar [151]). Realignment is possible using the same steering mechanism as described above but which seeks to reduce the offset between the current *phase* readout (e.g. a local compass locked onto visual features of the animals surroundings), and the recalled *phase* readout from the ANN.

We speculate that the most likely neural pathways for the new desired and current headings are from Optic Lobe via Anterior Optic Tubercle (AOTU) and Bulb (BU) to EB (CBL) of the CX [255] [256] (see Figure 3.5) with the desired heading terminating in the EB whereas the current heading continues to the PB forming a local compass that sits beside the global compass used by PI and VH systems. This hypothesis is further supported by the recently identified parallel pathways from OL via AOTU to the CX in *Drosophila* [257]. That's to say that, firstly, there are two parallel pathways forming two compass systems- the global (here based on celestial cues) and the local (based on terrestrial cues) compasses modelled by the activation of I-TB1 and II-TB1 neurons respectively. Four classes of CL1 neurons (or E-PG and P-EG neurons) [258] [33] and three classes of independent TB1 neurons [253] have been identified that provide potential sites for the parallel recurrent loops encoding independent local and global com-

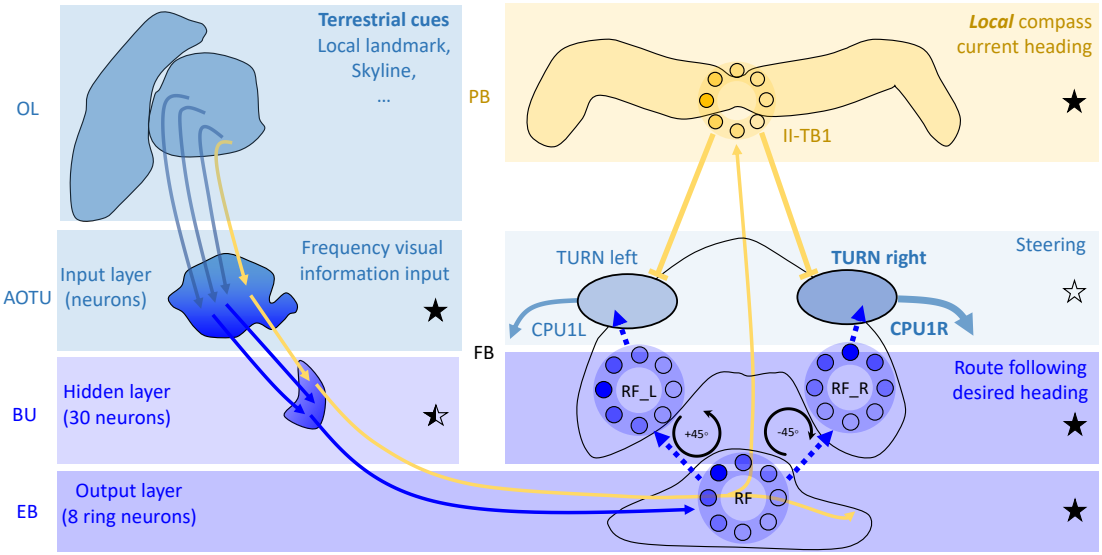

Figure 3.5: **Phase-based neural model of RF.** The visual pathway from the optic lobe via AOTU and Bulb to EB of the CX is modelled by a fully connected artificial neural network (ANN) with one hidden layer. The input layer receives the **amplitudes** of the frequency encoded views (as for the MB network) and the output layer is an 8-neuron ring whose population encoding represents the desired heading against to which the agent should align.

passes. Secondly, the desired heading, which is the recalled *phase* of a specific view, is generated through the neural plasticity from AOTU to BU and BU to EB, which is line with recent evidence of associative learning between the R-neurons transmitting visual information from BU to EB and the compass neurons (CL1a or E-PG neurons) that receive input from EB [155] [156]. This kind of learning endows the animal with the ability to flexibly adapt their local compass and also desired navigational orientation according to the changing visual surroundings. [137] reported a direct pathway from EB to FB neurons which we model to allow comparison of the local compass activity (II-TB1) with the desired heading. However, we note that this connectivity has not been replicated in recent studies [45] and thus further investigation of potential pathways is required.

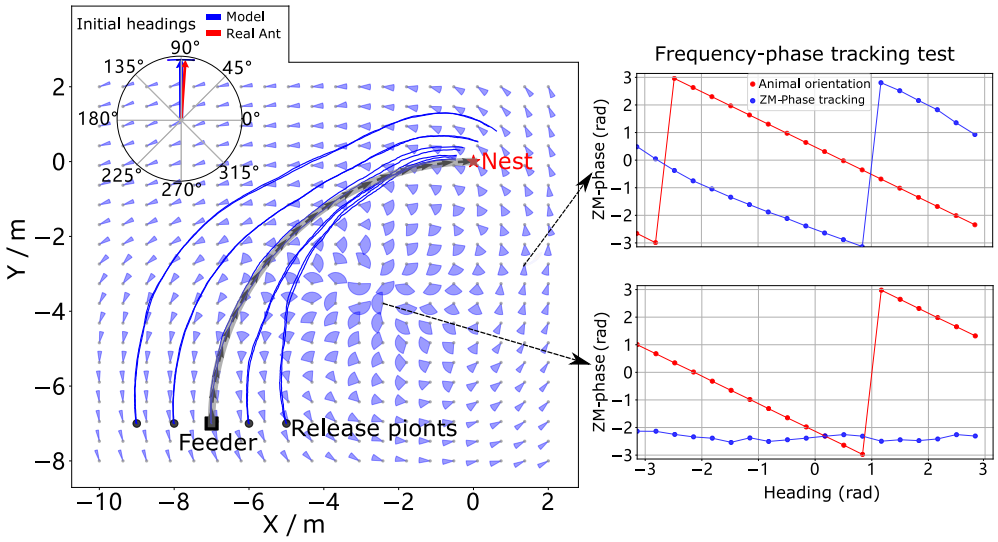

Figure 3.6: **Performances of RF model.** Blue and red arrows in the inserted polar plot (top left) display the mean directions and 95% confidential intervals of the initial headings of real [18] and simulated ants released at the start of the route $(-7, -7)$ respectively. Dark blue curves show the routes followed by the model when released at 5 locations close to the start of the learned path. The overlaid fan-plots indicate the circular statistics (the mean direction and 95% confidential interval) of the homing directions recommended by the model when sampled across heading directions (20 samples at 18°intervals). Data for entire rotations are shown on the right for specific locations with the upper plot, sampled at $(1.5, -3)$, demonstrating accurate phase-based tracking of orientation, whereas the lower plot sampled at $(-2.5, -3.5)$ shows poor tracking performance and hence produces a wide fan-plot.

The RF model accurately recovers the initial route heading in a similar manner to real ants returned to the start of their familiar route [18] (Figure 3.6, insert), and then follows the remaining route in its entirety back to the nest again reflecting ant data [100] [99] (Figure 3.6). The quiver plots displayed in the background of Figure 3.6 show the preferred homing direction output by the ANN when rotated on the spot across locations in the environment. Note that the confidence intervals are constructed by sampling different headings (20 samples at 18deg intervals). With different headings, we may get different recommended homing headings from RF network, thus 20 recommended headings are computed to generate the mean direction and standard deviations. This was done to show the robustness of the RF network against different headings. The noise in the results are due to errors in the tracking performance (see examples Figure 3.6 right) yet as these errors are in largely confined to the magnitude, the steering circuit still drives the ant along the route. We note that this effect is primarily a function of the specific frequency transformation algorithm used which we borrow

from computer graphics to investigate the utility of frequency encoding of visual information. The biological realism of such transforms and their potential implementation in the insect vision system are addressed in Chapter 3.4. The displaced routes also highlight the danger of employing solely RF which often shadows rather than converges with the route when displaced sideways, further demonstrating the necessity for integration with the Off-Route strategies that promote route convergence.

Further, the ability of ANN to encode the *phase* information is assessed by changing the value of highest order of frequency coefficients and the number of neurons in the hidden layer. Results are shown in Figure 3.7, suggesting that the ANN's performance of encoding the direction is not sensitive to the number of neurons in the hidden layer and the order of the frequency coefficients within the certain range, implying that the directional cue within the panoramic view is determined by the features with lower frequency and 1o neurons in hidden layer is enough for restoring the directions derived from the images sampled at the locations on the habitual route.

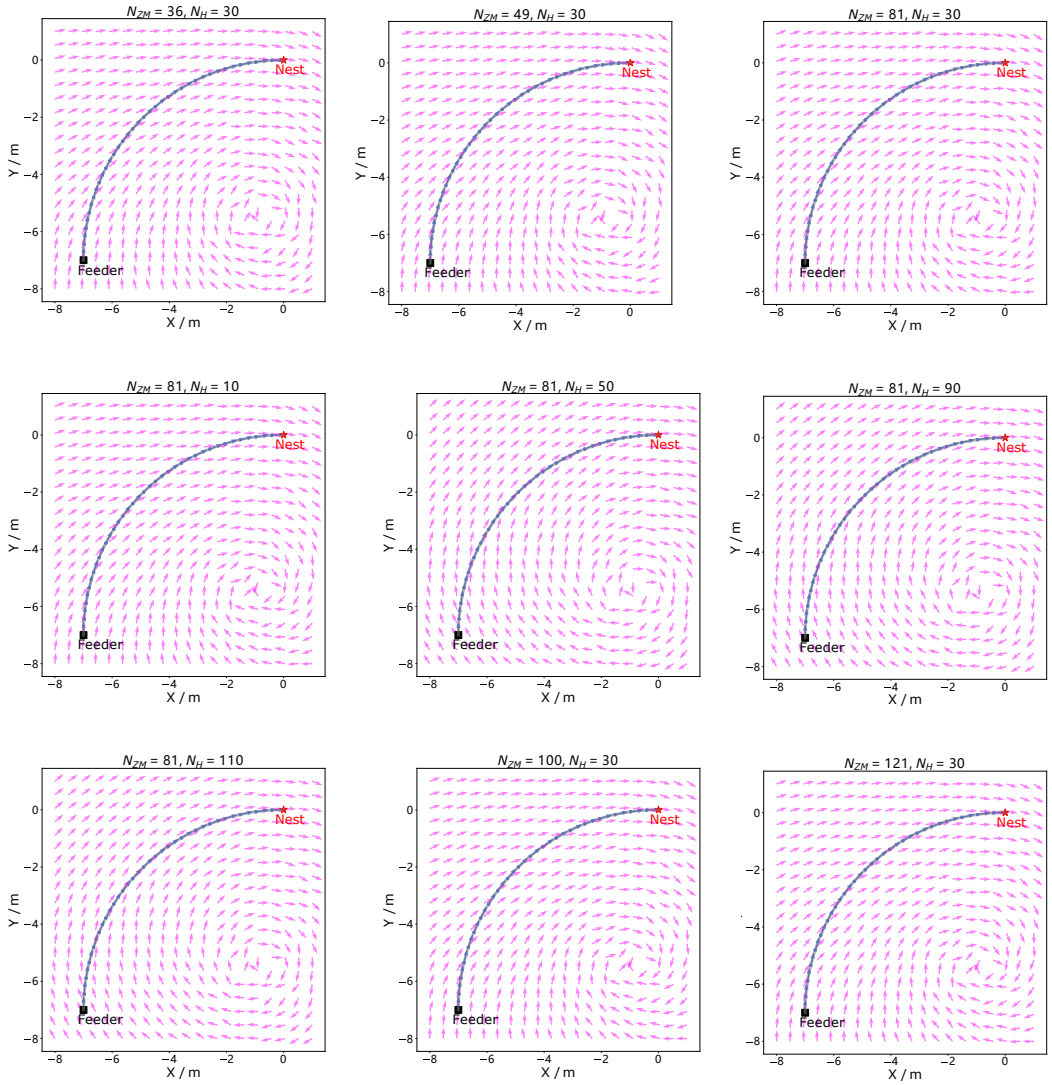

Figure 3.7: **Evaluating ANN (RF) model for encoding the route directions.** The quiver plots of the on-route homing direction recommended by the ANN. The first row shows the results for the ANN with 30 neurons in the hidden layer but with various number of frequency components 36, 49 and 81. The second row depicts the results for 81 frequency components with 10, 50 and 90 neurons in the hidden layer. Last low lists other results with the parameter from left to right: (81, 110), (100, 30), (121, 30).

3.3 Methods

All simulations and network models are implemented by Python 3.5 and make use of external libraries-*numpy*, *matplotlib*, *scipy*, *PIL* and *cv2*.

3.3.1 Simulated 3D World

The environment used in this study is that provided by [215] which is itself adapted from [220] (see Figure 3.8C). It is a virtual ant-like world consisting of randomly generated bushes, trees and tussocks based on triangular patches (for more details see [220]). Note that this is a visually sparse environment where the visual objects are placed rather far from the agents.

The data of this simulated world is stored in a matrix with the size of $N_P \times 3 \times 3$, defining the three dimensional coordinates (x,y,z) of the three vertices of N_P (number of patches) triangle patches. Agent movement was constrained to a $20m \times 20m$ training and test area allowing free movement without the requirement of an additional obstacle avoidance mechanism.

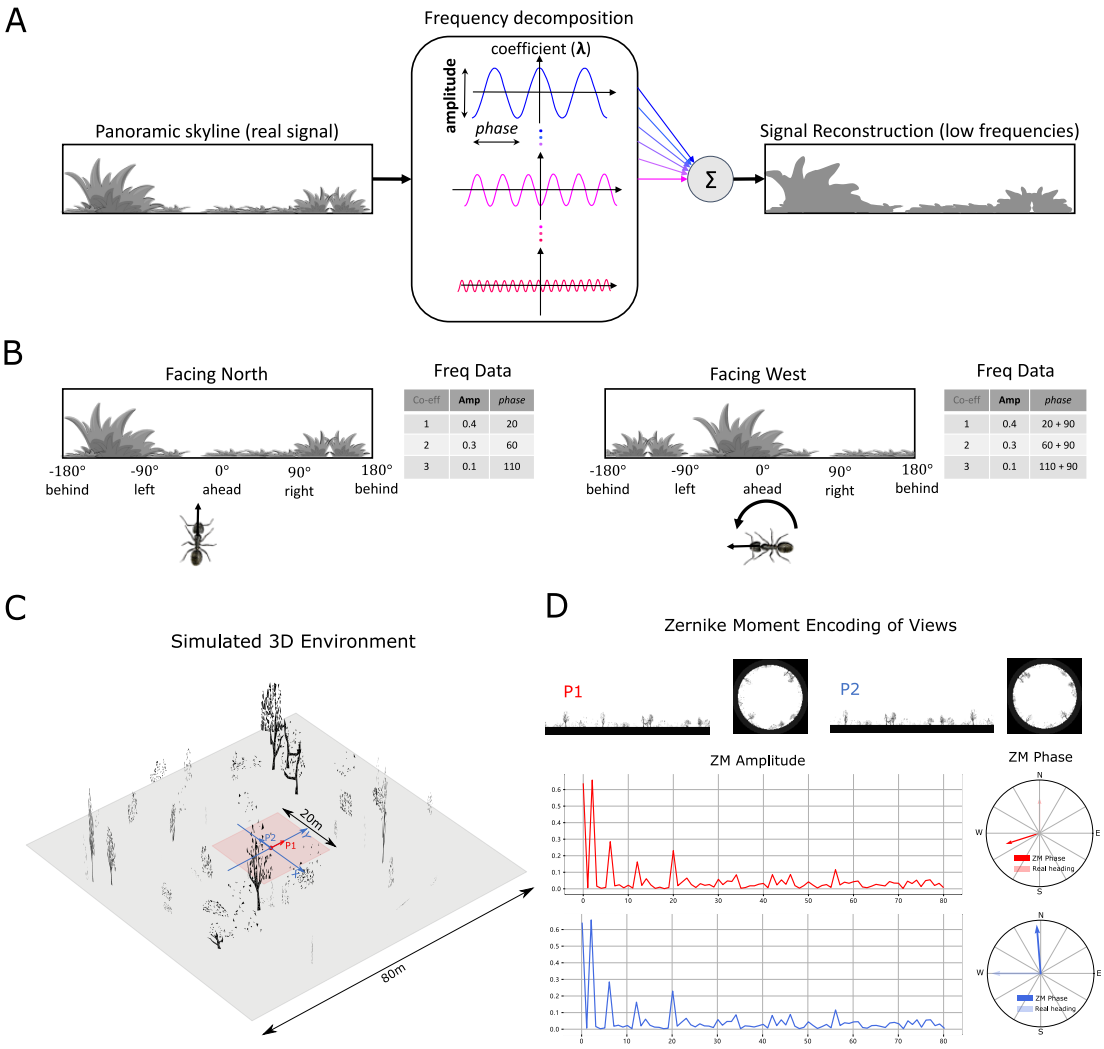

Figure 3.8: **information provided by frequency encoding in cartoon and simulated ant environments.** **(A)**: A cartoon depiction of a panoramic skyline, it's decomposition into trigonometric functions, and reconstruction through the summation of low frequency coefficients reflecting standard image compression techniques. **(B)**: Following a 90° rotation there is no change in the **amplitudes** of the frequency coefficients but the *phases* of the frequency coefficients track the change in orientation providing a rotational invariant signal useful for visual homing and rotationally-varying signal useful for route following respectively. **(C)**: The simulated 3D world used for all experiments. The pink area (size: $20m \times 20m$) is used for model training and testing zone for models allowing obstacle-free movement. **(D)**: The frequency encoding (Zernike Moment's **amplitudes** and *phase*) of the views sampled from the same location but with different headings (P1 and P2 in **(C)**, with $90°$ heading difference) in the simulated world. The first 81 **amplitudes** are identical while the *phases* have the difference of about $90°$.

3.3.2 Image Reconstruction

The agent's visual input at location (x, y) with the heading direction θ_h is simulated from a point 1cm above from the ground plane with field of view $360°$ wide by $90°$ high (centred on the horizon). This panoramic image (300×104) is then wrapped

onto a sky-centred disk as required by the Zernike Moments transformation algorithm used with the size of $208(104 \times 2) \times 208$ ready for image processing (see Figure 3.8D upper).

3.3.3 Image Processing

3.3.3.1 Frequency Encoding Conceptual Overview

Image compression algorithms such as JPEG encoding [259] have long utilised the fact that a complex signal can be decomposed into a series of trigonometric functions that oscillate at different frequencies. The original signal can then be reconstructed by summing all (for prefect reconstruction) or some (for approximate reconstruction) of the base trigonometric functions. Thus, compression algorithms seek a balance between using the fewest trigonometric functions to encode the scene (for example, by omitting high frequencies that humans struggle to perceive), and the accuracy of the reconstructed signal (often given as an option when converting to JPEG format). Figure 3.8A provides a cartoon of the frequency decomposition process for a panoramic view.

When such transforms are applied to fully panoramic images, or skylines, benefits beyond compression arise. Specifically, discrete transformation algorithms used to extract the frequency information generate a series of information triplets to describe the original function: frequency coefficients describe the frequency of the trigonometric function with associated **amplitudes** and *phase* values defining the vertical height versus the mean and the lateral position of the waveform respectively (Figure 3.8A). For panoramic views, regardless of the rotational angle of the image capturing device (eye or camera) the entire signal will always be visible and hence the **amplitudes** of the frequency coefficients do not alter with rotation (Figure 3.8B). This information has been used for successful place recognition in a series of robot studies [260] [261] [249]. Most recently [215] demonstrated that the difference between the **amplitudes** of the frequency coefficients recorded at two locations increases monotonically with distance producing an error surface suitable for visual homing. This feature of the frequency encoding underlies the visual homing results described in Chapter 3.2.2.

In addition, as the *phase* of each coefficient describes how to align the signal this will naturally track any rotation in the panoramic view (Figure 3.8B) providing a means to realign with previous headings. The *phase* components of panoramic images have been utilised previously to derive the home direction in a visual homing task [262]. This feature of the frequency encoding underlies the route following results described in Chapter 3.2.3.

The image processing field has created an array of algorithms for deriving the frequency content of continuous signals [263] [264]. To allow exploration of the usefulness of frequency information, and how it could be used by the known neural structures, we adopt the same Zernike Moment algorithm used by [215], but the reader should be clear that there are many alternate and more biologically plausible processes by which insects could derive similar information. It is beyond the scope of this proof of concept study to define precisely how this process might happen in insects but future research possibilities are outlined in the Chapter 3.4.

3.3.3.2 Zernike Moments Encoding

Zernike Moments (ZM) are defined as the projection of a function onto orthogonal basis polynomials called Zernike polynomials [265] [266]. This set of functions are defined on the unit circle with polar coordinates (ρ, θ) shown as:

$$V_{nm}(\rho, \theta) = R_{nm}(\rho)e^{jm\theta} \tag{3.1}$$

Where $n \in N^+$ is the order and m is the repetition meeting the condition: $m \in N$, $|m| \leq n$ and $n - |m|$ is even to ensure the rotational invariant property is met. $R_{nm}(\rho)$ is the radial polynomial defined as:

$$R_{nm}(\rho) = \sum_{s=0}^{n-|m|/2} (-1)^s \frac{(n-s)!}{s!(\frac{n+|m|}{2} - s)!(\frac{n-|m|}{2} - s)!} \rho^{n-2s} \tag{3.2}$$

For a continuous image function $f(x, y)$, the ZM coefficient can be calculated by:

$$Z_{nm}(\rho) = \frac{n+1}{\pi} \int \int_{x^2+y^2 \leq 1} f(x, y) V^*_{nm}(\rho, \theta) dx dy \tag{3.3}$$

For a digital image, summations can replace the integrals to give the ZM:

$$Z_{nm}(\rho) = \frac{n+1}{\pi} \sum_{x} \sum_{y} f(x,y) V^*_{nm}(\rho,\theta), \qquad x^2 + y^2 \leq 1. \tag{3.4}$$

ZM are extracted from the simulated insect views in wrapped format (Fig. Figure 3.8D) whose centre is taken to be the origin of the polar coordinates such that all valid pixels lie within the unit circle. For a given image I (P1 in Figure 3.8D) and the rotated version of this image I^{θ_r} (P2 in Figure 3.8D), the **amplitude** $A = |Z|$ and *phase* $\Phi = \angle Z$ of ZM coefficients of these two images will satisfy:

$$\begin{cases} |Z^{\theta_r}_{nm}| = |Z_{nm} e^{-jm\theta_r}| = |Z_{nm}| \quad i.e., \quad A^{\theta_r}_{nm} = A_{nm} \\ \Phi^{\theta_r}_{nm} = \Phi_{nm} - m\theta_r \end{cases} \tag{3.5}$$

From which we can see that the **amplitude** of the ZM coefficient remains the same while the *phase* of ZM carries the information regarding the rotation (see Figure 3.8A and D). This property is the cornerstone of the visual navigation model where the **amplitudes** encode the features of the view while the *phase* defines the orientation.

Amplitudes for ZM orders ranging from $n = 0$ to $n = 16$ were selected as they appeared to cover the majority of information within the image. From Equation 3.1 we know that $V_{n,m} = V_{n,-m}$, so we limited $m \in N^+$ to reduce the computational cost, which sets the total number of ZM coefficients (N_{ZM}) to $(16 \div 2 + 1)^2 = 81$ which was input to the visual navigation networks. For training the ANN network for RF, in Equation 3.5, if we set $m = 1$, such that $\Phi^{\theta_r}_{n,1} = \Phi_{n,1} - \theta_r$ which means that all ZM coefficients will provide the same information when the image is rotated. Further, the difference between the *phase* of ZM coefficients of the current view with those of the memorised view, will inherently provide the angle with which to turn to realign oneself, i.e. :

$$\Phi^{current}_{7,1} - \Phi^{memory}_{7,1} = \theta_h - \theta_m \tag{3.6}$$

Where the order n of this ZM is selected to be $n = 7$ manually by comparing the performance with different orders in this specific virtual environment, θ_h is the current heading of the agent while θ_m is the memorised heading direction (desired heading

direction).

3.3.4 Neural Networks

We use the simple firing rate to model the neurons in the proposed networks, where the output firing rate C is a sigmoid function of the input I if there is no special note. In the following descriptions and formulas, a subscript is used to represent the layers or name of the neuron while the superscript is used to represent the value at a specific time or with a specific index.

3.3.4.1 Current Headings

In the proposed model, there are two independent compass systems based on the global and the local cues respectively so named global and local compass correspondingly. These two compass systems have similar neural pathways from OL via AOTU and BU to the CX but ended distinct groupings of TB1 neurons: I-TB1 and II-TB1 in the PB.

Global Compass The global compass neural network applied in this study is the same as that of [10], which has three layers of neurons: TL neurons, CL1 neurons and I-TB1 neurons. The 16 TL neurons respond to simulated polarised light input and are directly modelled as:

$$I_{TL} = \cos(\theta_{TL} - \theta_h) \tag{3.7}$$

Where $\theta_{TL} \in \{0, \pi/4, \pi/2, 3\pi/4, \pi, 5\pi/4, 3\pi/2, 7\pi/4\}$ is the angular preference mapped over twice to the 16 TL-neurons. The 16 CL1-neurons are inhibited by TL-neuron activity which invert the polarisation response:

$$I_{CL1} = 1.0 - C_{TL} \tag{3.8}$$

The 8 I-TB1 neurons act as a ring attractor creating a sinusoidal encoding of the current heading. Each I-TB1 neuron receives excitation from the CL1 neuron sharing the same directional preference and inhibition from other I-TB1 neurons via mutual

connections:

$$W^{ij}_{I-TB1} = \frac{\cos(\theta^i_{I-TB1} - \theta^j_{I-TB1}) - 1}{2} \tag{3.9}$$

$$I^{t,j}_{I-TB1} = (1-c)C^{t,j}_{CL1} + c\sum_{i=1}^{8} W^{ij}_{I-TB1} C^{t-1,j}_{I-TB1} \tag{3.10}$$

Where c is a balance factor to modify the strength of the inhibition and the CL1 excitation. Finally, the population coding $C^{t,j}_{I-TB1}, j = 0, 1, ...7$ represents the heading of global compass of the agent at time t.

Local Compass The local compass is derived from the terrestrial cues through a similar visual pathway as the global compass and also ends in a ring attractor network. As for the global compass, the local compass heading is directly modelled by the population encoding of II-TB1 neurons:

$$C^i_{II-TB1} = \cos(\Phi_{7,1} - \theta^i_{II-TB1}) \qquad i = 0, 1, ...7 \tag{3.11}$$

Where θ_{II-TB1} is the angular preference of the II-TB1 neurons and $\Phi_{7,1}$ is the *phase* of ZM. Therefore, the firing rate of C_{II-TB1} encodes the heading of the local compass.

3.3.4.2 Visual Homing

The neural network of visual homing is an associative network constrained by the anatomical structure of the mushroom body (MB) of the insects. In contrast to [17] where a spiking neural network is implemented to model the MB, we apply a simple version of MB where the average firing rates of neurons are used.

The visual projection neurons (vPNs) directly receive the **amplitudes** of the ZM coefficients as their firing rates:

$$C^i_{vPN} = A^i, \qquad i = 0, 1, 2...N_{vPN} \tag{3.12}$$

Where N_{vPN} is the number of the vPN neurons which is the same as the total number of ZM **amplitudes** applied and in this study $N_{vPN} = N_{ZM} = 81$. The A^i denotes the i^{th} **amplitudes** of ZM coefficients.

The vPNs project into Kenyon cells (KC) through randomly generated binary connections W_{vPN2KC}, which result in the scenario wherein one KC receives 10 randomly selected vPNs' activation:

$$I_{KC}^{j} = \sum_{i=0}^{N_{vPN}} W_{vPN2KC}^{ji} C_{vPN}^{i} \tag{3.13}$$

Where I_{KC}^{j} denotes the total input current of j^{th} KC from the vPN and the KCs are modelled as binary neurons with the same threshold Thr_{kc}:

$$C_{KC} = \begin{cases} 0 & if \quad I_{KC} \leq Thr_{KC} \\ 1 & if \quad I_{KC} > Thr_{KC} \end{cases} \tag{3.14}$$

The MBON neuron sums all the activation of Kenyon cells via plastic connections W_{KC2EN}:

$$C_{MBON} = \sum_{i=0}^{N_{KC}} W_{KC2MBON}^{i} C_{KC}^{i} \tag{3.15}$$

An anti-Hebbian learning rule is applied for the plasticity of $W_{KC2MBON}$ in a simple way:

$$W_{KC2MBON}^{t} = W_{KC2MBON}^{t-1} - \eta_{KC2MBON} \quad if \quad C_{KC}^{i} \geq W_{KC2MBON}^{i} \quad and \quad C_{reward}^{t} > 0 \tag{3.16}$$

Where $\eta_{KC2MBON}$ is the learning rate. The learning process will happen only when the reward signal is turned on. The activation of EN C_{MBON} represents the familiarity of the current view and the change of the C_{MBON} is defined as:

$$\Delta C_{MBON} = C_{MBON}^{t} - C_{MBON}^{t-1} \tag{3.17}$$

ΔC_{MBON} is used to track the gradient of the familiarity to guide the agent to the more familiar locations by shifting the I-TB1 neurons' activation C_{I-TB1}.

$$C_{VH}^{i} = C_{I-TB1}^{j}, j = \begin{cases} i + offset & if \quad i + offset \leq 7 \\ i + offset - 7 & otherwise \end{cases} \qquad i = 0, 1, ...7 \tag{3.18}$$

The relationship between the ΔC_{MBON} and the $offset$ is shown as following:

$$offset = \begin{cases} 0 & if \quad \Delta C_{MBON} < 0 \\ \min(\lfloor k_{VH} \Delta C_{MBON} \rfloor, 4) & otherwise \end{cases} \tag{3.19}$$

Where the function $min()$ constrains the maximum $offset$ to be 4 so that the max angle of shifting is $4 \times 45^\circ = 180^\circ$.

3.3.4.3 Route Following

The route following model is based on a simple artificial neural network (ANN) with just one hidden layer. The input layer directly takes the **amplitudes** of the ZM coefficients as the activation in the same way as that of visual projection neurons in MB network. This is a fully connected neural network with the sigmoid activation function, so the forward propagation is ruled by:

$$\begin{cases} Z_l^i = \sum_{i=0}^{N} W^{ji} Y_{l-1}^j \\ \\ Y_i^l = sigmoid(Z_l^i) = \frac{1}{1+e^{-Z_l^i}} \end{cases} \qquad i = 0, 1, ...7 \quad and \quad l = 0, 1, 2 \tag{3.20}$$

Where Z_l^i and Y_l^i denote the input and output of the i^{th} neuron in l^{th} layer, thus the input is the same as the MB network $Z_0^i = A^i, i = 0, 1, ...N_{ZM}$ and the output of the ANN is consequently the population coding of the RF desired heading, i.e.:

$$C_{RF}^i = Y_i^2 \qquad i = 0, 1, ...7 \tag{3.21}$$

For a fast and efficient implementation, the learning method applied here is back propagation with gradient descend. Training data is derived from the **amplitudes** and the population encoded *phases* of the ZM coefficients of the images reconstructed along a habitual route. II-TB1 neurons encode the heading of local compass, therefore, the training pair for the RF network can be defined as $\{A, C_{II-TB1}\}$. After training, this network will correlate the desired ZM *phase* with the specific ZM **amplitudes**, and when RF is running, the output of this neural network C_{RF} will represent the desired

heading with respect to the current heading of the local compass represented by the population encoding of II-TB1 neurons.

3.3.4.4 Steering Circuit

The steering neurons, i.e., CPU1 neurons ($C^i_{CPU1}, i = 0, 1, 2...15$) receive excitatory input from the desired heading ($C^i_{DH}, i = 0, 1, 2...15$) and inhibitory input from the current heading ($C_{CH}, i = 0, 1, 2...15$) to generate the turning signal:

$$C^i_{ST} = C^i_{DH} - C^i_{CH} \qquad i = 0, 1, ...15 \tag{3.22}$$

The turning angle is determined by the difference of the activation summations between left ($i = 0, 1, 2...7$) and right ($i = 8, 9, 10...15$) set of CPU1 neurons:

$$\theta_M = k_{motor}(\sum_{i=0}^{7} C_{CPU1} - \sum_{i=8}^{15} C_{CPU1}) \tag{3.23}$$

which corresponds to the difference of the length of the subtracted left and right vectors in Figure 3.3A. In addition, as it is illustrated in Figure 3.3A, another key part of steering circuit is the left/right shifted desired heading, in this thesis, this is achieved by the offset connectivity pattern ($W_{DH2CPU1L}$ and $W_{DH2CPU1R}$) from the desired heading to the steering neurons [45] [10]:

$$\begin{cases} C^{0-7}_{DH} = C_{SN1}C_{RF}W_{DH2CPU1L} + C_{SN2}C_{VH}W_{DH2CPU1L} \\ C^{8-15}_{DH} = C_{SN1}C_{RF}W_{DH2CPU1R} + C_{SN2}C_{VH}W_{DH2CPU1R} \end{cases} \tag{3.24}$$

Where the $W_{DH2CPU1L}$ and $W_{DH2CPU1R}$ are:

$$W_{DH2CPU1L} = \begin{bmatrix} 0 & 1 & 0 & 0 & 0 & 0 & 0 & 0 \\ 0 & 0 & 1 & 0 & 0 & 0 & 0 & 0 \\ 0 & 0 & 0 & 1 & 0 & 0 & 0 & 0 \\ 0 & 0 & 0 & 0 & 1 & 0 & 0 & 0 \\ 0 & 0 & 0 & 0 & 0 & 1 & 0 & 0 \\ 0 & 0 & 0 & 0 & 0 & 0 & 1 & 0 \\ 0 & 0 & 0 & 0 & 0 & 0 & 0 & 1 \\ 1 & 0 & 0 & 0 & 0 & 0 & 0 & 0 \end{bmatrix} \tag{3.25}$$

$$W_{DH2CPU1R} = \begin{bmatrix} 0 & 0 & 0 & 0 & 0 & 0 & 0 & 1 \\ 0 & 1 & 0 & 0 & 0 & 0 & 0 & 0 \\ 0 & 0 & 1 & 0 & 0 & 0 & 0 & 0 \\ 0 & 0 & 0 & 1 & 0 & 0 & 0 & 0 \\ 0 & 0 & 0 & 0 & 1 & 0 & 0 & 0 \\ 0 & 0 & 0 & 0 & 0 & 1 & 0 & 0 \\ 0 & 0 & 0 & 0 & 0 & 0 & 1 & 0 \\ 0 & 0 & 0 & 0 & 0 & 0 & 0 & 1 \end{bmatrix} \tag{3.26}$$

which defines the connection pattern realising the left/right shifting of the desired headings used throughout our model ((Figure 3.2, Figure 5.5, Figure 3.5, Figure 5.8 and Figure 5.11A).

The current heading input to the steering circuit is also switched between global and local compass input via the SN1 and SN2 neuron as VH uses global compass (I-TB1) while RF uses local compass (II-TB1):

$$\begin{cases} C_{CH}^{0-7} = C_{SN1}C_{II-TB1} + C_{SN2}C_{I-TB1} \\ C_{CH}^{8-15} = C_{SN1}C_{II-TB1} + C_{SN2}C_{I-TB1} \end{cases} \tag{3.27}$$

3.3.5 Simulations

Equation 3.23 gives the turning angle of the agent, thus the instantaneous "velocity" ($\boldsymbol{v}$) at every step can be computed by:

$$\boldsymbol{v}^t = S_L[\cos\theta_M^t, \sin\theta_M^t] \tag{3.28}$$

Where S_L is the step length with the unit of centimetres. Note that we haven't defined the time accuracy for every step of the simulations, thus the unit of the velocity in this implementation is $cm/step$ rather than cm/s. Then the position of agent $\boldsymbol{P}^{t+1}$ in the Cartesian coordinates is updated by:

$$\boldsymbol{P}^{t+1} = \boldsymbol{P}^t + \boldsymbol{v}^t \tag{3.29}$$

3.3.5.1 Reproduce Visual Navigation Behaviours

Inspired by the benchmark study of real ants in [18], we test our model of VH and RF by reproducing the homing behaviours in that study. This is achieved by constructing a habitual route with a similar shape (arc or banana shape) in our simulated 3D world. The position $\boldsymbol{P}_{R-Arc}$ and heading θ_{R-Arc} along that route is manually generated by:

$$\begin{cases} \theta_{R-Arc}^i = \frac{\pi}{2} - i\frac{\pi}{2N_M} \\ \boldsymbol{P}_{R-Arc}^i = [-R\sin\theta_{R-Arc}^i, -7 + R\cos\theta_{R-Arc}^i] \end{cases} \quad i = 0, 1..N_M \tag{3.30}$$

Where the $R = 7m$ is the radius of the arc and $N_M = 20$ in this case is the number of the sampling points where view images are reconstructed along the route (see Figure 3.9). The reconstructed views then be wrapped and decomposed by ZM into **amplitudes** and *phases* are used to train the ANN network of RF and MB network of VH respectively.

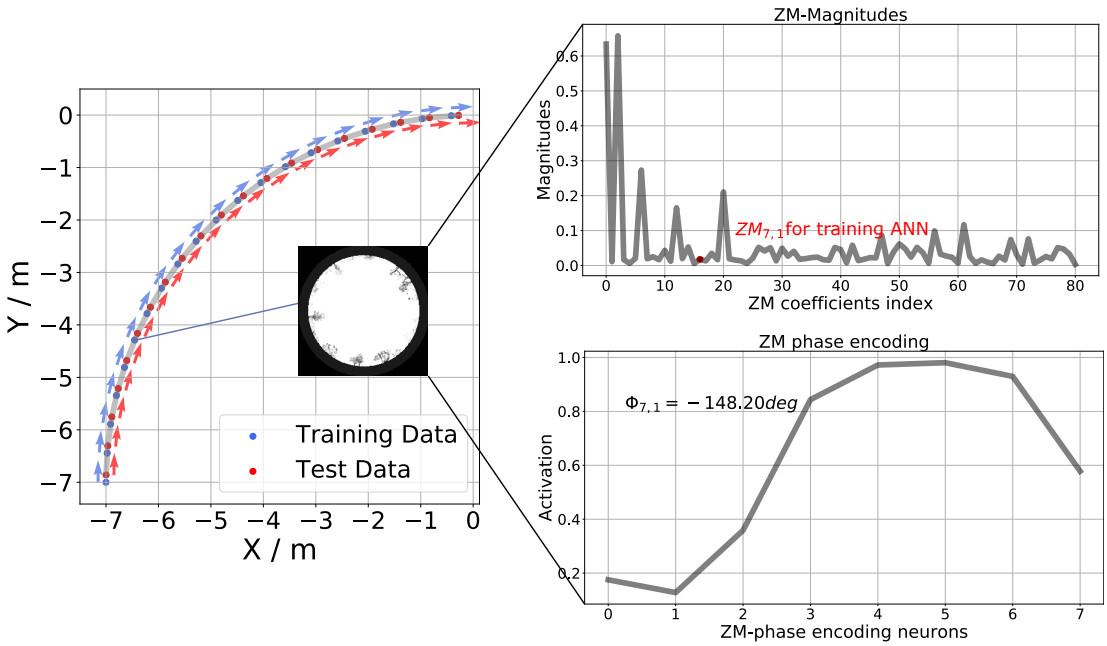

Figure 3.9: **The images used to train the MB network.** The training data and test data are labelled with red and blue dots respectively. The arrow along the route indicates the heading direction on the route. Frequency component $ZM_{7,1}$ used to train ANN is highlighted.

Visual Homing After training (see Figure 3.10 for an example of the training process of the MB network), 12 agents with different initial headings that were evenly distributed in $[0, 360)$ were released at the sideways release point ($\boldsymbol{P} = [0, -7]$) for the simulation of VH (Figure 3.3C). The headings of the agents at radius 2.5m from the release point (manually selected to ensure that the all the agents have completed any large initial loop) are taken as the initial headings.

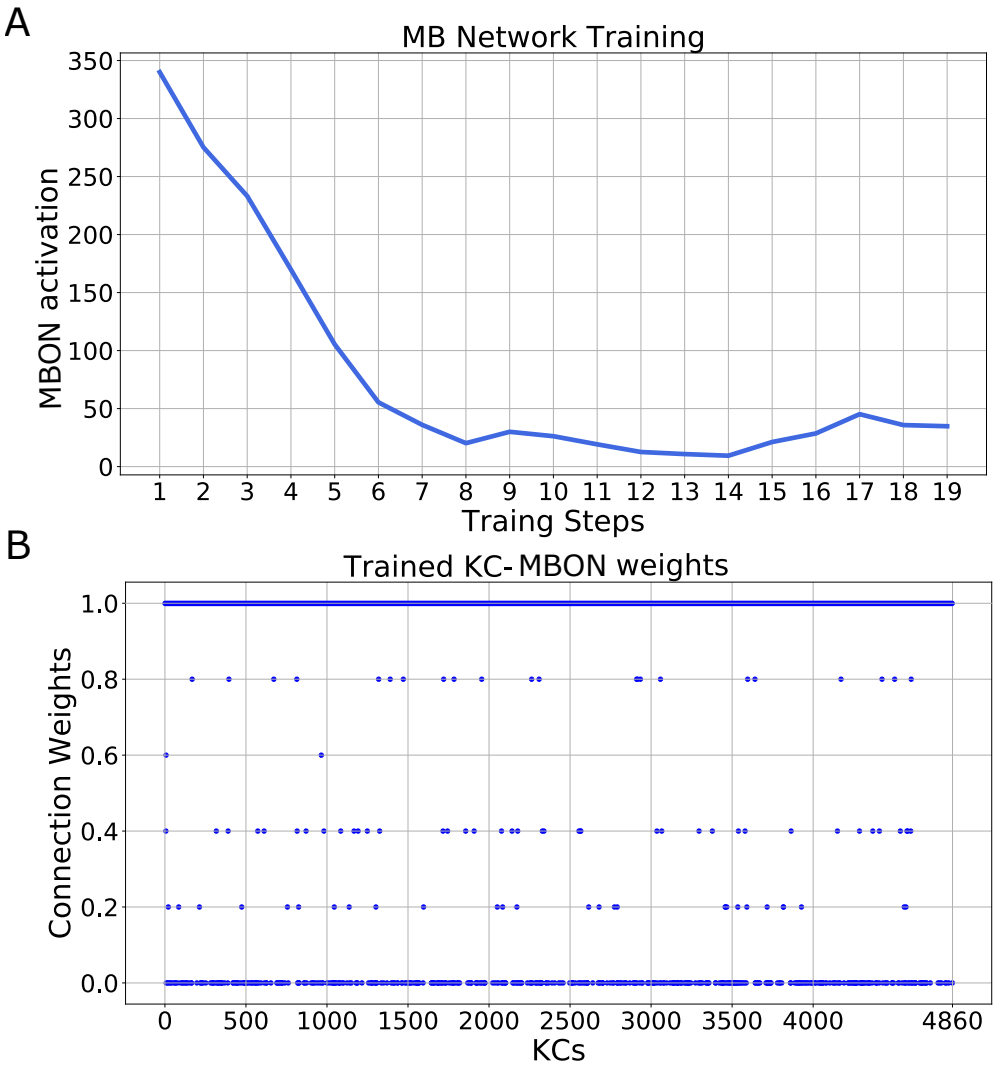

Figure 3.10: **The training process of MB network.** **(A)** The MBON activation decreases during training. **(B)** KC-MBON connection weights after training.

Route Following After training (see Figure 3.11 for a example of the training process of the ANN network), 2 agents with $0°$ and $180°$ are released at the different release points ($\boldsymbol{P} = [-9, -7]$, $[-8, -7], [-7, -7], [-6, -7], [-5, -7]$) for the simulation of RF (see Figure 3.6) to generate the homing path. And then, we release 12 agents on the route ($\boldsymbol{P} = [-7, -7]$) with different initial headings that is evenly distributed in $[0, 360)$ to compare the results with the real ant data in [18]. The heading of each agent at the position that is 0.6m from the release point is taken as the initial heading.

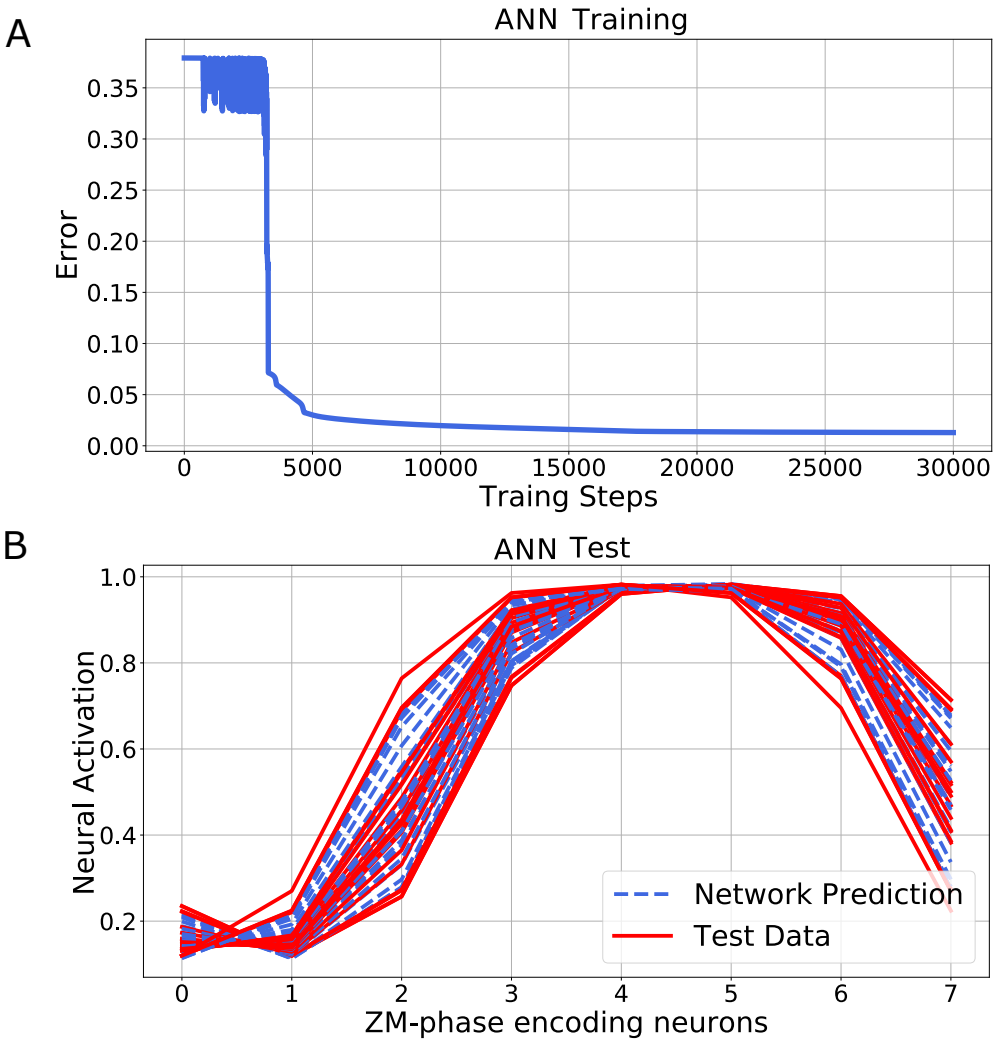

Figure 3.11: **The training process of ANN network. (A)** The error decreasing as the training. **(B)** The output of the network match well the test data.

3.4 Conclusion and Discussion

We show how VH and RF can be realised using frequency-encoding of panoramic skylines to separate information into rotationally-invariant **amplitudes** for VH and rotationally-varying *phases* for RF. The current model utilises frequency encoding schema from the computer graphics but behavioural studies support the use of spatial frequency by bees [267] [268], with neurons in the lobula of dragonflies [269] and locusts [270] found to have receptive fields akin to basis functions, providing a mechanism by which to extract the frequency information necessary for the local compass system. Our model allows for this information extraction process to happen at multiple stages ahead of its usage in the central learning sites such as the MBs opening the pos-

sibility for its application in either the optic lobes or subsequent pathways through regions such as the AOTU. Further, neurophysiological data is required to pinpoint both the mechanisms and sites of this data processing in insects. Similarly, following [10] the global compass signal directly mimics the firing pattern of compass neurons in the CX without reference to sensory input but [271] recently presented a plausible neural model of the celestial compass processing pipeline that could be easily integrated into the current model to fill this gap. Follow-on neuroanatomically constrained modelling of the optic lobes presents the most obvious extension of this work allowing the neural pathway from sensory input to motor output signal to be mapped in detail. Conversely, modelling the conversion of direction signals into behaviour via motor generating mechanisms such as central pattern generators (see [272] [273]) will then allow closure of the sensory-motor loop.

Visual homing is modelled on neural circuits found along the OL-MB-SMP pathway [274] [275] before terminating in the CX steering circuit [10] and shown capable of producing realistic homing paths. In this schema the MBs do not measure rotationally-varying sensory valence as recently used to replicate RF [17] [224], but rather the spatially varying (but rotationally-invariant) sensory valence more suited to gradient descent strategies such as visual homing [204] [215] and other taxis behaviours [228]. This is inline with the hypothesis forwarded by [241] that suggest that the MBs output ”whether” the current sensory stimulus is positive or negative and the CX then adapts the animal heading, the ”whither”, accordingly. Always turning left may not be realistic, but this could be partly explained by the insect handedness shown also controlled by the CX [276]. Or adding a CPG control mechanism could also allow the agent to oscillating left and right while keeping the desired moving direction.

Route following is shown possible by learned associations between the **amplitudes** (i.e. the place) and the *phase* (the orientation) experienced along a route, allowing realignment when later at a proximal location. This kind of neural plasticity based correlation between the visual surroundings and the orientations fits with data recently observed in fruit flies [155] [156]. These studies provide the neural explanation for the animal’s ability to make flexible use of visual information to navigate while the

proposed model gives a detailed implementation of such ability in the context of insect's route following schema. Neurophysiological evidence suggests that the layered visual pathway from OL via AOTU and BU to the EB of the CX [277] [255] [256] with its suggested neural plasticity properties [277] [278] provides a possible neural pathway but further analysis is needed to identify the circuit structures that might underpin the generation of RF desired heading. In addition to the desired heading, the current heading of RF is derived from the local compass system anchored to animal's immediate visual surroundings. This independent compass system may be realised parallel to the global compass system in an similar but independent circuit [258] [253] [33]. Our model therefore hypothesises that insects possess different compass systems based on varied sensory information and further that insects possess the capability (via CX-based RAs) to coordinate their influence optimally according to the current context. Since the global compass, the local compass and the desired heading of RF share the same visual pathway (OL→AOTU→BU→CX), distinct input and output patterns along this pathway may be found by future neuroanatomical studies. In addition, in the proposed model, the activation of current heading and desired heading of RF overlap in the EB, and therefore separation of activation profiles representing each output (e.g. following methods in [151]) presents another meaningful topic for future neurophysiological research.

Closed-loop behavioural studies during which the spatial frequency information of views is altered (similar to [279]) coincident with imaging of key brain areas [280] [151] offers a means to investigate which neural structures make use of what visual information. Complimentary behavioural experiments could verify the distinct VH and RF systems by selectively blocking the proposed neural pathways with impacts on behaviour predicted by Figure 3.3C and Figure 3.6 respectively. [85] report that visual homing abilities are lost for fruit flies with a blocked EB of the CX but not MB, which is predicted by our model if animals have learned target-facing views to which they can later align using their RF guidance system. Analysis of animal's orientation during learning is thus vital to unpacking precisely how the above results arise.

Chapter 4

Modelling Optimal Cue Integration- a Bio-plausible Ring Attractor Network

Animals and robots must constantly combine multiple streams of noisy information from their senses to guide their actions. Recently, it has been proposed that animals may combine cues optimally using a ring attractor neural network architecture inspired by the head direction system of rats augmented with a dynamic re-weighting mechanism. In this work we report that an older and simpler ring attractor network architecture, requiring no re-weighting property combines cues according to their certainty for moderate cue conflicts but converges on the most certain cue for larger conflicts. These results are consistent with observations in animal experiments that show sub-optimal cue integration (i.e., not constant optimal as switching from cue integration to cue selection strategies will happen under certain conditions). This work therefore demonstrates an alternative architecture for those seeking neural correlates of sensory integration in animals. In addition, performance is shown robust to noise and miniaturisation and thus provides an efficient solution for artificial systems.

4.1 Introduction

A fundamental principle underlying animal intelligence is the capacity to appropriately combine redundant sensory information (e.g. vision, olfactory and haptic) of the same percept (e.g. location of a sensory source) to achieve a more accurate and

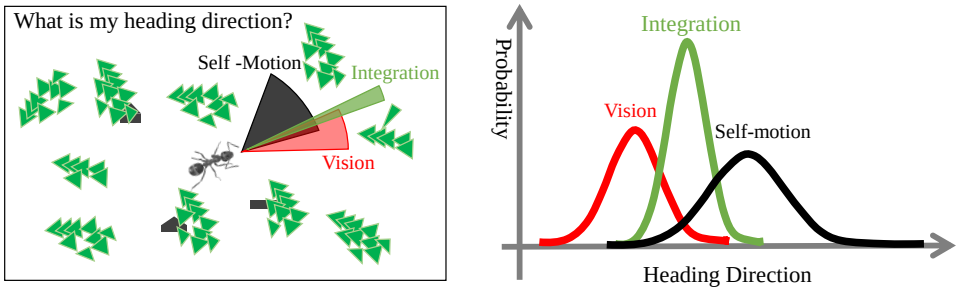

(a) (b)

Figure 4.1: **The cue integration problem**. Left: An example of an animal maintaining an estimate of it's current pose (green area) using different cues of varying certainty (Self-motion, black area, and vision, red area). Right: cues can be represented by conflicting Gaussian functions with the width describing the uncertainty of each and the optimal solution (green) given by weighting each cue according to their known variance as described by Bayes' rule.

robust estimate [281] [282]. For example, both mammals and insects constantly track their pose using head-direction cells which combine information from external cues (e.g. from surrounding visual features) with self-motion cues (from path integration) to maintain a precise estimate of their current orientation [283] [151] (Figure 4.1) (and also see Chapter 2.2.1.1). Yet, as all sensory information is subject to errors which can change drastically depending on the situation (e.g. relying on visual cues in a darkened room) animals must employ an adaptive cue combination strategy reflecting the known errors (variance) in the different sensory signals to achieve the optimal estimate of the desired environmental property.

Bayes' theorem (4.1) provides a mathematical framework describing the optimal way in which information from different sources should be combined, and it has been argued that animals have Bayesian brains [282] [128] [284] [285]. According to Bayes' Rule, the posterior probability $P\left(x_{true}|x_{cue}\right)$ (the probability of event x will happen when the cue about x is sensed) is proportional to the product of the prior probability $P\left(x_{true}\right)$ (the probability of event x happening based on prior knowledge) and the likelihood function $P\left(x_{cue}|x_{true}\right)$ (the probability of the cue when x truly happened, which represents the reliability of this cue). Assuming that the prior probability $P\left(x_{true}\right)$ is uniform and x_{cue} is corrupted by Gaussian noise with variance σ^2, then the posterior probability is proportional to $1/\sigma^2$. Therefore, when there are n cues all concerning x event and corrupted by Gaussian noise with variance $\sigma_i^2, i = 1, 2, ...n$, the optimal

way to reduce the uncertainty of estimating x (i.e., the maximum the posteriori probability) is averaging the cues weighted by their reciprocal variances $1/\sigma^2$, as indicated by (4.2), which is identical with results calculated by the maximum-likelihood estimate (MLE) [284] [286]. The theorem asserts that cues with low variance (i.e more reliable) should be weighted more than those with high variance (i.e less reliable) as demonstrated in Figure 4.1.

$$P\left(x_{true}|x_{cue}\right) = P\left(x_{cue}|x_{true}\right) P\left(x_{true}\right) / P\left(x_{cue}\right) \tag{4.1}$$

$$\hat{X} = \sum_{i}^{n} W_i X_i, W_i = \left(1/\sigma_i^2\right) / \left(\sum_{j}^{n} 1/\sigma_j^2\right) \tag{4.2}$$

Artificial systems must also solve the same problem although in robotics it is commonly known as sensor fusion. Sensor fusion for mobile robot navigation is a long standing issue and many statistical methods based on maximum *a posterior* and maximum-likelihood estimation have been applied to solve it [287]. Recent advances in deployment of robot systems such as cars with their suite of GPS, radar, cameras, and laser scanning sensors to estimate precise lane position, owe much to adoption of probabilistic integration of cues in line with the Bayesian formulation described above [288]. Yet, current SLAM methods [289], tend to be computationally expensive and unsuitable for application on small, cheap robot platforms. Learning from biology may bring significant benefits for solving these problems in artificial systems.

We therefore take a bio-inspired approach to firstly understand how animals resolve this task, which in turn may offer inspiration to engineers seeking efficient solutions. As a starting point, we use a classic neural network architecture known as a ring attractor network.

Ring attractors can be constructed such that the output activity resembles a Gaussian profile that is maintained even in the absence of sensory input. When new sensory input is presented, the activity profile will shift towards and stabilise at the new location. If this sensory input is driven by orientation cues such as path integration or visual features then the Gaussian mean will naturally track the animal orientation. Such net-

works have been proposed to underpin the head-direction cells in animals [290] [291]. Further when more than one input signal is presented ring attractors can be constructed such that the output settles on the weighted average of the combined cues as required for optimal cue integration [292]. In a recent review, Jeffery et al [293] proposed that ring-attractor networks may provide a general architecture for optimal cue integration. Their biomimetic model (constrained by physiological data from rats) used a re-weighting mechanism to achieve optimal integration. Specifically, in the region where conflicting cues overlap, Hebbian learning rapidly strengthens local synapses causing peak activity to shift towards the position consistent with optimal integration.

In this study, we revisit the Touretsky [292] ring attractor network and assess its ability to combine conflicting cues of different strengths. Specifically we seek to assess how this network performs when given cues of different strengths and with different levels of conflict. Further, we wish to document if and when the network optimally integrates cues or if it adheres to a winner-takes-all (WTA) solution, or switches strategy depending on the situation. Our results suggest that a Touretsky ring attractor network can integrate cues in a manner approaching optimal (i.e, consistent with MLE) for small conflicts. For larger conflicts the network switches to WTA mode, mirroring results of ethological experiments [19]. Performance is shown to be robust to noise and significant reduction in the network size, and thus provides a simple (no re-weighting mechanism required), compact ring attractor solution to cue integration that can provide inspiration for those seeking similar integration networks in animals or act as a bio-inspired method for optimal sensor fusion in robots.

4.2 Methods

4.2.1 Artificial Neurons

The network is constructed using two populations of CTRNN (continuous time recurrent neural network) neurons which are simple nonlinear and continuous dynamical neurons suitable for simulating the subset of real numbers as required for our ring attractor model [294]. The average membrane potential c_i of a CTRNN i^{th} neuron is

updated by the differential equation (4.3), where τ is the positive time constant and I_i is the total number of inputs into the neuron which equals the weighted sum of other neurons' outputs $O_j, j = 1, 2, ...n$ and the external inputs, as shown in (4.4), where W_{ji} is the weight matrix representing the connection strength from j^{th} to i^{th} neuron, g is the activation function and X_i is the external input. To acquire the nonlinear property of the network, the activation function of g should be a nonlinear function. Here we simply applied a semi-linear threshold function with a threshold defined by θ as indicated in (4.5).

$$\tau \frac{c_i}{dt} = -c_i + I_i \tag{4.3}$$

$$I_i = \sum_{j=1}^{n} W_{ji} O_j + X_i = \sum_{j=1}^{n} W_{ji} g(c_j) + X_i \tag{4.4}$$

$$g(c) = max(0, \theta + c) \tag{4.5}$$

4.2.2 Network Geometry

We implemented a variant of the classic ring attractor network [290] (Figure 4.2(a)) which replaces the inhibitory interneurons with a single global inhibitory (uniform inhibitory) neuron making the network easier to tune while giving the same performance [292]. Each excitatory neuron in the network has recurrent excitatory connections to all other neurons in the ring with weights decreasing with distance which is crucial for generating the bell-shape activation profile in stable state, as revealed in (4.6), where d_{ij} is the distance between the i^{th} and j^{th} neuron. Our network posses a single dynamic inhibitory neuron that sums inputs from the excitatory neurons and then proportionally inhibits the entire network. Note, for ease of understanding the recurrent connections from a single excitatory cell are shown in Figure 4.2(a) but in reality each neuron has the same set of recurrent connections.

$$W_{ji}^{E \to E} = e^{\frac{-d_{ji}^2}{2\sigma^2}} \tag{4.6}$$

Figure 4.2(b) shows the process by which the network combines input from multiple cues. We simulate cues of different strengths using Gaussian functions (see equation (4.7) where K is the scale factor, μ defines the peak position of the Gaussian curve (estimation of the certain property based on the cue) and σ^2 is the variance of the Gaussian function determining the reliability of the signal). Note that other distribution like the von-Mises and sinusoidal can also be applied (simulations imply identical performances and results), here we use the Gaussian to achieve generality. To have a corresponding connection with the integration neurons in the attractor, the cues are represented by the activation profile of N neurons with their preference p_i, and so the Gaussian curve is sampled by N points at intervals. This input is then passed to the integration population which is shown in unwrapped form in Figure 4.2 (b), and with the recurrent connections omitted for ease of reading. The integration population (and also population representing cue 1 and cue 2) has N neurons labeled with their preferences (for example, if these neurons represent the heading directions of the animal, the preferences will be the preferred directions evenly distributed around the entire 360° of possible directions). The inhibitory population has a single dynamic postulated inhibition neuron summing the activations from all integration neurons and which recurrently inhibits all integration neurons. Therefore, in accordance with equations (4.3) - (4.5), the average membrane potential of the output neurons (neurons in integration population) is computed by equation (4.8), where $X1$ and $X2$ represent the activation vectors of cue 1 and cue 2 respectively and u is the membrane potential of the uniform inhibitory neuron (calculated by equation (4.9)). Note that in order to maintain the nonlinear property and simultaneously guarantee the positive output of the model, we tuned the total input I to c and u using function g according to [292].

Note that in this paper, as an example, we use the ring attractor to represent the heading direction system so all the values have the unit-degree. But generally the unit could be other meanings when this model is applied to other specific contexts.

$$F(i) = \frac{K}{\sqrt{2\pi}\sigma} e^{-\frac{(p_i-\mu)^2}{2\sigma^2}} + \xi N(0,1), i = 1, 2, ...N \tag{4.7}$$

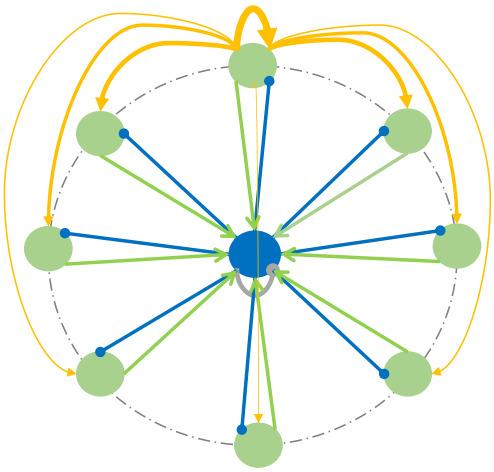

(a) Touretzky Ring Attractor

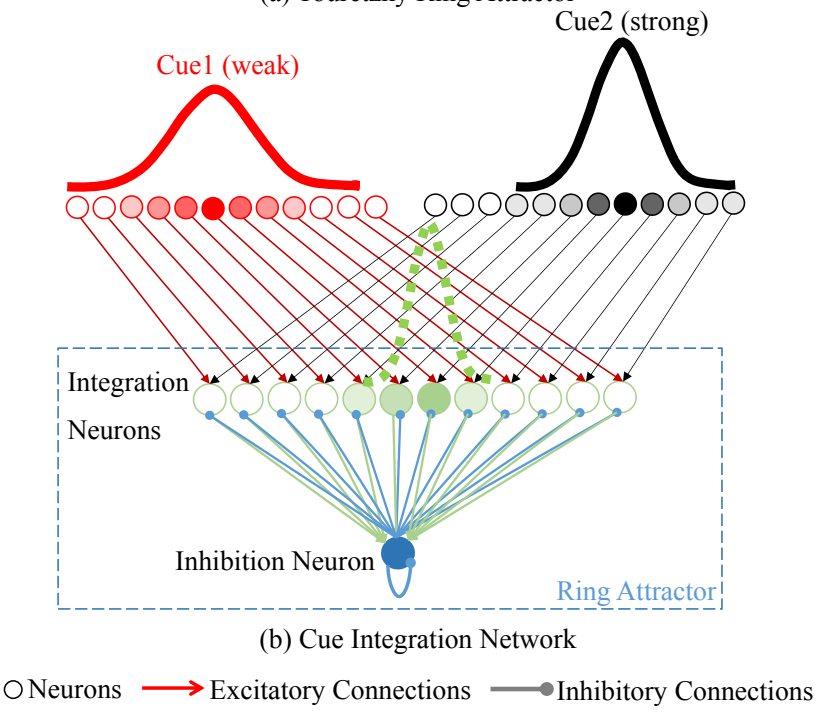

(b) Cue Integration Network

Figure 4.2: **The implemented Touretzky ring attractor network.** (a) Excitatory neurons are shown by green circles, and the global inhibitory neuron depicted by the blue circle. The recurrent excitatory interneurons are shown by orange arrows with connection strength decreasing with distance between neurons. Excitatory and inhibitory connections between the global inhibitory neuron are also shown in blue and green respectively. (b) The full integration network shown in unwrapped form (minus recurrent connections for ease of reading) with example inputs and optimal output overlaid.

$$\tau \frac{dc_i}{dt} = -c_i + g\left(\sum_{j=1}^{n} W_{ji}^{E\to E} c_j + X1_i + X2_i + W^{I\to E} u\right) \tag{4.8}$$

$$\tau \frac{du}{dt} = -u + g\left(W^{I\to I} u + W^{E\to I} \sum_{k=1}^{n} c_k\right) \tag{4.9}$$

4.3 Results

Figure 4.3(a) shows the response of our ring attractor network configured with 100 neurons when stimulated with two conflicting cues (65° apart) with different variances ($\sigma_{cue1} = 40°, \sigma_{cue2} = 35°$) shown by red and black lines. The response of the network (green line) approaches the MLE, i.e., the optimal integration (blue dashed line) rather than following the WTA solution. Figure 4.3(b) shows that the network response is robust to noise with each cue corrupted by Gaussian white noise ((4.7) with $\xi = 0.01$). Finally, inspired by recent anatomical results showing that insects encode their heading direction using populations of only 8 directional neurons in each hemisphere of the central complex [146] [12] we reduced the number of neurons in our integration network from 100 to 8. Figure 4.3(c) demonstrates that the cue integration properties of the network remained stable despite the obvious loss of resolution in the Gaussian functions.

To assess the performance of the network across likely scenarios we performed two more experiments using the noise free network with 100 neurons. Firstly, we assessed the performance of the network when presented with cues that were increasingly disparate. Cue 1 ($\mu_{cue1} = 0°, \sigma_{cue1} = 40°$) was presented at the same position throughout the tests, while Cue 2 was presented at increasingly distant positions (from 0° to 180° in 5° steps). We performed this analysis under three conditions: (a) cues with identical variance ($\sigma_{cue1} = \sigma_{cue2} = 40°$); (b) cues with slight differences in variance ($\sigma_{cue1} = 40°, \sigma_{cue2} = 35°$); and (c) cues with significantly different variance ($\sigma_{cue1} = 40°, \sigma_{cue2} = 20°$). Figure 4.4(a-c) shows the peak response of the network (green line) overlaid on the MLE (blue line) and WTA (red line) solutions. With cues of equal variance (Figure 4.4(a)) the network response approaches (though never very precisely matches) the MLE solution but changes to WTA-like responses when cue-conflict exceeded approximately 100°. With small differences in variance (Figure 4.4(b)), the network again weights cue in an approximately optimal manner but shifts to a WTA response at higher values ($> 110°$). In contrast when more significant differences in variance were presented (Figure 4.4(c)), the network changes from the MLE to WTA response at much smaller conflicts ($> 60°$).

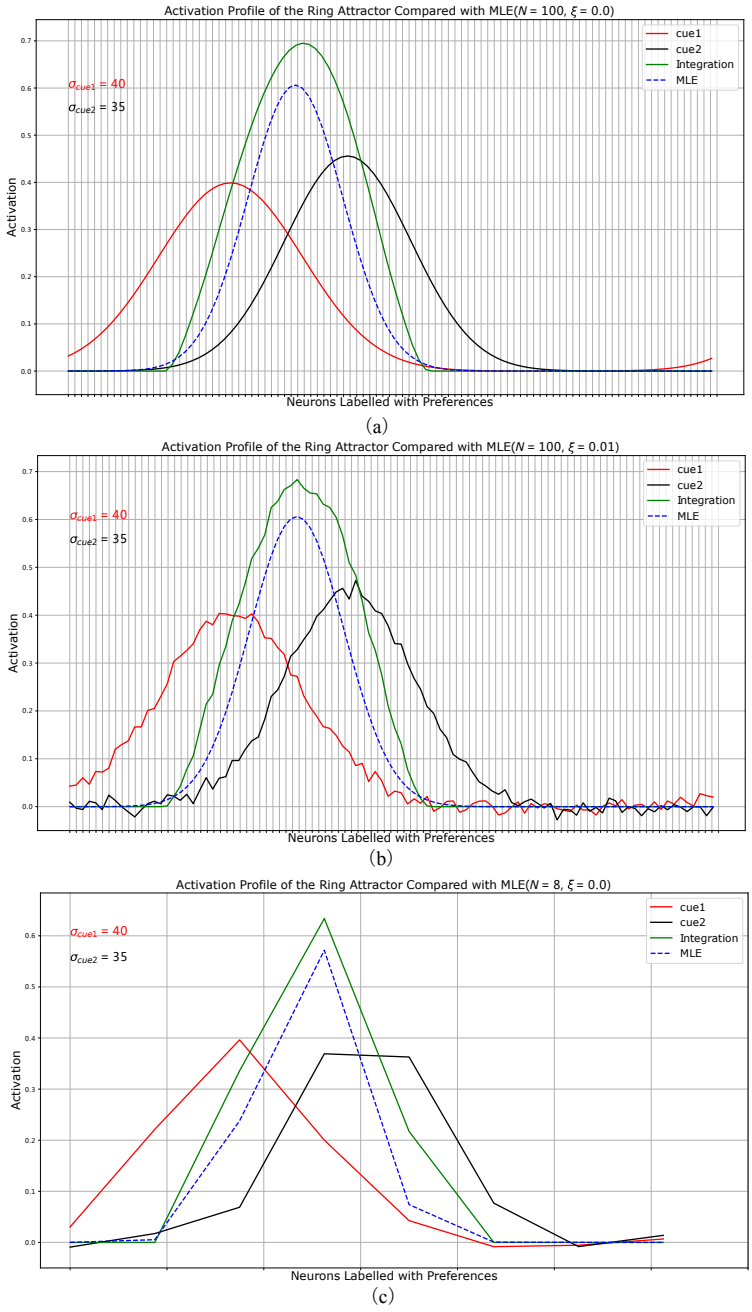

Figure 4.3: **Integration of conflicting cues by a ring attractor network**. Activation profiles of cues are shown by the red and black curves, the output profile of RA (the ring attractor) by the green line, and the MLE by the blue dashed line. (a) shows the results for a noise-free network with 100 neurons, (b) shows the results of the same network with added white noise, and (c) show the results when the number of neurons is reduced to 8.

Figure 4.4(d) shows data from a previous cue-combination experiment in rats [19] (black line) overlaid with the bioligically constrained ring attractor network with re-weighting mechanism [20] (orange line) as the cue conflict is increased as in our experiment. We note that our model response (Figure 4.4(a)) adheres closely to the animal data.

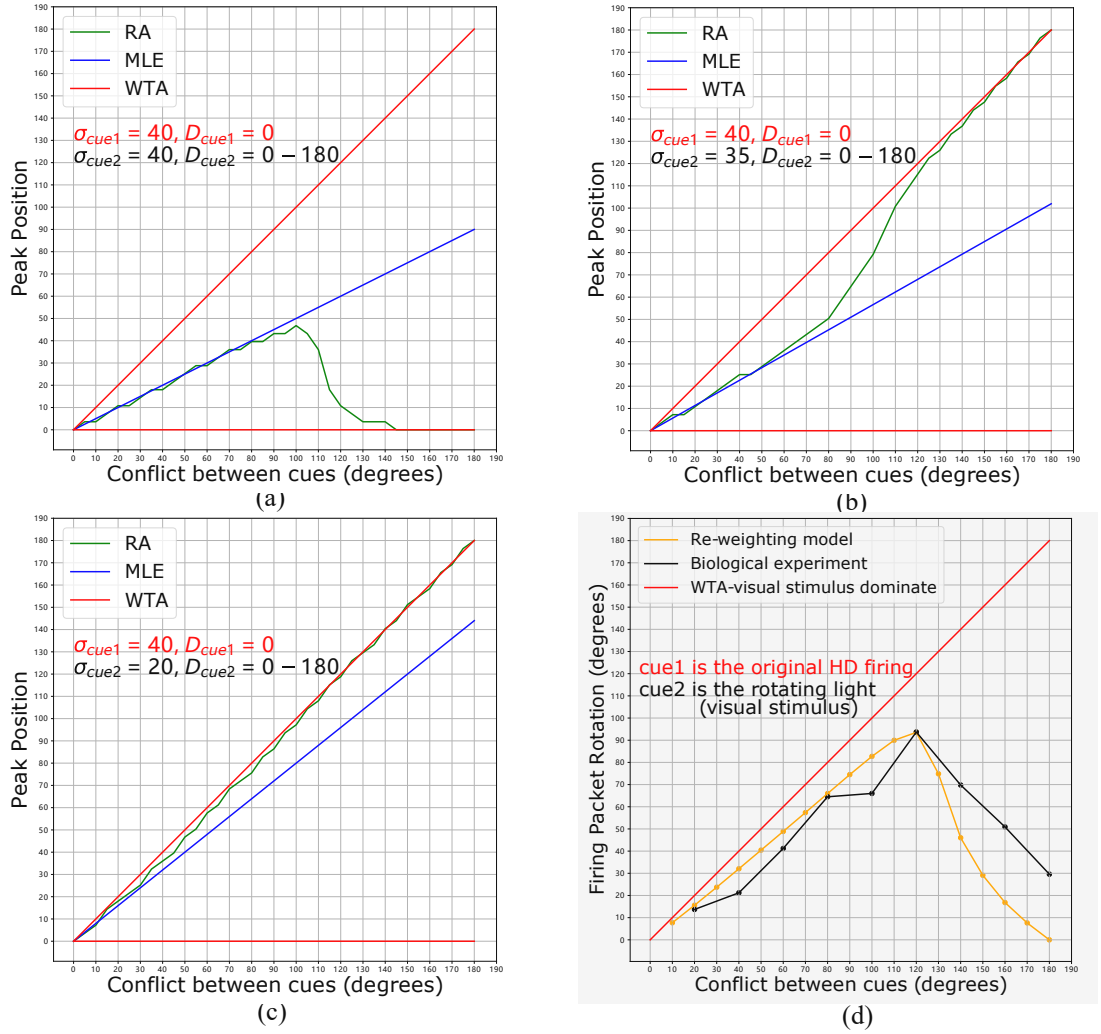

Figure 4.4: **Network performance with increasing cue conflict**. Cue 1 was presented in the same location while cue 2 was presented at increasing distances. For (a), (b) and (c), the response of the RA (ring attractor) is shown by the green line, the WTA prediction by the red line, and the MLE by the blue line. (a) Cues of equal variance (b) Cue 1 with slightly higher variance than Cue 1, (c) Cue 1 with significantly higher variance than cue 1. (d) data from similar cue combination study in rats (black line) [19] and alternative re-weighting model (orange line) [20] (data provided with thanks by Dr. Hector Page and Prof. Kate Jeffery). Note the same tendency of switching from 'cue combination' to 'cue selecting' emerged from the biological data (black curve in (d), re-weighting model (orange curve in (d)) and our model (blue curve in (a)).

Secondly we assessed the performance of the network when the certainty of one cue was altered while the other was held constant. Specifically, cue 1 and cue 2 were presented 90° apart. While cue 2 variance was held at 40°, the variance of cue 1 was increased from 5° to 200°. Figure 4.5 shows the peak position of the activation profile of the network changes from a WTA state for uncertainty of cue 1 below 15° and above 160° but performs a weighted average when uncertainty of cue 1 in the range 20° to 155°. Thus, although not acting in a truly optimal manner the switch from WTA to

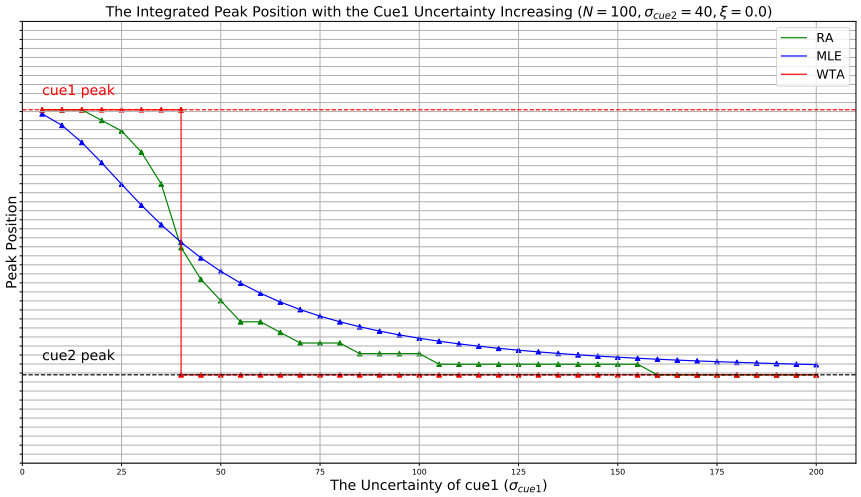

Figure 4.5: **Network performance with changes in cue variance**. Cue 1 and cue 2 were presented at the same location 90° apart. The variance of cue 2 was kept at 40° while cue 1 changed from 5° to 200° in intervals of 5°. The position the peaks of activation profile of cues 1 and 2 are shown by the dashed red and black lines respectively; the WTA response by the solid red line; the MLE by the blue line; and the RA (ring attractor) output by the green line.

weighted-average and back again follows the general profile of the MLE prediction.

4.4 Discussion

In this work, we re-visited the classic ring-attractor network described by Touretsky [292] to assess if it could be configured for optimal cue integration, and if so whether this might give inspiration for those seeking such networks in animals or provide a biologically-inspired solution for robotics.

We report that that our implementation of the classic Touretsky ring attractor network perform optimal-like cue integration when presented with conflicting cues rather than tending to a winner-takes-all solution as often cited [293], [295]. The network output is also shown to be robust to noise on the sensory input and to reduction to 8 neurons encoding direction (as in insects). Our sweep tests showed that both the variance and distance between conflicting cues strongly affect the network properties. With equal or small differences in variance of cues the network performs a weighted average for small cue conflicts, but switches to a WTA response for larger conflicts. For larger differences the network switches to WTA responses at much small conflicts. This changing of response is akin to meta-Bayesian decision making where it is highly

sub-optimal to integrate two hugely conflicting cues e.g. one should not go West, when one cue states North and the other South. Instead one should choose the best single option, but how does the agent know when to apply each strategy? We show that the [292] ring attractor network inherently possesses this capacity.

Over two decades ago the ring attractor network was proposed as a possible solution underpinning the head direction cells in mammals that integrate directional cues from different sensory modalities to maintain an accurate read-out of their current orientation [290]. Recent models of the head direction cells of mammals have moved away from the original ring attractor architecture because the physiology does not mirror the excitatory interconnections required by the original model [20] [295], and the belief that ring attractors will tend to a WTA outcome over the weighted-average observed in behavioral experiments [293]. Through augmentation of these models with a re-weighting mechanism (Hebbian learning) [20] it has been proposed that this network architecture may be a ubiquitous neural circuit underlying optimal cue integration across many functions [293]. Here we provide new evidence that the original ring attractor network can also perform weighted cue integration (closely matching the performance of the re-weighting network [20] Figure 4.4(d)), or cue selection in a manner closely approximating data from rats [19] (Figure 4.4(d)).

Direction cells have recently been revealed in insects (*Drosophila*) with so-called E-PG neurons [151] forming a bump of activity that moves in response to both rotation of vision cues and self-motion and combines in both cue selection (Extended Data Figure 6(e) in [151]) or cue integration like a averaged weighted (Extended Data Figure 6(f) in [151]). These E-PG neurons have also been shown to have ring attractor dynamics [58]. Biomimetic models constrained by the anatomy of the animal have successfully recreated the activation phenomena of behavioral experiments [251] [252] but have not, as yet, been extended to the broader cue integration problem discussed here and in [293]. We note that [251] showed that fixed connection weights are sufficient to track the self-motion and visual cues well with the dynamic re-weighting with slower learning rates giving improved performance describing a trade-off between computational complexity and required robustness.

By analyzing the Touretzky ring attractor network, we show that it should still be considered a biologically plausible mechanism to achieve cue integration of the animals. Although not well suited to describe the head-direction system of mammals due to physiological constraints, it is an open question whether other areas of animal brains that perform cue integration may use this ring attractor architecture. For instance, the lateral accessory lobe (LAL) of insects brain, which is a converging point of sensory information and has inputs from sensory lobes, mushroom body and the central complex [296] [297] provides a candidate to search for such network architectures. To date, we know little about how different cues (like vision memory from mushroom body and path integration from central complex) might be integrated in this area and wherein ring attractors may also play crucial roles. As a bio-inspired neural network, the ring attractor is a compact but efficient model to solve the similar problems in sensor fusion and its anti-noise and stable performance with only 8 neurons endow it the advantage of implementation on robots with limited computation resources.

Chapter 5

The Unified Model- How the MB and the CX Work in Tandem to Realise Multi-guidance Coordination

Now we have the frequency encoding based visual navigation model (see Chapter 3) and the bio-plausible ring attractor network for optimal cue integration (see Chapter 4). The next challenge in addressing the current gap of building a unified model for the extended insect navigation toolkit (see Figure 5.1B) is to designing a biologically realistic coordination circuit that can account for the observed context-depended navigational behaviours (see Figure 5.1A). This chapter presents the ring attractor based multiple guidences coordination circuit modelling the context-depend insect navigation behaviour that can replicates main behavioural data from real insects.

5.1 Introduction

As described in Chapter 2.2, despite increasing neuroanatomical evidence suggesting that premotor regions of the CX coordinate navigation behaviour [146] [242] [13], a theoretical hypothesis explaining how this is achieved by the neural circuitry has yet to be developed.

With the necessary elemental guidance systems defined, a unifying model must then convert the various directional recommendations into a single motor command

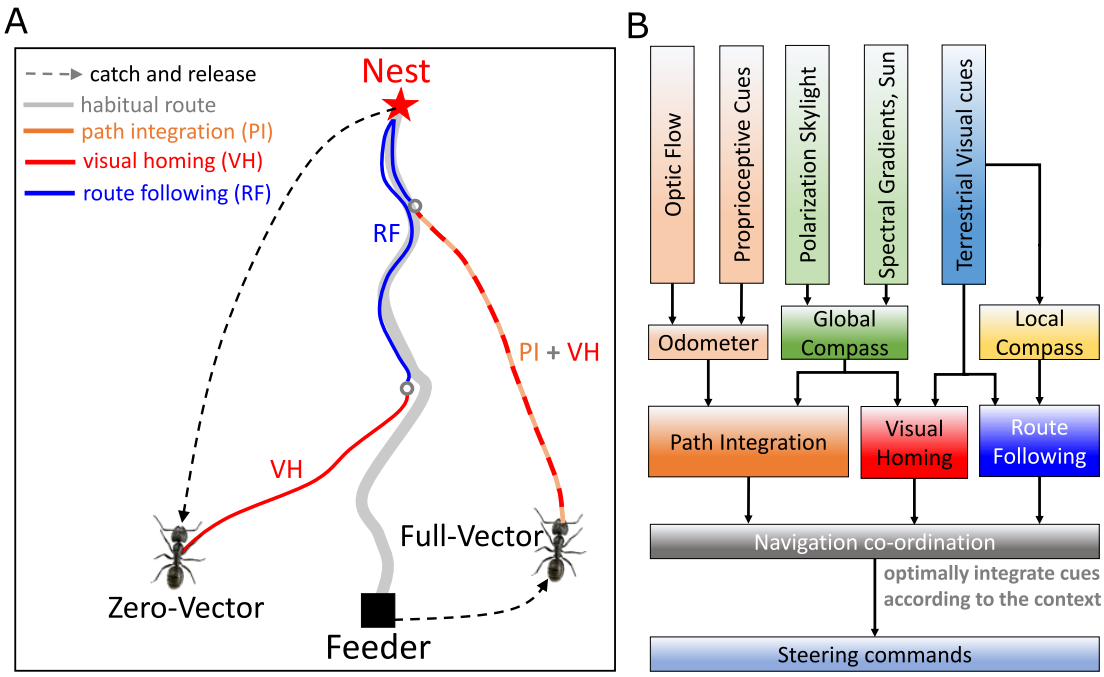

Figure 5.1: **Overview of insects' homing capabilities and the extended toolkit.** (**A**) The homing behaviours to be produced by the model when displaced either from the nest and having no remaining PI home vector (zero vector), or from the nest with a full home vector (full vector). Distinct elemental behaviours are distinguished by coloured path segments, and stripped bands indicate periods where behavioural data suggests that multiple strategies are combined. Note that this colour coding of behaviour is maintained throughout the remaining figures to help the reader map function to brain region. (**B**) The proposed conceptual model of the insect navigation toolkit from sensory input to motor output. Three elemental guidance systems are modelled in this paper: path integration (PI), visual homing (VH) and route following (RF). Their outputs must then be coordinated in an optimal manner appropriate to the context before finally outputting steering command.

appropriate to the context [126] [239] [131] [27]. Behavioural studies show that when in unfamiliar visual surroundings ("Off-route") insects combine the outputs of their PI and VH systems [298] [6] [7] relative to their respective certainties consistent with optimal integration theory [9] [8] (Figure 5.1A "Full Vector"). Upon encountering their familiar route, insects readily recognise their surroundings, recover their previous bearing and retrace their familiar path home [299] [100] [300] [18] [99].

Thus, the navigation coordination model must posses two capabilities: (a) output a directional signal consistent with the optimal integration of PI and VH when Off-Route (b) switch from Off-Route (PI and VH) to On-Route (RF) strategies when familiar terrain is encountered. Mathematical models have been developed that reproduce aspects of cue integration in specific scenarios [126] [16], but to date no neurobiologically constrained network revealing how insects might realise these capabilities has been

developed.

To address these questions a functional modelling approach is followed that extends proposing a neurally-based model of the CX neuropil that integrates competing cues optimally and generates a simple steering command that can drive behaviour directly. Performance is bench-marked by direct comparison to behavioural data reported by [18] (showing different navigation behaviours on and off the route), [9] [8] (demonstrating optimal integration of PI and VM), and through qualitative comparison to extended homing paths where insects switch between strategies according to the context [50]. Biological realism is enforced by constraining models to the known anatomy of specific brain areas, but where no data exists an exploratory approach is taken to investigate the mechanisms that insects may exploit.

5.2 Results

5.2.1 Optimally Integrating Visual Homing and Path Integration

We have demonstrated how ants could use visual cues to return to the route in the absence of PI (see Chapter 3.2.2) but in most natural scenarios (e.g. displacement by a gust of wind) ants will retain a home vector readout offering an alternative, and often conflicting, guidance cue to that provided by VH. In such scenarios desert ants strike a comprise by integrating their PI and VH outputs in a manner consistent with optimal integration theory by weighting VH relative to the familiarity of the current view [9] and PI relative to the home vector length (a proxy for directional certainty) [8].

Various ring-like structures of the CX represent directional cues as bumps of activity with the peak defining the specific target direction, and the spread providing a mechanism to encode cue certainty as required for optimal integration (for an example see increased spread of HD cell activity when only proprioceptive cues are present [151]). Besides their excellent properties to encode the animal's heading ring attractors also provide a biologically realistic means to optimally weight cues represented in this format [292] (see also Chapter 4) without the need for dedicated memory circuits to store means and uncertainties of each cue.

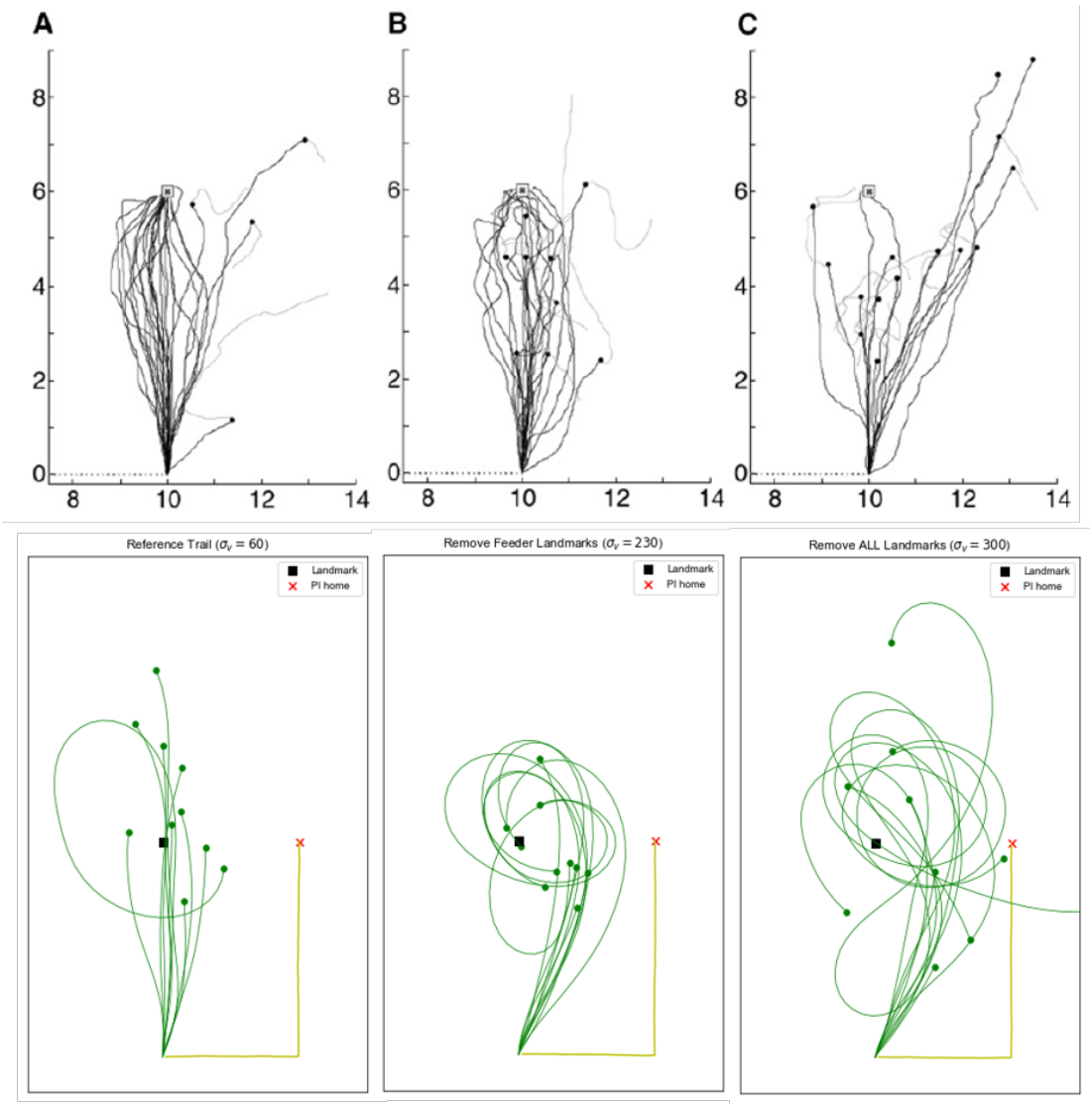

Figure 5.2: **Simulation results of integration of PI and visual cues to reproduce behavioural data in [7].** Green curves are the homing trajectories of the simulated ants and the green dots at the end of each path marks the start points of searching. Cross marks indicates the position of home predicted by PI and black square indicates the positions of landmarks.

First, to preliminary test the performance of ring attractor network to do ants-like integration of visual cues and path integration, we have undertaken simulations to reproduce the behavioural data published in [7] and [6] (see also Figure 2.2A and B). The PI model proposed by [10] is used, and the direction guidance provided by visual cues is calculated directly by the angle between the position of the landmark and nest. For each setting (different PI length and landmark position), we run 10 trials and the homing routes are shown in Figure 5.2, Figure 5.3 and Figure 5.4, from which we can infer that the proposed ring attractor network is capable of generating ant-like integrating results.

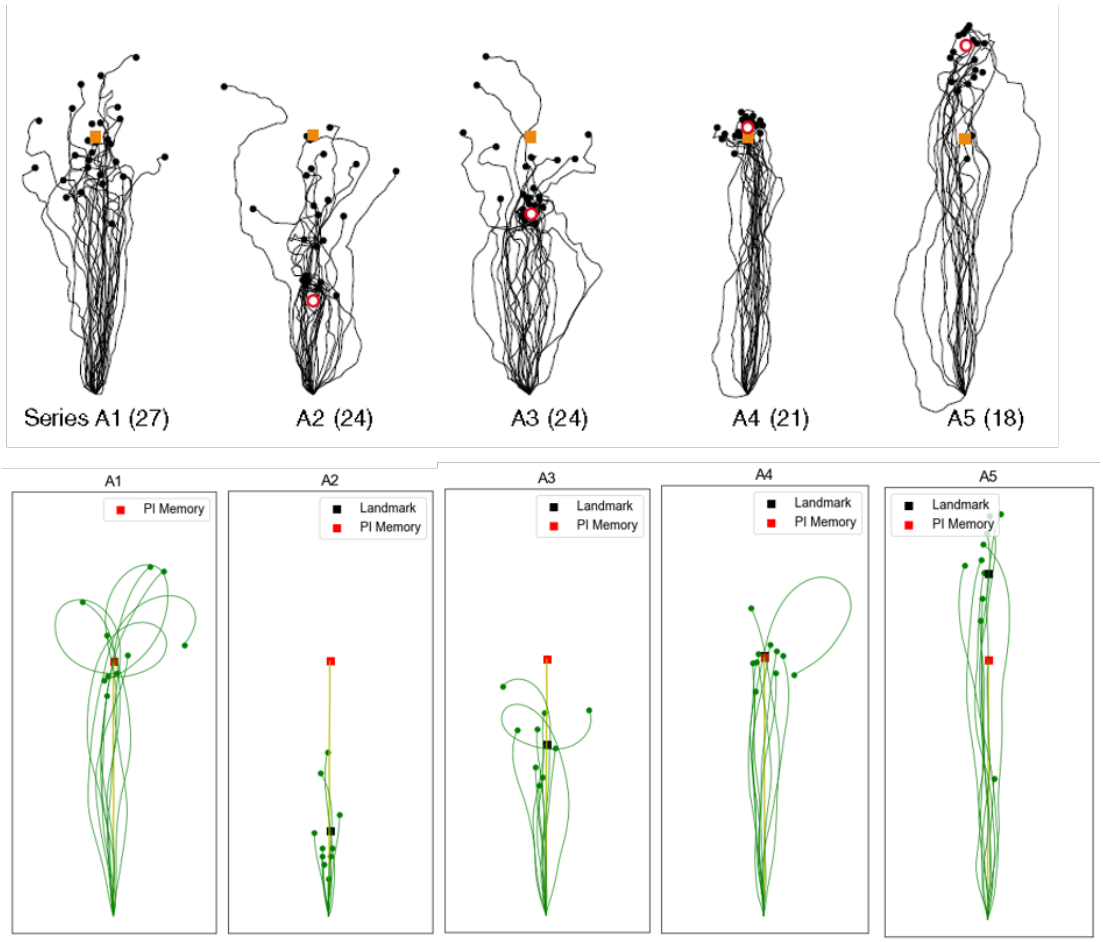

Figure 5.3: **Simulation results of integration of PI and visual cues to reproduce behavioural data in [6].** Green curves are the homing trajectories of the simulated ants and the green dots at the end of each path marks the start points of searching. Cross marks indicates the position of home predicted by PI and black square indicates the positions of landmarks.

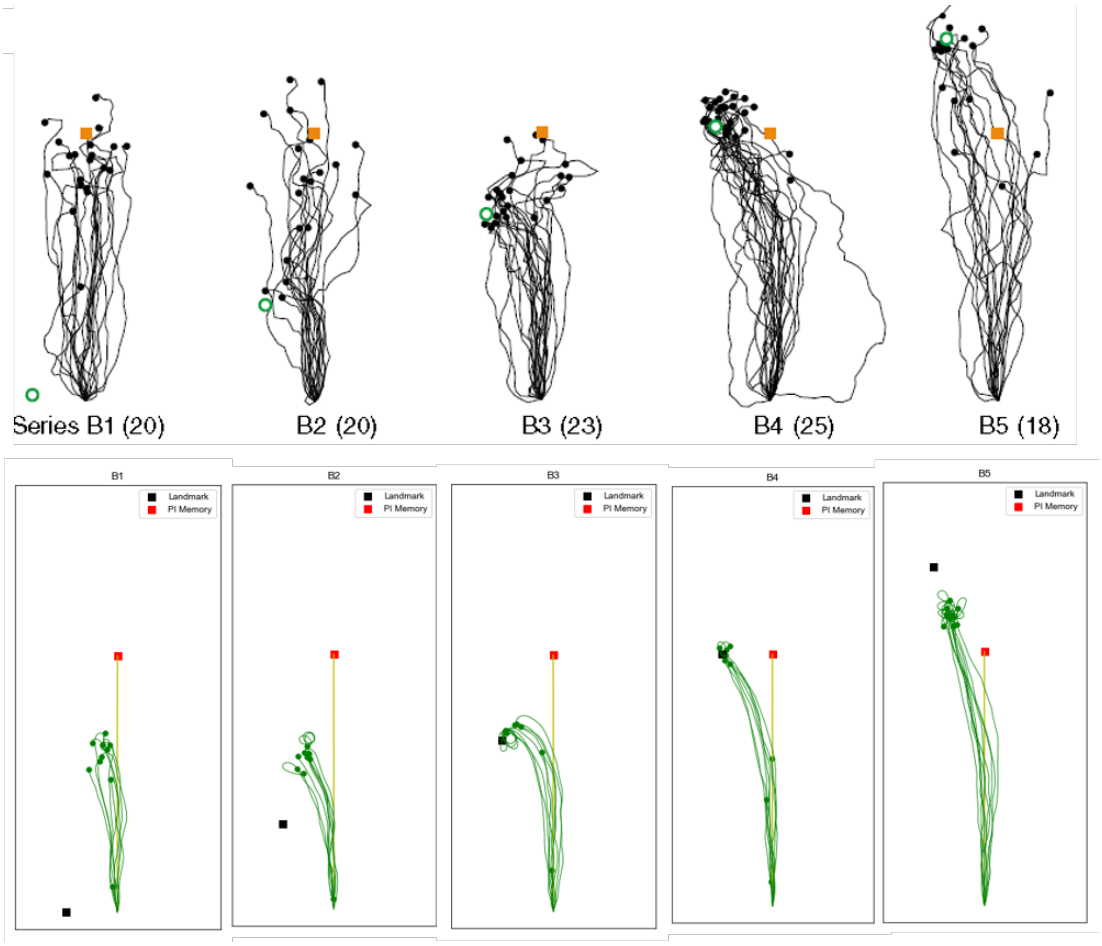

Figure 5.4: **Simulation results of integration of PI and visual cues to reproduce behavioural data in [6].** Green curves are the homing trajectories of the simulated ants and the green dots at the end of each path marks the start points of searching. Cross marks indicates the position of home predicted by PI and black square indicates the positions of landmarks.

Thus we introduce a pair of integrating ring-attractor networks to the CX model (Figure 5.5A grey neural rings: RA_L and RA_R) that take as input the desired headings from the above proposed VH model (red neural rings: VH_L and VH_R) and [10]'s PI model (orange neural rings: PI_L and PI_R) and output combined Off Route desired heading signals that are sent to the steering circuits (blue neural rings: CPU_L and CPU_R). [10] mapped the home vector computation to a population of neurons (CPU4) owing to their dual inputs from direction selective compass neurons (I_TB1) and motion sensitive speed neurons (TN2) as well as their recurrent connectivity patterns facilitating accumulation of activity as the animal moves in a given direction.

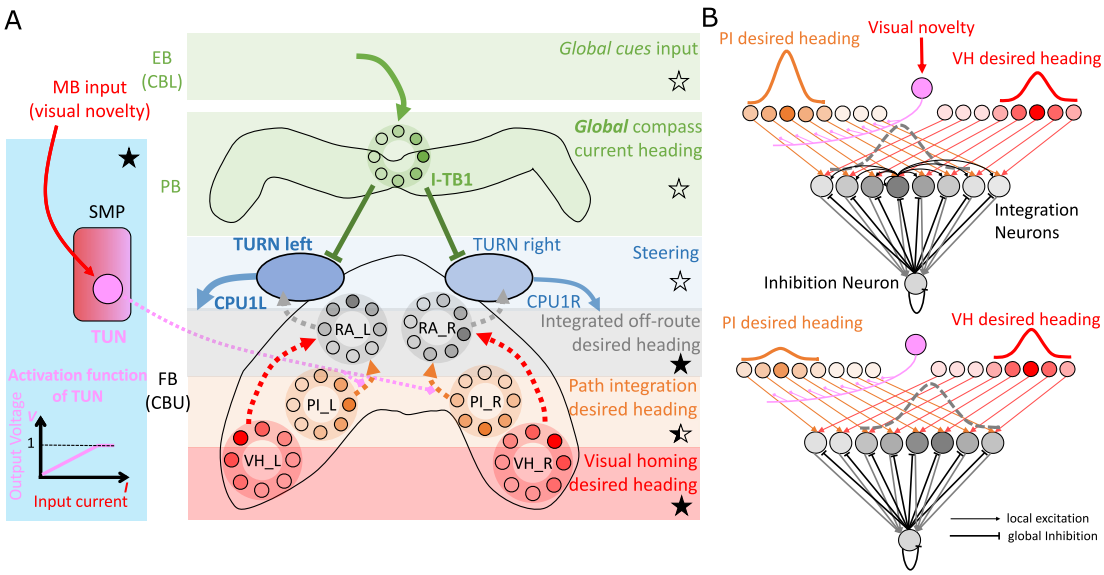

Figure 5.5: **Modelling optimal cue integration in the CX.** (**A**) Proposed model for optimally integrating PI and VH guidance systems. In each hemisphere, ring attractors (RAs) (grey neural rings) (speculatively located in FB/CBU) receive the corresponding inputs from PI (orange neural rings) and VH (red neural rings) with the outputs sent to the corresponding steering circuits (blue neural rings). Integration is weighted by the visual novelty tracking tuning neuron (TUN) whose activation function is shown in the leftmost panel. (**B**) Examples of optimal integration of PI and VH headings for two PI states with the peak stable state (grey dotted activity profile in the integration neurons) shifting towards VH as the home vector length recedes. Note that VH distribution stays the same height and width, while the PI activation (inherently encoded the uncertainty (PI length)) is scaled by the visual novelty via TUN neuron.

[8] showed that the certainty of PI automatically scales with the home-vector length owing to the accumulating effect of the memory neurons which correlates with directional uncertainty, and thus the output PI network is directly input to the ring attractor circuits. In our implementation the VH input has a fixed height and width profile and influences the integration through tuning neurons (TUN) (see the plotted activation function in Figure 5.5B and Chapter 5.3.3.1) that we suggest reside in the SMP and modulate the PI input to the integration network. Altering the weighting in this manner rather than by scaling the VH input independently allows VH to dominate the integrated output at sites with high visual familiarity even in the presence of a large home vector without having large stored activity, i.e., to make it possible to sufficiently suppress the PI output. We note however, that both approaches remain feasible and further neuroanatomical data is required to clarify which, if either, mechanism is employed by insects.

Figure 5.6A shows the initial headings produced by the model which replicates the

trends reported in cue-conflict experiments by [9] (linear regression, $\beta_{model,real} = 0.86$) and [8] (linear regression, $\beta_{model,real} = 0.82$) when the uncertainty of PI and VH cues were altered independently. Example extended paths of independent PI and VH models and the ring-attractor-based combined PI and VH model are plotted in Figure 5.6B with the combined model showing the most ant-like behaviour [100] [99] by initially following predominantly the home-vector direction before switching to visual homing when the home-vector length drops leading the simulated ant back to familiar terrain. The reported model results are obtained after careful parameter tuning as the MB model is very brittle and the ring attractor network is also sensitive to the parameters. By trying different parameters and checking the output from the model with the aid of the developed GUI, the best parameters that have been found are listed in Table 5.2. Note that the PI-only and PI+VH models are drawn back towards their fictive nest sites indicated by their home vectors which if left to run would likely result in emergent search-like patterns as in [10]. Moreover, upon encountering the route the VH-based models (VH-only and PI+VH) are unable to distinguish the direction in which to travel and hence again (see meander around the valley of familiarity Figure 3.3C and Figure 5.6B) further demonstrating a need for a route recovery mechanism.

5.2.2 Route Recovery Through Context-dependent Modulation of Guidance Systems

Homing insects readily recognise familiar route surroundings, recover their bearing, and retrace their habitual path home, irrespective of the status of other guidance system such as PI. Replicating such context-dependent behavioural switching under realistic conditions is the final task for the proposed model. The visual novelty measured by the MBON provides an ideal signal for context switching with low output when close to the route when RF should dominate versus high output further away from the route when PI and VH should be engaged (see Figure 3.3C). Also the fact that Off-route strategies (PI and VH) compute their turning angles with reference to the global compass whereas the On-route RF strategy is driven with reference to a local compass provides a means to modulate their inputs to the steering circuit independently. This

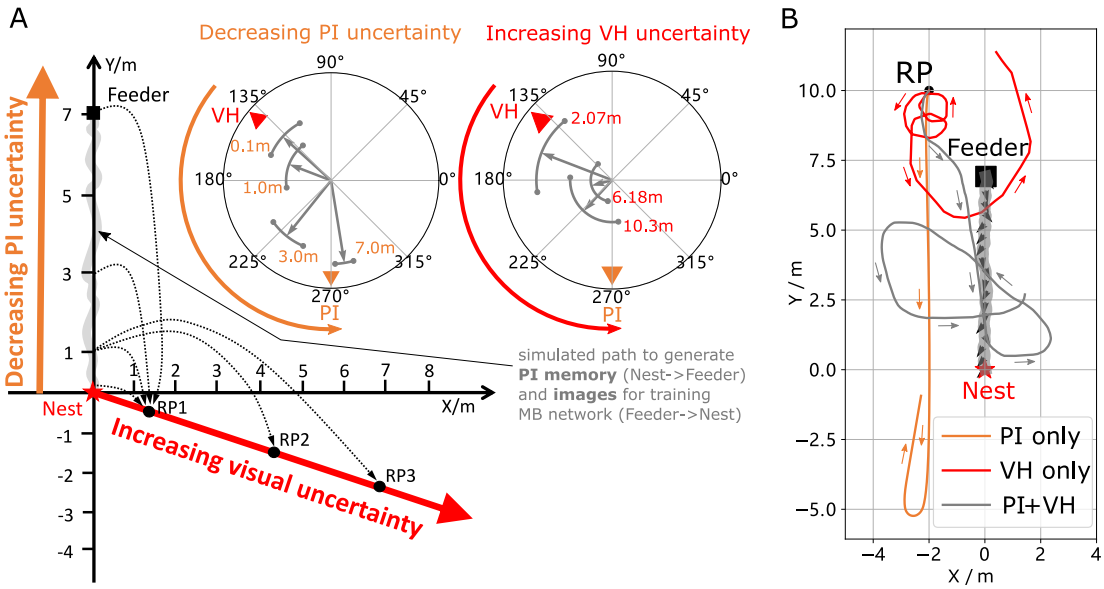

Figure 5.6: **Modelling optimal cue integration in the CX.** (**A**) Replication of optimal integration studies of [8] and [9]. Simulated ants are captured at various points (0.1m, 1m, 3m and 7m) along their familiar route (grey curve) and released at release point 1 (RP1) thus with the same visual certainty but with different PI certainties as in [8] (see thick orange arrow). The left polar plot shows the initial headings of simulated ants increasingly weight their PI system (270°) in favour of their VH system (135°) as the home vector length increases and PI directional uncertainty drops. Simulated ants are also transferred from a single point 1m along their familiar route to ever distant release points (RP1, RP2, RP3) thus with the same PI certainty but increasingly visual uncertainty as in [9] (see thick red arrow). The right polar plot shows the initial headings of simulated ants increasingly weight PI (270°) over VH (135°) as visual certainty drops. (see Chapter 5.3.5.1 for details) (**B**) Example homing paths of the independent and combined guidance systems displaced from the familiar route (grey) to a fictive release point (RP).

is realised through a non-linear weighting of the On and Off-route strategies which we propose acts through the same SMP pathway as the VH model (see the SN1 and SN2 neurons in Figure 5.8) (see Chapter 5.3.3.2 for neuron details and Figure 5.11 for a force-directed graph representation of the final unified model).

The activity of the proposed switching circuit and the paths that it generates in simulated zero vector and full vector displacement trials are shown in Figure 5.10 A & B respectively. In the full vector trial (Figure 5.10A (upper), Figure 5.10B (solid line)) as visual novelty is initially high (see high TUN activity until step 78) SN2 is activated which enables Off-Route strategies (PI and VH recommends moving at a 45° bearing but VH prevents ascension of the visual novelty gradient that this would cause with the compromise being a bearing closer to 90° i.e. toward the route. As the route is approached the visual novelty decreases (again see TUN activity), until at step 78,

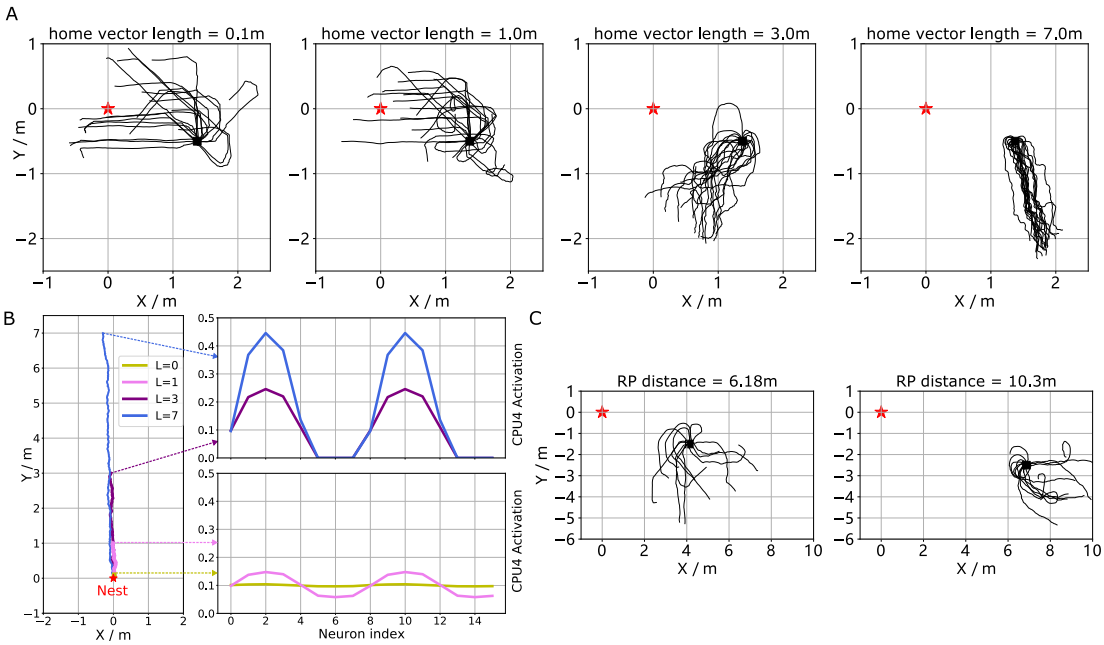

Figure 5.7: **The extended homing paths and the PI memory in the simulations. (A)** The extended homing path of 20 agents released at RP1 in Figure 5.5B with different home vector length. **(B)** The activation of CPU4 neurons (PI memory) encoding home vectors with different lengths from 0 to 7.0m. **(C)** The extended homing paths of 20 agents released at RP2 and RP3 in Figure 5.5B.

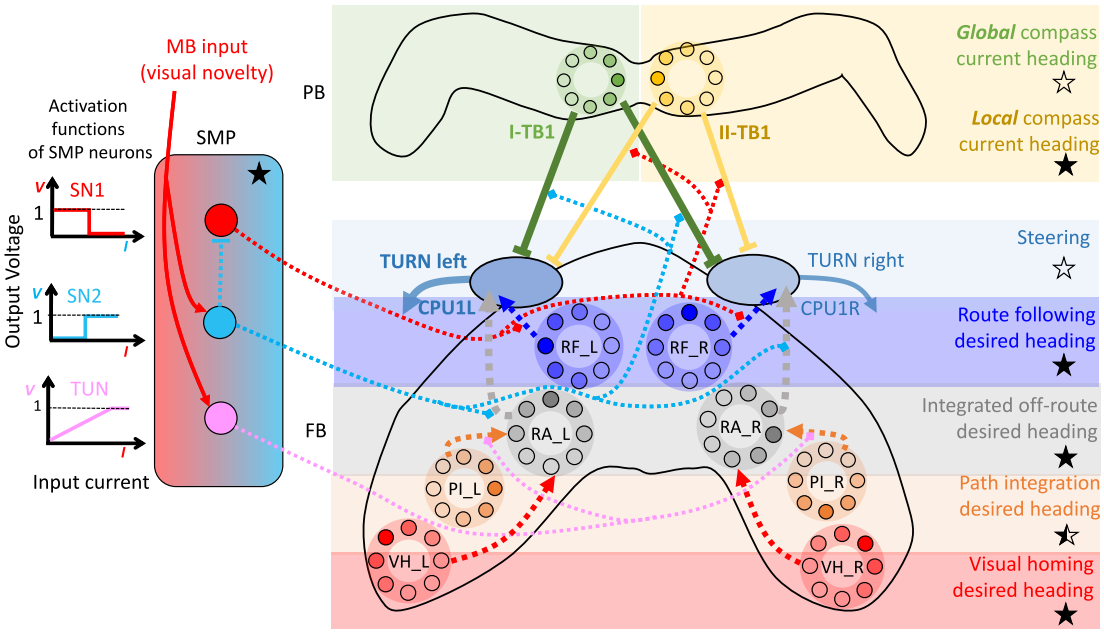

Figure 5.8: **Unified model realising the full array of coordinated navigational behaviours.** Context-dependent switching is realised using two switching neurons (SN1, SN2) that have mutually exclusive firing states (one active while the other is in active) allowing coordination between On and Off-Route strategies driven by the instantaneous visual novelty output by the MB. Connectivity and activation functions of the SMP neurons are shown in the left side of panel. Note that the illustration of the global and local compass is for the easy of understanding not implying the real anatomy, actually they occupy the same set of PB columns.

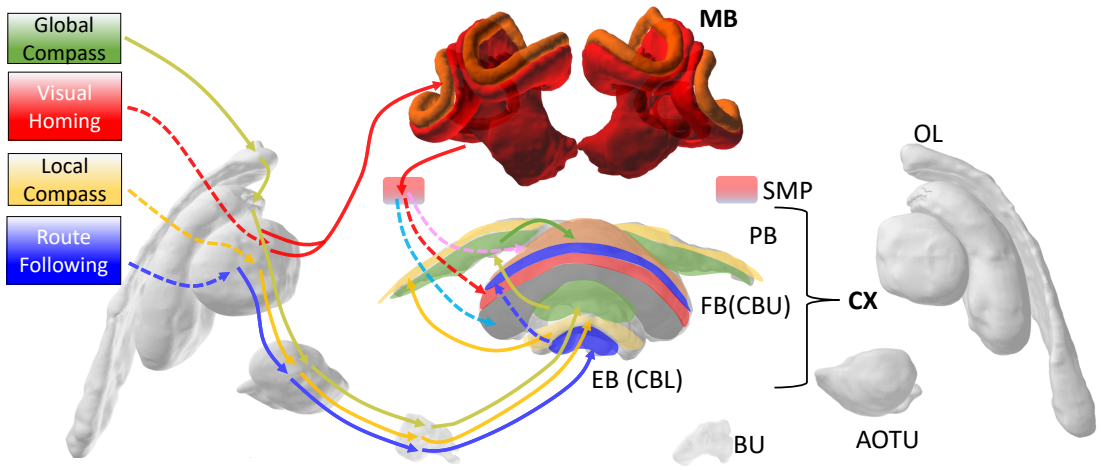

Figure 5.9: **Unified model mapped to brain regions.** The unified navigation model maps the elemental guidance systems to distinct processing pathways: ***RF***: OL → AOTU → BU → CX; ***VH***: OL → MB → SMP → CX; ***PI***: OL → AOTU → BU → CX. The outputs are then optimally integrated in the proposed ring attractor networks of the FB in CX to generate a single motor steering command. Connections are shown only for the left brain hemisphere for ease of visualisation but in practice are mirrored on both hemispheres. Hypothesised or assumed pathways are indicated by dashed lines whereas neuroanatomically supported pathways are shown by solid lines (a convention maintained throughout all figures).

SN2 falls below threshold and deactivates the Off-Route strategies while conversely SN1 activates and engages On-Route strategies. After some initial flip-flopping while the agents converges on the route (steps 78-85) RF becomes dominant and drives the agent back to the nest via the familiar path. In the zero vector trial (Figure 5.10A (lower), (Figure 5.10A (dashed line)) Off-route strategies (here only VH) largely dominate (some false positive route recognition (e.g step 60)) until the route is recovered (step 93), at which point the same flip-flopping during route convergence occurs (steps 93-96) followed by RF alone which returns the agent to the nest via the familiar path. It should be noted that the data presented utilised different activation functions of the TUN neuron that weights PI and VH (see Table 5.2 for parameter settings across trials and Chapter 5.4 for insights into model limitations and potential extensions), yet the results presented nevertheless provide a proof-of-principle demonstration that the proposed unified navigation model can fulfil all of the criteria defined for replication of key adaptive behaviour observed in insects (Figure 5.1A).

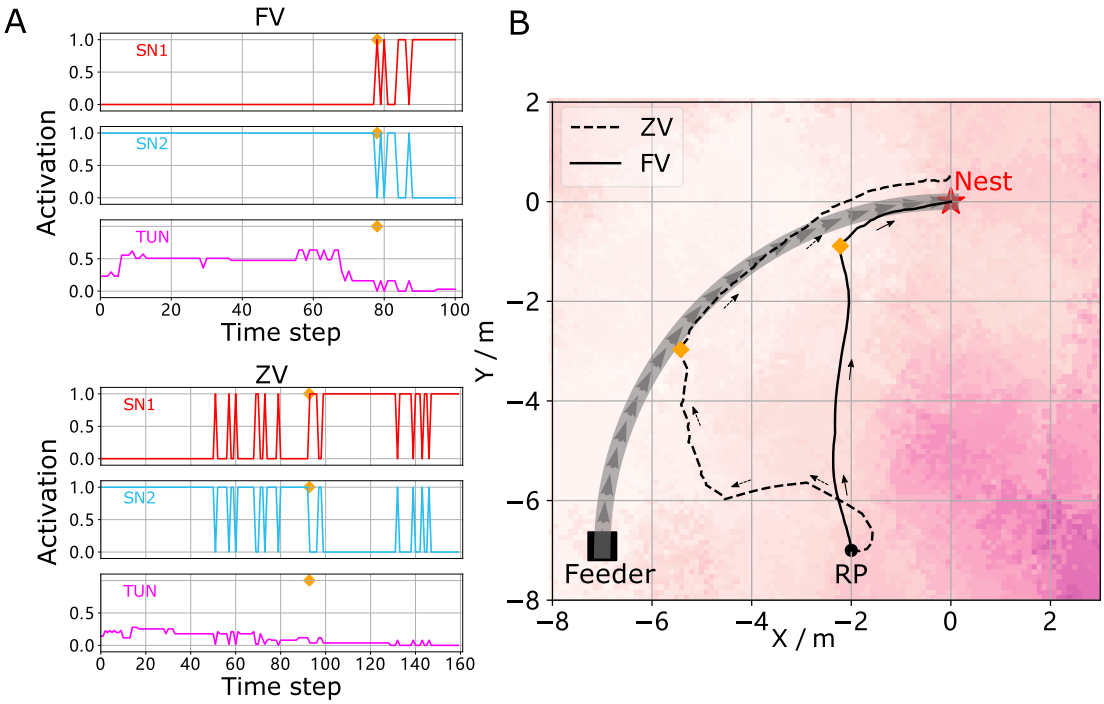

Figure 5.10: **Homing performances of the unified model reproducing main behaviours in insect navigation.** (**A**) Activation history of the SN1, SN2 and TUN (to demonstrate the instantaneous visual novelty readout of the MB) neurons during the simulated displacement trials. (**B**) Paths generated by the unified model under control of the context-dependent switch circuit during simulated FV (solid line) and ZV (dashed line) displacement trials.

5.3 Methods and Materials

All simulations and network models are implemented by Python 3.5 and make use of external libraries-*numpy*, *matplotlib*, *scipy*, *PIL* and *cv2*. The developed GUI are based on *PyQt5*. The UI design are based on the tool- *PyQt desinger* and then converted to Python code using *PyUIC*

5.3.1 Current Headings- Local and Global Compass

Current headings are modelled in the same way as that in Chapter 3.3.4.1.

5.3.2 Path Integration

The PI model implemented is that published by [10]. The core functionality arises from the CPU4 neurons that integrate the activation of TN2 neurons that encode the speed of the agent and the inverted activation of direction-sensitive I-TB1 neurons. The result is that the population of CPU4 neurons iteratively track the distance and

orientation to the nest (a home vector) in a format akin to a series of directionally-locked odometers.

The firing rate of the CPU4 neurons are updated by:

$$I^t_{CPU4} = I^{t-1}_{CPU4} + r(C^t_{TN2} - C^t_{I-TB1} - k) \tag{5.1}$$

Where the rate of the memory accumulation $r = 0.0025$; the memory loss $k = 0.1$; the initial memory charge of CPU4 neurons $I^0_{CPU4} = 0.1$.

The input of the TN2 neurons encoding the speed is calculated by:

$$\begin{cases} I_{TN2_L} = [\sin(\theta_h + \theta_{TN2})\cos(\theta_h + \theta_{TN2})]\boldsymbol{v} \\ I_{TN2_R} = [\sin(\theta_h - \theta_{TN2})\cos(\theta_h - \theta_{TN2})]\boldsymbol{v} \end{cases} \tag{5.2}$$

where $\boldsymbol{v}$ is the velocity (see Equation 3.28) of the agent and θ_{TN2} is the preference angle of the TN2 neurons. In this study $\theta_{TN2} = \pi/4$. The activation function applied to TN2 neurons is the rectified linear function given by:

$$C_{TN2} = \max(0, 2I_{TN2}) \tag{5.3}$$

As CPU4 neurons integrate the speed and direction of the agent, the desired heading of PI can be represented by the population encoding of these neurons, thus:

$$C_{PI} = C_{CPU4} \tag{5.4}$$

5.3.3 Coordination of Elemental Guidance Strategies

The coordination of the three main navigation strategies PI, VH and RF are realised in distinct stages. Firstly, Off-route strategies (PI and VH) are optimally integrated by weighing according to the certainly of each before a context-dependent switch activates either On-route (RF) or Off-route strategies depending on the current visual novelty.

5.3.3.1 Optimal Cue Integration

A ring attractor neural network is used to integrate the cues from the VH and PI guidance systems. As reported in [16] summation of directional cues represented in vector format leads to optimal angular cue integration which is the same case as real insects. Chapter 4 gives a biology plausible way to do this kind of computation based on a simple ring attractor neural network. There are two populations of neurons in this network, the first is the integration neurons (IN) which is the output population of the network. Constrained by the number of columns in each hemisphere of the insects CX, we set the number of the IN to be 8, and its firing rate is updated by:

$$\tau \frac{dC_{IN}}{dt} = -C_{IN} + g\left(\sum_{j=1}^{n} W_{E2E}^{ji} C_{IN}^{j} + X_1^i + X_2^i + W_{I2E} C_{UI}\right) \qquad i = 0, 1, ...7. \tag{5.5}$$

Where W_{E2E}^{ji} is the recurrent connections from j^{th} neuron to i^{th} neuron, $g(x)$ is the activation function that provides the non-linear property of the neuron:

$$g(c) = max(0, \rho + c) \tag{5.6}$$

Where ρ denotes the offset of the function.

In Equation 5.5, X_1 and X_2 generally denote the cues that should be integrated. In this study, X_1 and X_2 represent the desired heading of path integration (C_{PI}) and visual homing (C_{VH}). The desired heading of PI is also tuned by the tuning neuron (TUN) in SMP which is stimulated by the MBON of MB (see Figure 5.5A) and its activation function is defined by a rectified linear function, i.e.:

$$C_{TUN} = \min(k_{TUN} C_{EN}, 1) \tag{5.7}$$

Where k_{TUN} is the scaling factor.

Thus, the X_1 and X_2 for this ring attractor network can be calculated by:

$$\begin{cases} X_1^i = C_{TUN} C_{PI}^i \\ X_2^i = C_{VH}^i \end{cases} \quad i = 0, 1, ...7 \tag{5.8}$$

The second population of the ring attractor is called the uniform inhibition (UI) neurons modelled by:

$$\tau \frac{dC_{UI}}{dt} = -u + g\left(W_{I2I} C_{UI} + W_{E2I} \sum_{k=1}^{n} C_{IN}^k\right) \qquad i = 0, 1, ...7. \tag{5.9}$$

After arriving at a stable state, the firing rate of the integration neurons in this ring attractor network provides the population encoding of the optimal integrated output C_{OI}:

$$C_{OI} = C_{CN} \tag{5.10}$$

5.3.3.2 Context-dependent Switch

The model generates two current/desired headings pairs: the current heading of global compass decoded by C_{I-TB1} with the desired heading optimally integrated by the integration neurons of the ring attractor network C_{OI} and the current heading of local compass decoded by II-TB1 neurons C_{II-TB2} with the desired heading decoded by the output of the RF network C_{RF}. These two pairs of signal both are connected to the steering circuit (see Figure 5.8 and Chapter 5.3.3.3) but are turned on/off by two switching neurons (SN1 and SN2) in the SMP (Figure 5.8). SN2 neuron receives the activation from MBON neuron and is modelled as:

$$SN2 = \begin{cases} 0 & if \quad C_{MBON} < Thr_{SN2} \\ 1 & otherwise \end{cases} \tag{5.11}$$

While SN1 will always fire unless SN2 fires:

$$SN1 = \begin{cases} 0 & if \quad C_{SN2} = 1 \\ 1 & otherwise \end{cases} \tag{5.12}$$

Therefore, the context-depend switch is achieved according to the current visual novelty represented by the activation of MBON.

5.3.3.3 Steering Circuit

Steering circuit used in this chapter is the same as that in VN (see Chapter 3.3.4.4). But as now we should integrate the PI with VN based on the ON- and OFF-route assumption, the input of desired heading to the steering circuit should be changed to:

$$\begin{cases} C_{DH}^{0-7} = C_{SN1}C_{RF}W_{DH2CPU1L} + C_{SN2}C_{OI}W_{DH2CPU1L} \\ C_{DH}^{8-15} = C_{SN1}C_{RF}W_{DH2CPU1R} + C_{SN2}C_{OI}W_{DH2CPU1R} \end{cases} \tag{5.13}$$

The input of current heading to steering circuit is the same as (3.27).

5.3.4 Detailed Neural Connectivity of the Unified Model

Figure 5.11A shows a complete picture of the proposed model. Specifically, it highlights the final coordination system showing that CX computing the optimal navigation output with the modulation from the MB and SMP. In addition, offset connectivity pattern from the desired heading to the steering circuit that underpin the left/right shifting is clearly shown. Figure 5.11BC shows the network generating the desired heading of RF and VH respectively.

In addition, Table 5.1 provides details of all modelled neural circuits with their function and naming conventions with links to biological evidence for these neural circuits where it exists and the animal that they were observed in.

5.3.5 Simulations

The main parameter settings for all the simulations in this chapter and also that in Chapter 3 can be found in Table 5.2.

5.3.5.1 Reproduce the Optimal Cue Integration Behaviour

We evaluated the cue integration model by reproducing the results of [8] and [9]. The ants' outbound routes in [8] is bounded by the corridor, so here we simulate the

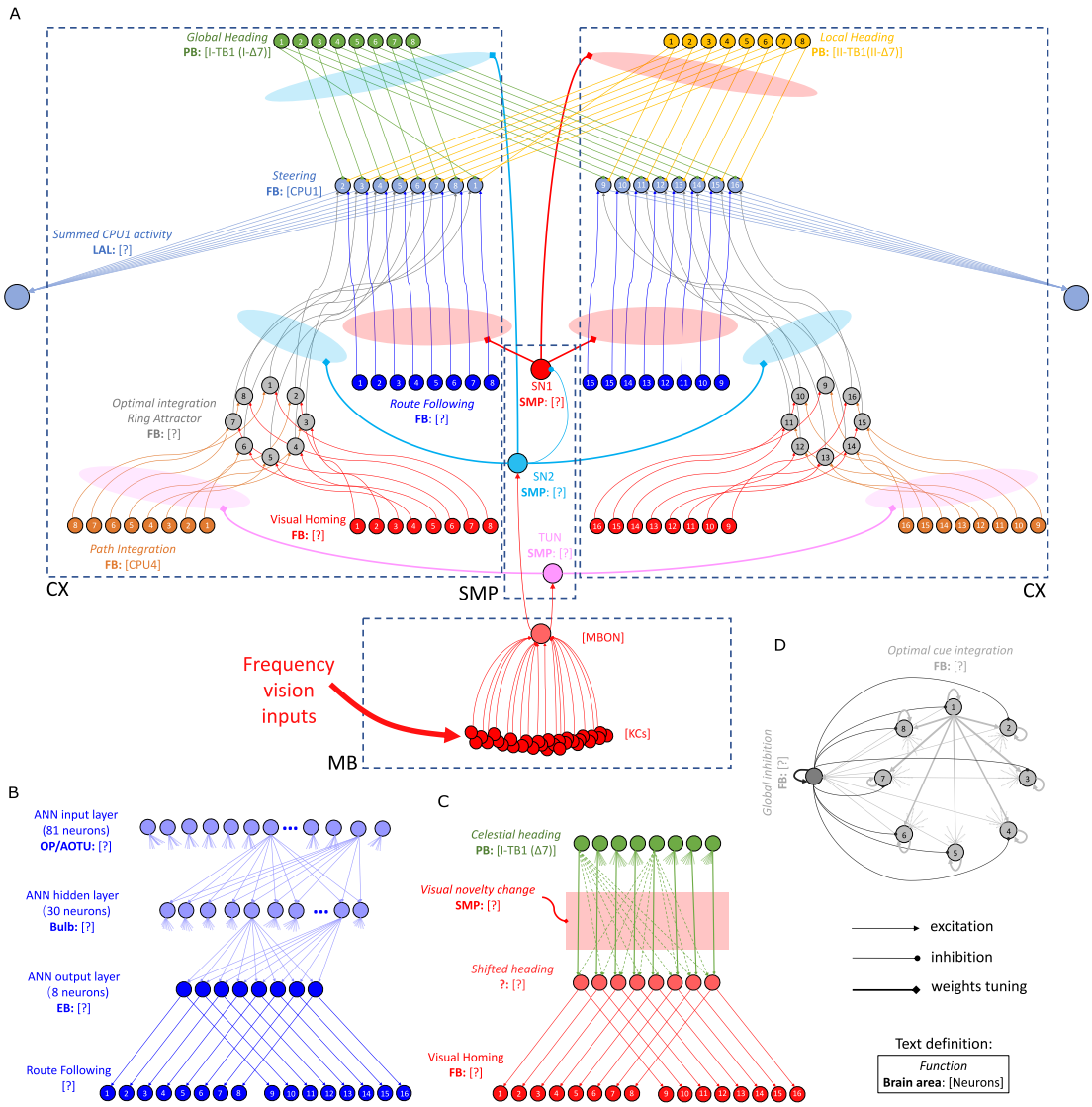

Figure 5.11: **The detailed neural connections of the proposed model.** (**A**): The detailed neural connections of the navigation coordination system. Note that the illustration of the global and local compass is for the easy of understanding not implying the real anatomy, actually they occupy the same set of PB columns. (**B**): The neural connection of the route following network. The input layer to the hidden layer is fully connected, so does the hidden layer to the output layer. (**C**): The network generating the visual homing memory. (**D**): The detailed neural connection of the ring attractor network for optimal cue integration.

velocity of the agent by:

$$\boldsymbol{v}_{out}^{t} = [rand(0, 2V_0) - V_0, V_0], \quad t = 0, 1...T_{out} \tag{5.14}$$

Where the function $rand(0, x)$ generates a random value from the uniform distribution of $[0, x]$, thus the speed of x-axis will be in $[-V_0, V_0]$ and will cancel each other during the forging. The speed of y-axis is constant so it will accumulated and be recorded

Table 5.1: The details of the main neurons used in the proposed model

Name	Function	Num	Network	Brain region	Neuron in Species(e.g.)	Reference
I-TB1	Global compass current heading	8	Ring attractor	CX	TB1 in *Schistocerca gregaria* and *Megalopta genalis*	[150] [10]
II-TB1	Local compass current heading	8	Ring attractor		Δ7 in *Drosophila*	[301]
S I-TB1	Copy of shifted global heading	8	Ring		No data	/
VH-L	VH desired heading left	8	Ring		No data	
VH-R	VH desired heading right	8	Ring		No data	
PI-L	PI desired heading left	8	Ring		CPU4 in *Schistocerca gregaria* and *Megalopta genalis*	[45] [10]
PI-R	PI desired heading right	8	Ring		P-F3N2v in *Drosophila*	[301]
RF-L	RF desired heading left	8	Ring		No data	/
RF-R	RF desired heading right	8	Ring		No data	
RA-L	Cue integration left	8	Ring attractor		No data	
RA-R	Cue integration right	8	Ring attractor		No data	
CPU1	Comparing the current and desired heading	16	Steering circuit		CPU1 in *Schistocerca gregaria* and *Megalopta genalis* PF-LCre in *Drosophila*	[45] [10] [301]
vPN	visual projection	81	Associative learning	MB	MB neurons in *Drosophila*	[193]
KCs	Kenyon cells	4000			*Camponotus*	[302]
MBON	visual novelty	1			*Apis mellifera*	[303]
TUN	Tuning weights from PI to RA	1	/	SMP	No data	/
SN1	Turn on/off the RF output to CPU1	1	Switch circuit		No data	
SN2	Turn on/off the RA output to CPU1	1	Switch circuit		No data	

by the PI model. And $V_0 = 1cm/step$ is the basic speed of the agent and T_{out} is the total time for outbound phase determining the length of the outbound route. As for the simulated homing route, we duplicate the outbound route when $T_{out} = 300$ but with a inverted heading direction. And then the visual navigation network was trained with images sampled along a simulated route (grey curve in Figure 5.5B and see details in Figure 5.12). Training process and results of the MB network are illustrated in Figure 5.13.

Tuning PI Uncertainty The agent in this simulation was allowed to forage to different distances of 0.1m, 1m, 3m or 7m from the nest to accrue different PI states and directional certainties before being translated to a never-before-experienced test site 1.5m from the nest. (RP1 in Figure 5.5B). For each trial, we release 20 agents with

Table 5.2: The detailed parameters settings for the simulations

Para.	Visual Homing	Optimal Integration tuning PI	Optimal Integration tuning VH	Route Following	Whole model ZV	Whole model FV
Thr_{KC} (3.14)	0.04	0.04	0.04	0.04	0.04	0.04
$\eta_{KC2MBON}$ (3.16)	0.1	0.1	0.1	0.1	0.1	0.1
k_{VH} (3.19)	2.0	2.0	2.0	/	0.5	0.5
k_{TUN} (5.7)	/	0.1	0.1	/	0.025	0.0125
Thr_{SN2} (5.11)	/	/	/	/	2.0	3.0
k_{motor} (3.23)	0.125	0.125	0.125	0.125	0.375	0.375
S_L (cm/step) (3.28)	4	4	4	4	8	8
initial heading (deg)	0∼360	0∼360	0∼360	0 / 180	90	0

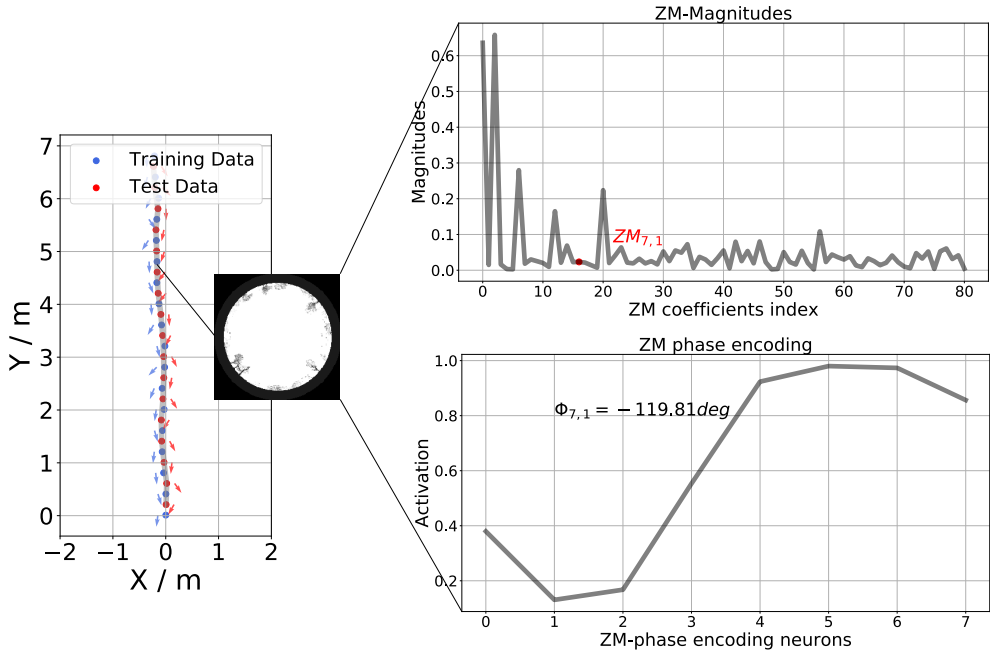

Figure 5.12: **The images used to train the MB network.** The training data and test data are labelled with red and blue dots respectively. The arrow along the route indicates the heading direction on the route.

different initial headings that is evenly distributed in $[0, 360)$. The headings of every agent at the position that is 0.6m from the start point is taken as the initial headings, and the mean direction and the 95% confidential intervals are calculated. As in the biological experiment, the angle between the directions recommended by the PI and visual navigation systems differed by approximately $130°$. As the length of the home vector increase (0.1m $\rightarrow$ 7m) the activation of PI memory becomes higher (Figure 5.7B), and increasingly determines the output of the ring attractor integration. Since the length of the home vector is also encoded in the activation of the PI memory neurons, the ring attractor can extract this information as the strength of the cue. As the visual familiarity is nearly the same in the vicinity of the release point, the strength of visual homing circuit remains constant and has more of an influence as the PI length drops.

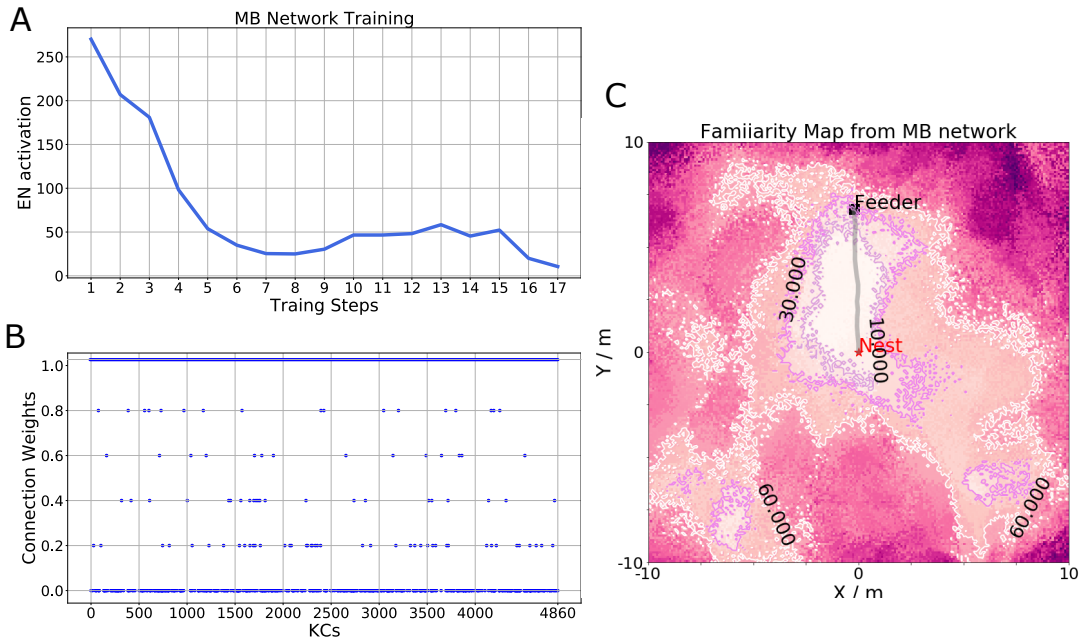

Figure 5.13: **The training process of MB network. (A)** The MBON activation decreases during training. **(B)** KC-MBON connection weights after training. **(C)** Heatmap of the visual familiarity measured by the trained MB network.

Tuning Visual Uncertainty The agent in this simulation was allowed to forage up to 1m from the nest to accrue its PI state and directional certainty before being translated to three different release points (RP1, RP2 and RP3 in Figure 5.5B). As the distance from nest increases (RP1→RP2→RP3) so does the visual uncertainty. For each trial, we release 12 agents with different initial headings that is evenly distributed in $[0, 360)$. The headings of each agent at the position that is 0.3m from the start point is taken as the initial headings, and the mean direction and the 95% confidential intervals are calculated.

Whole Model The simulated habitual route remains the same as in the simulation of visual navigation (Chapter 3.3.5.1) as is the learning procedure. The zero- and full-vector agents are both released at $[-2, -7]$ with the heading $0°$ and $90°$ respectively. The full-vector agent's PI memory is generated by letting the agent forage along the route from nest to feeder.

5.3.6 A GUI for Running the Simulation of the Unified Model

For the ease of running and exploring the proposed unified model and to efficiently visualise the model performance and the homing results, a GUI was developed (see

Figure 5.14). In this GUI, one can easily run the simulation of insect navigation from loading the simulated world, training the neural network to checking real-time homing trajectories and neuron activities.

5.4 Conclusion and Discussion

We propose that the insect navigation toolkit [36] [27] should be extended to include independent visual homing (VH) and route following (RF) systems (see Figure 5.1B for updated Insect Navigation Toolkit).

With the elemental guidance strategies defined, we propose that their outputs are coordinated through the combined action of the MBs and CX. Specifically, we demonstrate that a pair of ring attractor networks that have similar connectivity patterns of the CX-based head-direction system [153] [250] [157], are sufficient for optimally weighting multiple directional cues from the same frame of reference (e.g. VH and PI). The use of a pair of integrating RAs is inspired by the column structure of the FB which has 16 neural columns divided into two groups of 8 neural columns that each represent the entire 360°space. The optimal integration of PI and VH using a ring attractor closely matches the networks theorised to govern optimal directional integration in mammals [293] and supports hypothesis of their conserved use across animals (see Chapter 4). Optimality is secured either through adapting the shape of the activity profile of the input as is the case for PI which naturally scales with distance, or by using a standardised input activity profile with cross-inhibition of competing cues as is the case for VH in the model. The later schema avoids the need for ever increasing neural activity to maintain relevance.

To replicate the suite of navigational behaviours described in Figure 5.1 our network includes three independent ring attractor networks: the global compass head direction system [157]; the local compass head direction system [151] [153] [250]; and an Off-route integration system (modelled here). We would speculate that it is likely that central place foraging insects also possess a similar integration network for ”On-Route” cues (not modelled here) bringing the total number of RAs to four. The utility of RAs for head-direction tracking arises from their properties in converging

activity to a signal bump that can easily be shifted by sensory input and is maintained in the absence of stimulation. In addition, RAs also possess the beneficial property that they spontaneously weight competing sensory information stored as bumps of activity in an optimal manner. Thus, there are excellent computational reasons for insects to invest in such neural structures. Yet, it should be clear that the model proposed here represents a proof-of-concept demonstrating that the underlying network architectures already mapped to the CX (directional cues encoded as bumps of activity [151] [150]; various lateral shifting mechanisms [10] [152] [154]; RAs [153] [250] [157]) are sufficient to generate adaptive navigation but further studies are required to critique and refine the biological realism of this hypothesis.

While this assemblage recreates optimal integration of strategies that share a compass system, it does not easily extend to integration of directional cues from other frames of reference (e.g. VH and PI reference the global compass versus RF that references a local compass). Indeed as the CX steering network seeks to minimise the difference between a current and a desired heading, calibrating input signals from different frames of reference would require a similar calibration of their respective compass systems. Rather, the proposed model incorporates a context-dependent non-linear switching mechanism driven by the output of the MB that alternates between strategies: global compass based PI and VH are triggered when the surroundings are unfamiliar, but when in familiar surroundings engage local compass based RF. In summary, the adaptive behaviour demonstrated is the result of distinct guidance systems that converge in the CX, with their relative weighting defined by the output of the MB. This distributed architecture is reminiscent of mechanisms found in the visual learning of honeybees [254], and supports the hypothesis that the CX is the navigation coordinator of insects [12] [13] but shows how the MB acts as a mediator allowing the CX to generate optimal behaviour according to the context.

The resultant unified model of insect navigation Figure 5.1B and Figure 5.9 represents a proof-of-principle framework as to how insects might co-ordinate core navigational behaviours (PI, VH and RF) under standard field manipulations Figure 5.1A. Neuroanatomical data has been drawn from across insect classes (see Table 5.1) to

ensure neural realism where possible with performance compared to ant navigation behaviour in a single simulated desert ant habitat. The framework can be easily extended to new navigation behaviours observed in other insects from idiothetic PI [58] to straight line following [304] to migrations [305] as well as more nuanced strategies that flexibly use directional cues from different sensory modalities [221] [306] [307]. A priority of future works should be the investigation of the differences and commonalities in sensory systems, neural structures and ecology of different insect navigators and how they impact behaviour allowing for extension and refinement of the framework for different animals. Complementary stress-testing of models across different environments in both simulation and robotic studies are also required to ensure that model performance generalises across species and habitats and to provide guidance to researchers seeking the sensory, processing and learning circuits underpinning these abilities.

We proposed that the use of global and local frames in the navigation model could allow effective coordination enabling the agent to keep approaching the global destination while being responsive to local stimuli such as landmarks and obstacles. Although this idea of using global and local frames is inspired by observed facts of insects (like [308]), it is also a useful robotics engineering technique. For example, the route planning algorithm that consists of global and local planner [309] caring about the whole map and dynamic objects respectively. Thus, applying global and local compass could be an effective strategy in solving a wide range of problems especially those related to navigation.

In this thesis, we focus on 2D motion (i.e., only take yaw into account) simulation. How about the motion of flying insects where pitch and roll are also involved? Although theoretically by adding another same two circuits we can extend our model to the 3D version (similar to the recent implementation of pose estimation in [310]), we don't think there is a need for doing so. Because pitch/roll and yaw may act at different levels, namely, a navigation system is only responsible for generating the desired navigating heading (yaw) output, while the pitch and roll are controlled by the motor system as they are more related to kinetics and aerodynamics. A recent study has

shown that the learned visual memories during flight can also be used when navigating on the ground [311] may support this argument.

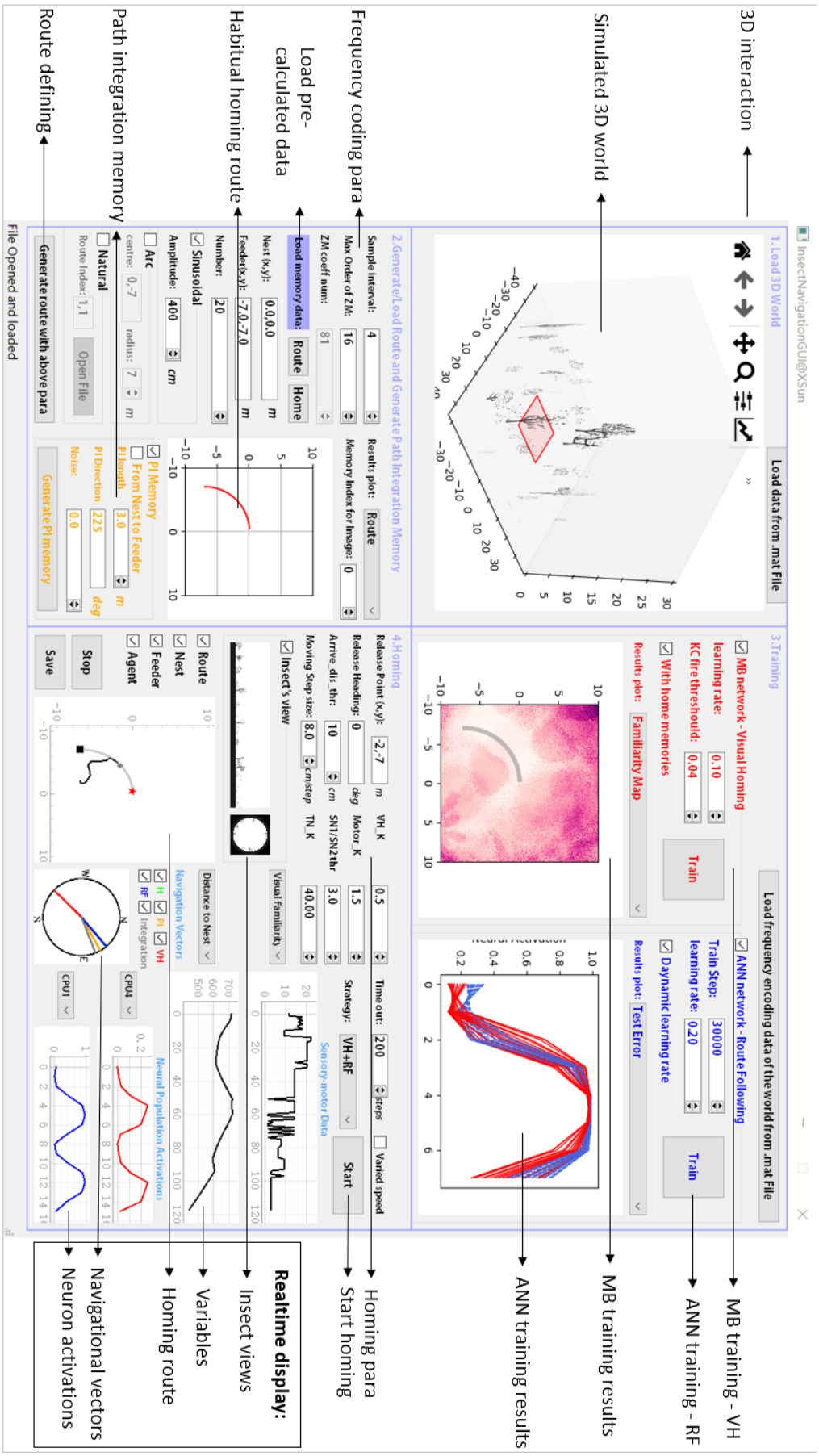

Figure 5.14: **The developed GUI for running the proposed model.** Panels are labelled with the functions.

Chapter 6

This Unified Model Can Also Replicate Odour Navigation Behaviours

Although the unified model presented in previous chapters can account for path integration, visual navigation, and their optimal coordination, as another crucial sensory information that insects rely on, olfactory cue also plays its role in navigational tasks. In this chapter, based on the similarities between the observed olfactory navigation behaviours and our unified model, an adapted model for reproducing olfactory related behaviour is presented. Simulation results of this extension of the unified model further demonstrate the bio-plausibility of the presented model.

6.1 Introduction

One of the most principal abilities for living animals to survive on the earth is to make use of varies sensory information provided by the natural environment to appropriately control their behaviour. The insect is such a class of animal with great capacity of using multiple sensory cues to navigate, which has fascinated researchers for more than a century. Among these cues, as introduced in Chapter 2.1, insects combines celestial cues (e.g. polarised light, sun position etc.) to maintain a stable compass for measuring heading direction, use visual cue for pinpointing the goal or following habitual routes. Recent neurobiology and modelling studies greatly push forward our understanding of these observed navigation behaviours in insects, especially the path

integration wherein the column neurons in CX continuously integrates the heading and velocity to update a home vector and then guide the agent back to the original points (see Chapter 2.3.1). Based on this model, we have previously shown how navigation based on visual information can be uniformly modelled and how insects could optimally coordinate different guidance systems at the neural level (see Chapter 3 and Chapter 5). However, except collective navigation based on pheromone trial, we know comparatively few about the neural mechanism of how individual insects may use olfactory cues for navigation.

To elucidate new behaviours, if possible, using the exiting model is always the first option because it requires no additional complexity. Given the observed olfactory related navigational behaviours introduced in Chapter 2.1.3 and our unified model, several similarities can be found: 1) chemotaxis that moving towards the location with a higher concentration of rewarded odour is analogical with the visual homing model guiding the agent to the location with higher visual familiarity; 2) odour-gated upwind following [114] wherein the agent will go upwind direction once sensed the odour, is similar with low-visual-familiarity triggered route following; 3) Behaviour of path integration's controlling the odour plume tracking in ants [21] resembles the optimal integration of PI and VH in our model. Based on these similarities, we want to ask if the presented model with small adaption can allow for the reproducing of olfactory navigation behaviours? To this end, we change the sensory input in our previous model from vision to olfactory, replace the learnt on-route RF direction by the upwind direction encoding and integrate it with PI via the same RA network. Results show that the unified model with small adaption can account for olfactory navigation behaviours both in flies and ants, thus filling the gap in understanding the neural basis of olfactory based navigation and further prove the plausibility of our model in deducing insect navigation behaviours. This work also suggests that the *sensory processing* $\rightarrow$ *CX* $\rightarrow$ *motor* chain may be a ubiquitous and conserved neural circuitry for mediating behaviour and coordinating multimodal cues and further demonstrate the coordinating role the CX plays in the insect brain.

6.2 Results

In the previous chapters, we have demonstrated that in the context of visual navigation, the output of trained MB can be regarded as the measurement of visual novelty and sequentially CX can use this signal to do gradient tracking (OFF-route: visual homing), memory retrieving (ON-route: route following) and contextual coordination (switching from OFF-route strategy to ON-route strategy) (Chapter 5). Likewise, when it comes to *Drosophila*'s odour navigation behaviours, the similar sensorimotor strategy seems to be applied: chemotaxis are like visual homing where agents aim to go to the sites with the higher value of preference (odour concentration or visual familiarity); Odour-gated upwind following (or anemotaxis) resembles the memory retrieving of route-following triggered by high visual familiarity. The following two subsections show the detailed results of adapting the unified model to reproduce these two kinds of olfactory navigation behaviours.

6.2.1 Adapted Visual Homing Model Can Reproduce Chemotaxis

As a classical behavioural assay, the larval taxis has been intensively studied. Evidence has shown that the key sensory information used by larva during taxing is the change of the perceived odour concentration [312]. Physiological and modelling research also shown that olfactory sensory neurons both in larvae and adult fly response to the decrease and increase of odour concentration [313] [314] [315] and then convey this information to modulate the motor pattern [316] [315] [228]. Interestingly, visual homing in our previous model (Chapter 3.2.2) was also implemented by following this idea. Therefore, based on the previous model, chemotaxis can be simply realised by changing the modulation signal from the change of visual familiarity to the change of odour concentration (see Figure 6.1A). As shown in Figure 6.1, the temporal change of odour concentration modulates the shifting of the current heading to generate the desired heading of chemotaxis, namely, with the increase of odour concentration the agent should go on moving in the current direction (run behaviour) while a turn should be made when concentration decreases (cast behaviour).

Figure 6.2 and Figure 6.3 demonstrates that the agents guided by the model can

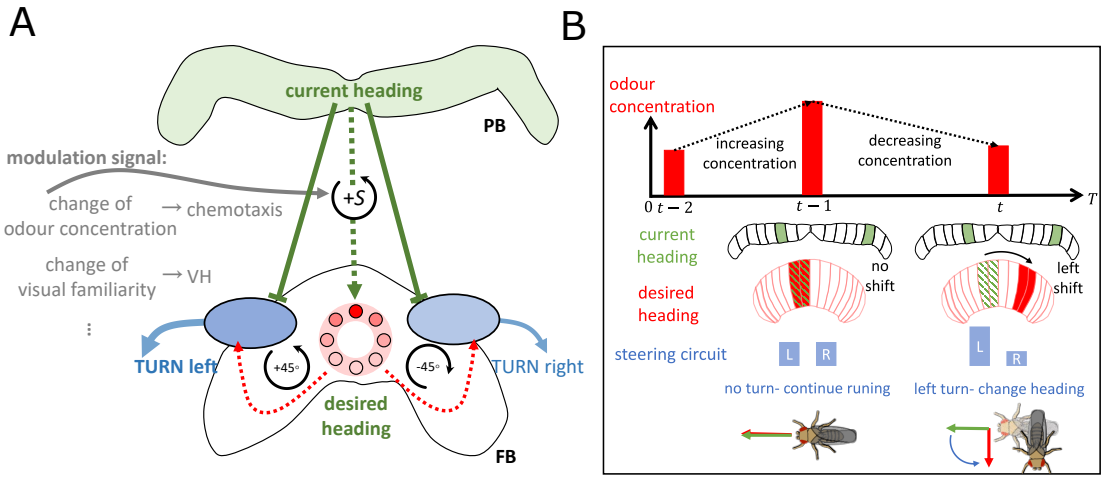

Figure 6.1: **The adapted VH model for generating chemotaxi behaviour. (A)** Schematic diagram of the general neural model generating gradient tracking behaviour like visual homing and chemotaxis. **(B)** Schematic diagram of the chemotaxis model based on the main idea that when perceived odour concentration temporally decreases, shift the current heading as the desired heading to make a turn through the steering circuit.

successfully track the odour concentration gradient. Start from different points, all the agents are moving towards the sites with higher concentration (see Figure 6.2 and Figure 6.3) and will stay within the region with the highest concentration has ever experienced (see Figure 6.2). These performances resemble some of the distinctive characteristics in behavioural data [317] [315] and therefore demonstrate that visual homing and chemotaxis could share the same neural mechanism that is suitable for this kind of behaviour with gradient tracking paradigm involved.

6.2.2 The CX Coordination Modulated by the MB/LH Can Account for Odour-gated Anemotaxis

Unlike in the laminar environment where the odour concentration can provide smooth gradient information that can be used to navigate, in a more turbulent environment, odour distribution is formed by the air or water dynamics [318], navigating in this type of environment seems more challenging but animals have developed a compact and effective strategy. Modelling and behavioural studies in moth [78] [231], flying fly [232], walking fly [233] [114] and marine plankton [319] suggested that the key of successful navigation in turbulent environment lies on the detecting of both the odour and flow direction. The main mechanism applied by these organisms is that

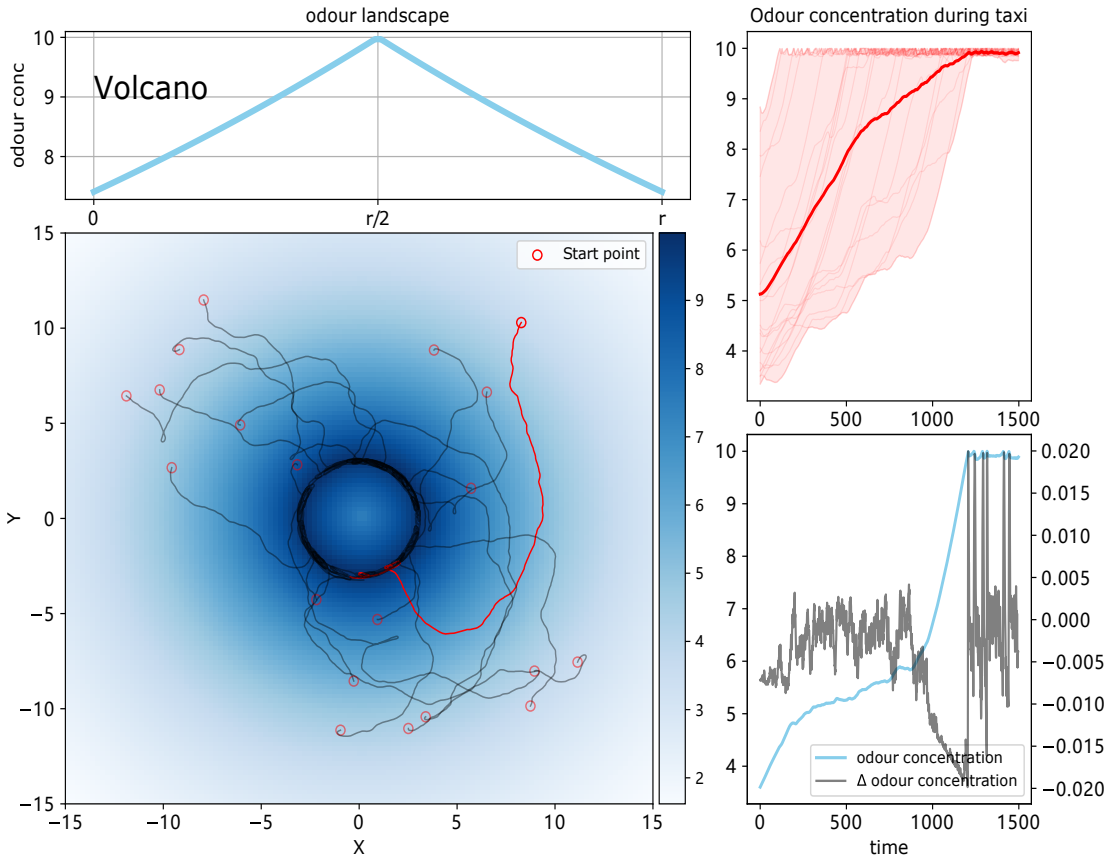

Figure 6.2: **The simulation performance of the model in two different odour landscapes- 'volcano'.** Odour landscape and trajectories are shown in the left and the sensed odour concentration of all the trials and the highlighted trial are shown in the right top and bottom respectively.

upwind (upstream) direction following (anemotaxis) is triggered by the onset of attractive odour. As demonstrated in previous chapters and several other studies [13] [44], the CX is is believed to be the navigational centre computing directional information, therefore, we assumed that wind direction is also encoded in CX (or at least has a copy stored in the CX). Similarly, the odour processing neurons in MB and/or LH conveying valence signal (non-directional) will activate the neurons carrying wind direction (directional) as the desired heading to dominate the steering circuit. The following subsection will introduce how the upwind direction can be neurally encoded based on known physiological data and the sequential subsection presents the adapted model for odour-gated anemotaxis.

6.2.2.1 Wind Direction Encoded by the Shifted Heading Direction

Experiments and studies have shown that *Drosophila* uses its antennae to gauge the wind direction as wind from varies directions will differentially displaces the two

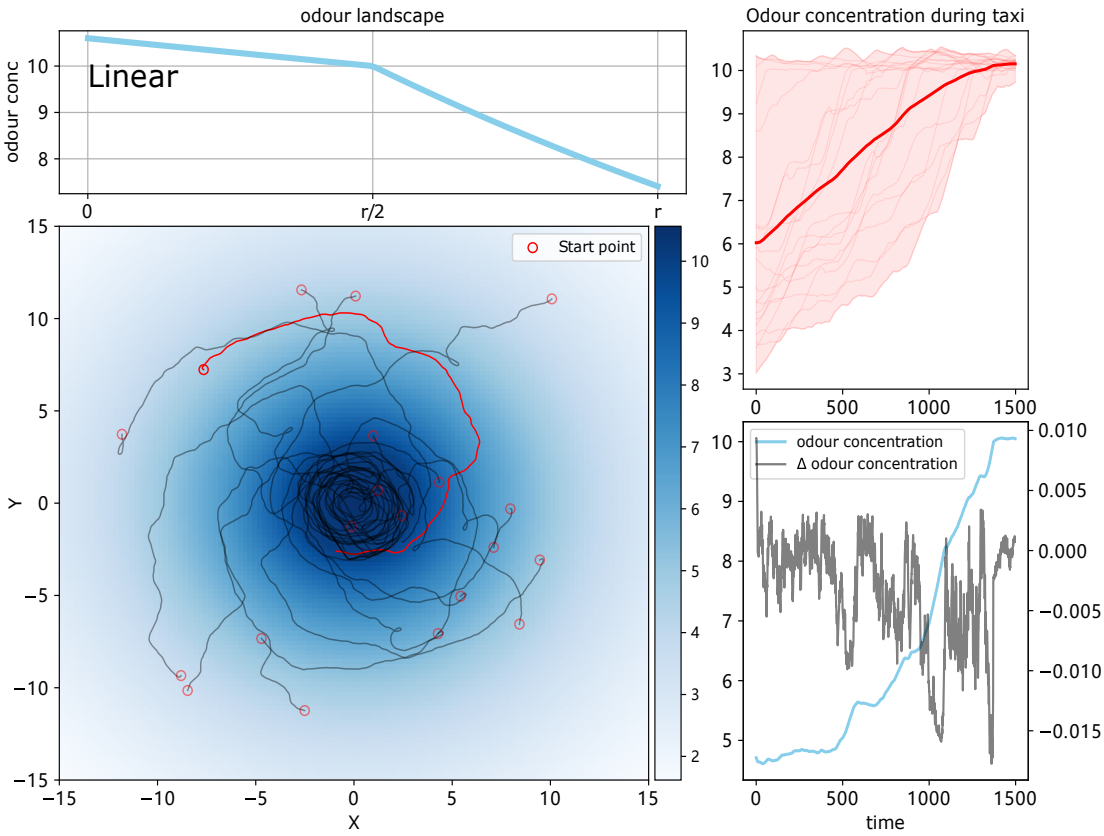

Figure 6.3: **The simulation performance of the model in two different odour landscapes- 'linear'.** Odour landscape and trajectories are shown in the left and the sensed odour concentration of all the trials and the highlighted trial are shown in the right top and bottom respectively.

antennae [320] [321] [322], consequently generating different mechanosensory signals. Here inspired by the very recent study shown that higher-order 'wedge project neurons' (WPNs) linearly encode this mechanosensory difference by integrating information from two antennae [322] and based on the evidence that neurons in the CX response to wind stimuli (bees: [140], locust: [296], cockroach: [162]), we assumed that WPNs could send its activation to the CX to modulate the shifting of the heading direction, then UWN (upwind encoding neurons) copy this shifted activation of current heading (i.e., I-TB1 neurons) to represent the upwind direction (see Figure 6.4A). The activation of WPNs with two different headings (0 and $\pi/2$) and swept wind direction (0 to π) are shown in Figure 6.4B. Note the different activation function for different heading direction as WPN neurons represent the relative angular difference between the wind and the heading direction, and that's also the reason why we can use its activation to modulate the shifting of current heading.

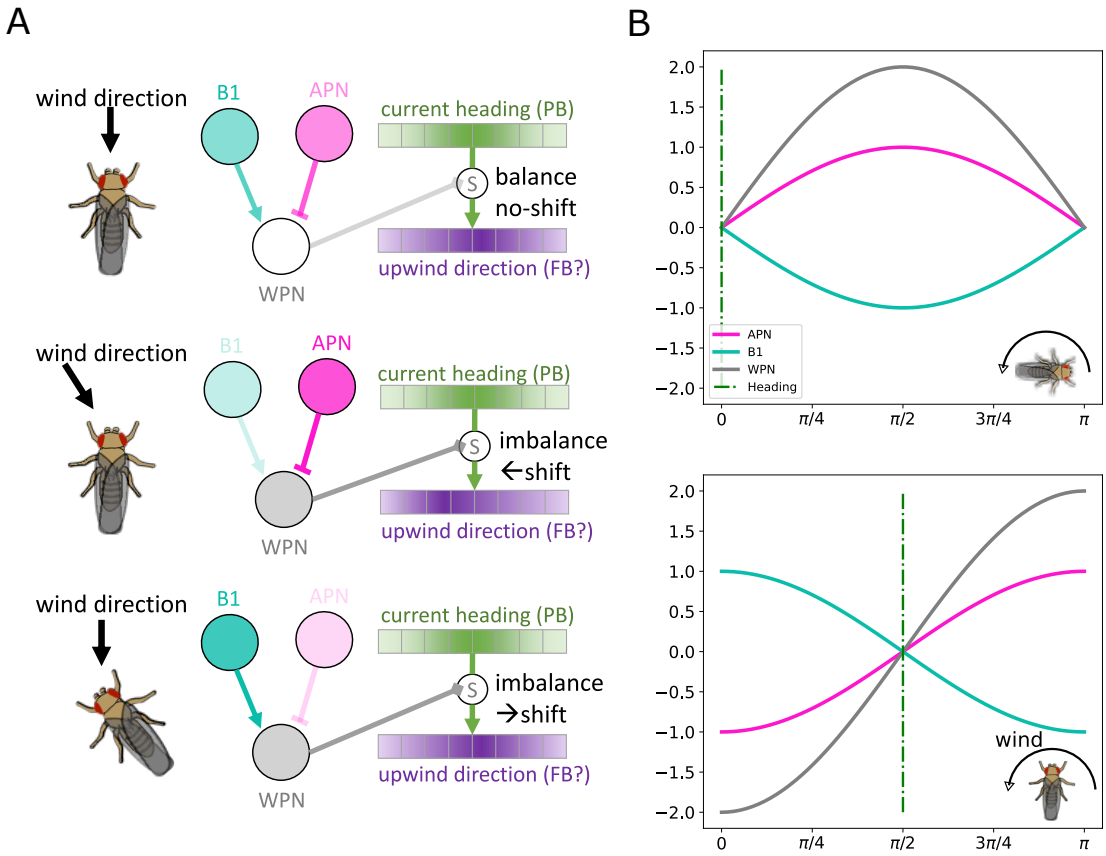

Figure 6.4: **The model of upwind direction encoding in insect brain. (A)** Schematic diagram of the upwind direction encoding in the insect brain. **(B)** Neural responses of the WPNs with different headings (0 and $\pi/2$) and wind direction stimuli is swept from 0 to π.

6.2.2.2 Output Neuron of Olfactory Processing Triggers Upwind Direction Encoding in the CX to Dominate Steering Circuit

In our previous model (Chapter 5.2.1), enough low visual novelty output from the MB will guide the CX to select the memory of route following (ON route strategy), similarly here, the output from the olfactory processing will trigger the selection of upwind direction as the desired heading (see Figure 6.5). As upwind direction is an egocentric cue which is determined by the relative angular difference to the agent's current head direction and anemotaxis should also lead the agent to go that direction, therefore injecting the upwind direction modelled in the way introduced in the previous section (see Figure 6.4) as the desired heading to the steering circuit will produce the ideal turning command. Hence, just by simply changing the modulating signal from visual novelty to odour concentration and changing the memory of route following to upwind direction encoding, we can build a model for odour-gated anemotaxis (see Fig-

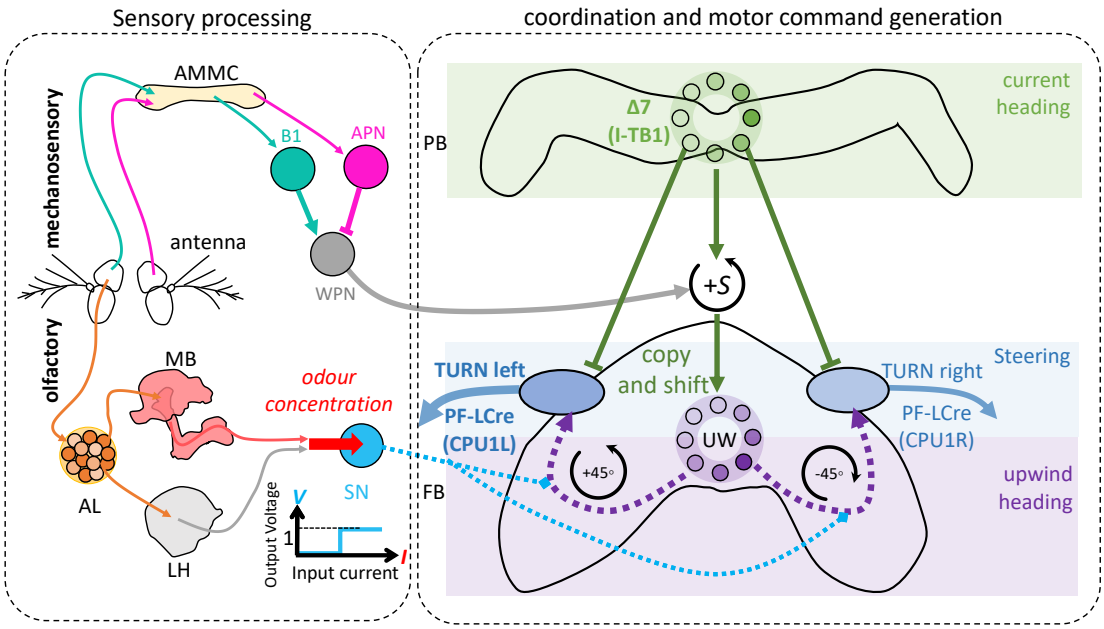

Figure 6.5: **The schematic diagram of the neural model generating the odour-gated anemotaxis behaviour.** Olfactory from the antenna is processed in MB/LH to get the odour concentration signal mediating the input inhibition encoded the upwind direction to the steering circuit. The upwind direction encoding is assumed to be stored in the FB of the CX. This neural pathway and circuits suit for similar types of mechanism where sensory information modulates the navigation behaviours.

ure 6.5). Performance of the model was tested in a scenario inspired by the behavioural study in [114], Figure 6.6 demonstrates the effectiveness of the model and shows the similar movement pattern observed in the real walking fly [114]. Note that when the perceived odour concentration is under the threshold, the agent will run randomly (for details see Chapter 6.3.

6.2.2.3 ON and OFF Response Based Contextual Strategy

When the chemotaxis and odour-gated anemotaxis are available in the fly's brain, the next challenge is to smartly select the optimal strategy given the current perceived environmental conditions. The flexibility of insects' contextually choosing different navigational strategies has been shown in [18]. Although the olfactory navigation algorithm can be divided into two types based on the odour dynamics [114], how insect coordinate different guidance systems in the natural environment remain unknown, here, inspired by the distinctive ON and OFF responses observed in *Drosophila* [114], we use the polarity of the modulation signal (Figure 6.1A) to determine the OFF and ON response and then use this signal to select the chemotaxis or anemotaxis behaviour

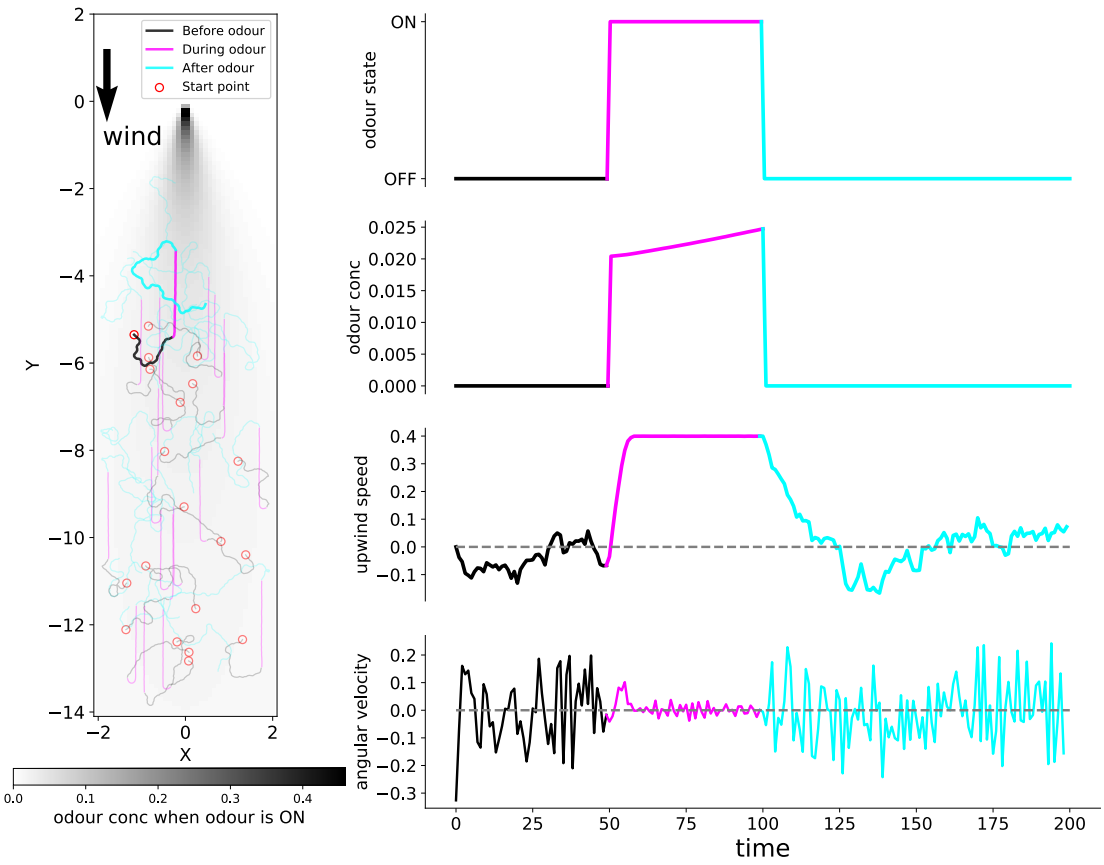

Figure 6.6: **The performances of the odour-gated chemotaxis model for 4 agents and each agent ran 5 trials.** The trajectories are coloured by the odour state (ON and OFF, illustrated in the first row of the right panel) and shown in left panel while averaged data of 20 trials are shown in the right panel (from the second row to the last row is the sensed odour, upwind speed and angular velocity respectively).

respectively. In fact, this ON and OFF response has the same function as to whether visual novelty is under or above the threshold determining whether the ON or OFF route strategy should be switched on in our previous model (Chapter 5). That's to say, the increase of the temporal change of the perceived odour produces an ON response and then anemotaixs is triggered, while the decrease of the temporal change of the odour defines an OFF response and then chemotaxis will dominate the steering circuit (Figure 6.7A). Figure 6.7B illustrates the connections of the hypothesised neurons from sensory information processing to the modulation of the navigational decision making in the integrated model. Using the ON and OFF response as the selector to coordinate different odour navigation strategies can maintain the main behavioural features observed in real animals [114] Figure 6.8) although sometimes the agent will perform not well due to the sensitive perception of odour dynamics (Figure 6.9).

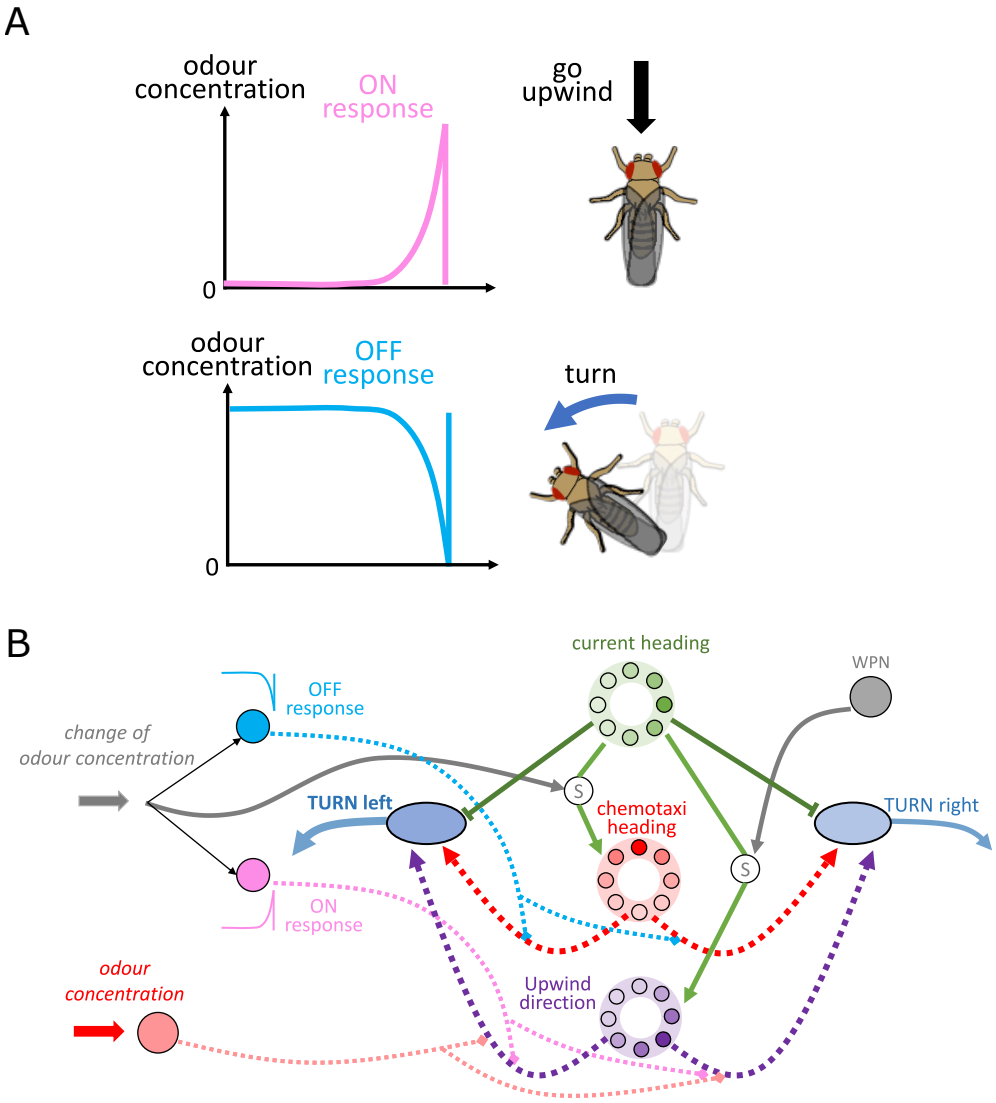

Figure 6.7: **The model of integration chemotaix and odour gated anemotaxis behaviour.** **(A)** Schematic diagram of the ON and OFF response and the corresponding behaviour it triggers. **(B)** Wire diagram showing the neural connections of the integrated model for the chemotaxis and odour gated anemotaxis behaviours.

6.2.3 Could This Model Also Deduce Ant's Odour Navigation Behaviours?

Although odour navigation in ants has not been studied so intensively as that of flies, several behavioural studies have already shown that ants take olfactory information as an important cue to find food [112] and use odour landmarks to pinpoint nest entrance [323] [130]. So here we ask if this model established based on data from fly can also explain some of the known odour navigation behaviours in ants. As demonstrated in [112] [113], The mechanism of odour-gate upwind following also exists in ant. Further, [21] has provided more precise data on how the odour navigation interacts

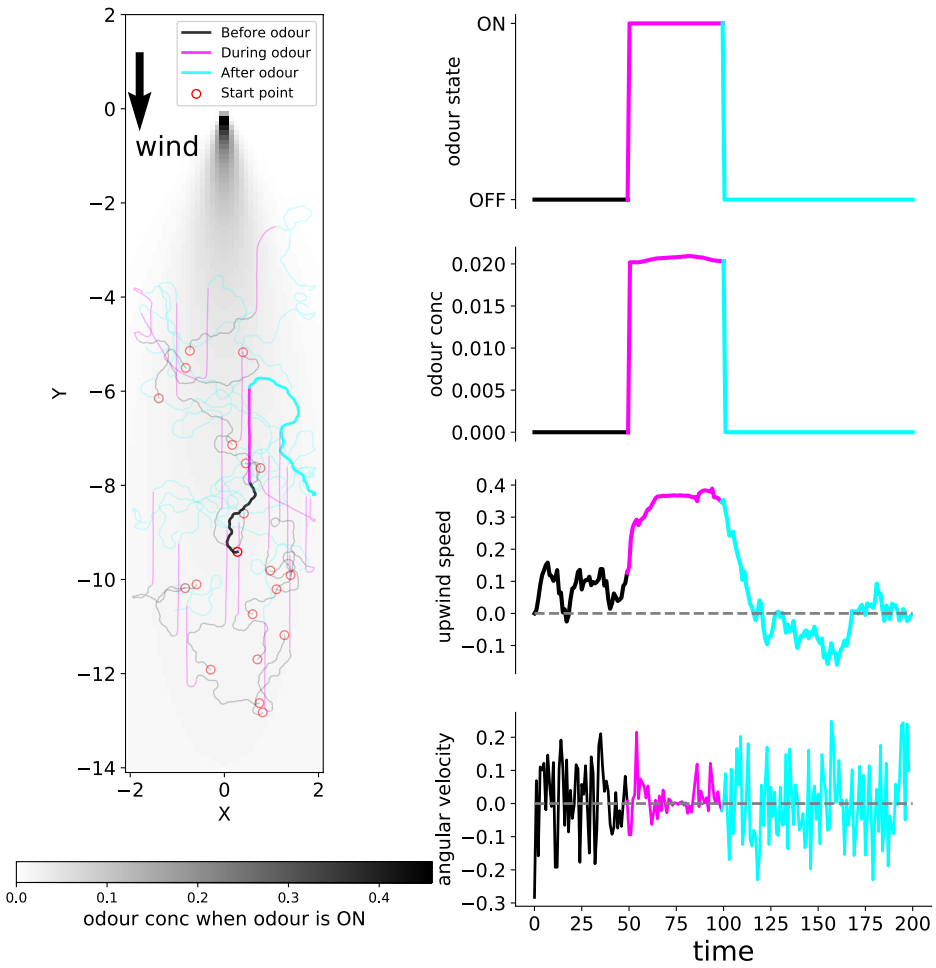

Figure 6.8: **The performances of integrated model can still reproduce the main characteristics of the observed behaviour.** The trajectories are colored by the odour state (ON and OFF, illustrated in the first row of the right panel) and shown in left panel while averaged data of 20 trials are shown in the right panel (from the second row to the last row is the sensed odour, upwind speed and angular velocity respectively).

with path integration. Here, based on our previous model optimally integrating PI and VH (Chapter 5.2.1), a unified model was established to integrate the odour navigation guidance including the chemotaxis (or in ant navigation, named odour homing) and the odour-gated anemotaxis with the PI (Figure 6.10A) using the same ring attractor (RA) network (Chapter 4). As depicted in Figure 6.10B, the desired headings recommended by OH and UW are gated by the OFF and ON response and are weighted by the odour concentration signal when injected to the RA to integrate with PI.

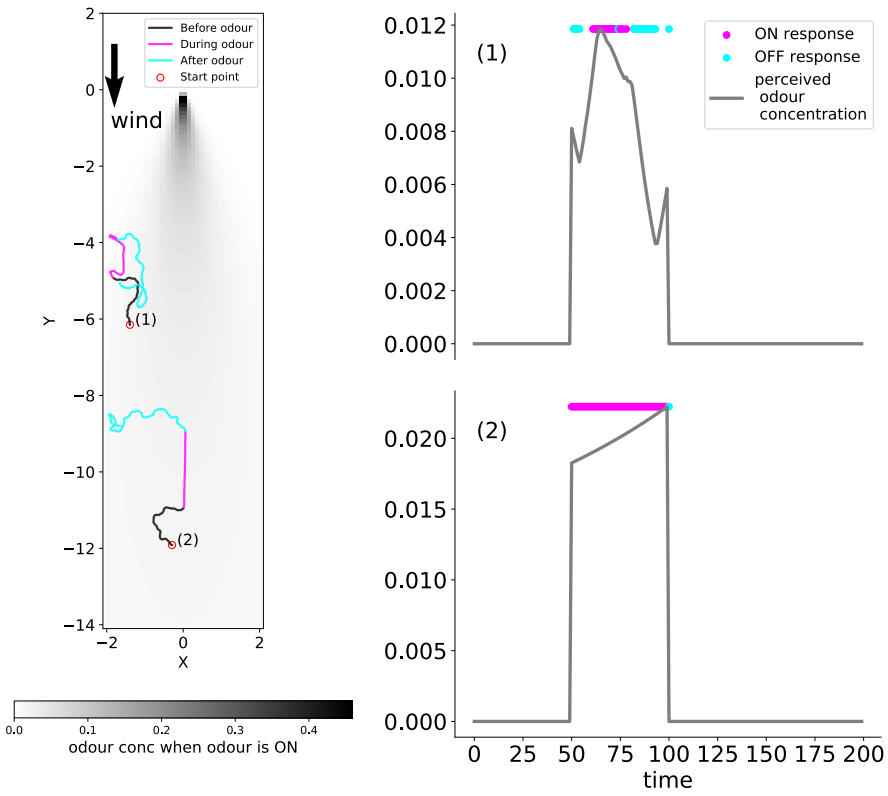

Figure 6.9: **Two examples of the trajectories of the selected agent and their ON and OFF responses.** Data were chosen from Figure 6.8. The trajectories are coloured by the odour state (magenta for odour ON and black and cyan for odour OFF) shown in the left panel, while the perceived odour concentration for these two agents are plotted in the right panel with the neural response states marked during odour.

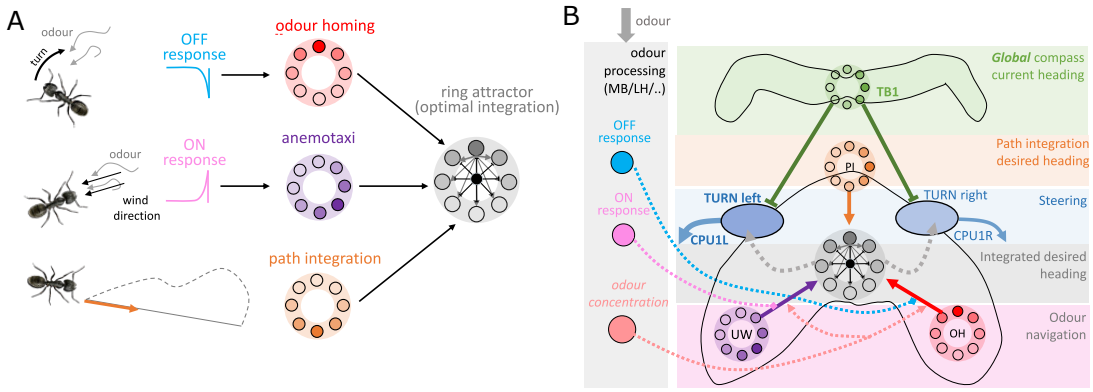

Figure 6.10: **The integrated model of ants navigation** Data were chosen from Figure 6.8. **(A)**: Schematic diagram showing ON and OFF response triggers different odour navigation behaviour and then be optimally integrated with PI by ring attractor network. **(B)**: Neural model illustrate how olfactory processing output mediates navigational coordination in the CX.

Behavioural data in [21] are benchmarked and results are shown in Figure 6.11A,B. Agents driven by the model will first be guided by PI memory (left panel in Figure 6.11C) as larger PI length dominate the RA output and then head to the upwind direction when the PI memory is going to zero and the rewarding odour is perceived

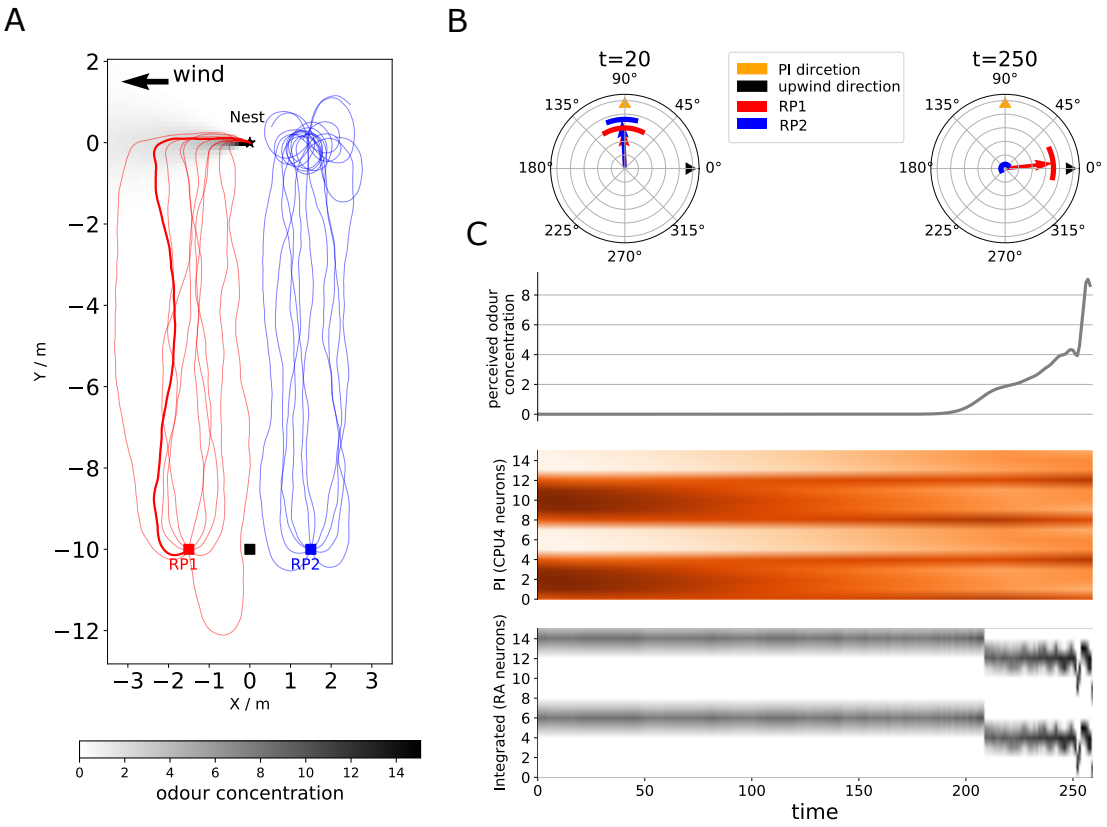

Figure 6.11: **The integrated model of ants navigation(A)**: The trajectories of the agents guided by the integrated model for ants. Simulation scenario is inspired by the experiment in [21]. **(B)**: Circular statistics showing the headings of the agents released from RP1 (red) and RP2 (blue) at the time of $t = 20$ (at the beginning of homing) and $t = 250$ (at the almost end of the homing). **(C)**: The instantaneous sensory value and neural activation of highlighted agent in **(A)** during homing. From top to bottom, the value of perceived odour concentration, the activation of PI memory neurons (CPU4) and the ring attractor excitation neurons.

to trigger the anemataxis (red lines in Figure 6.11A and red arrows in the right panel of Figure 6.11B) These replicate the real ants' data in [21]. Neural activation of PI and RA (integrated navigation output) during homing of the highlighted agent in Figure 6.11A are shown in Figure 6.11C and indicates the discharging of PI memory when homing and the ideal shift of the desired heading from OI to olfactory navigation.

6.3 Methods and Material

All simulations and network models are implemented by Python 3.5 and make use of external libraries-*numpy*, *matplotlib*, *scipy*.

6.3.1 Odour Field

As the basic sensory input, the spatial concentration distribution of the odour field is simulated simply based on the scaled exponential functions, with required changes according to the wind dynamics.

6.3.1.1 Odour Field without Wind

For the simulations in the static odour environment (i.e. no wind) as that in Figure 6.2 and Figure 6.3, the landscape of the odour concentration CON_o are modelled as, for 'volcano' shape:

$$CON_o = \begin{cases} ke^{\tau(r/2-d)} & if \quad d > r/2 \\ ke^{\tau(d-r/2)} & otherwise \end{cases} \tag{6.1}$$

and for 'linear' shape:

$$CON_o = \begin{cases} ke^{\tau(r/2-d)} & if \quad d > r/2 \\ k - 0.2e^{\tau(d-r/2)} & otherwise \end{cases} \tag{6.2}$$

where d is the distance from the position (x, y) to the odour source (x_s, y_s). Thus, $d = \sqrt{(x-x_s)^2 + (y-y_s)^2}$. k is the scale factor, r is the radius of the odour source and τ is decay factor.

6.3.1.2 Odour Field with Wind

To simplify the simulation of the odour plume dynamics, all the simulations in this chapter are conducted under the condition of constant wind speed u and wind direction θ_w, and we assume that the odour plume will ideally flow to the downwind area, i.e., the odour concentration in the upwind area will always be zero. The source of the odour constantly emits at the rate q , Then the odour concentration at position (x, y) can be calculated by:

$$CON_o = \begin{cases} \frac{q}{u\sigma_{xy}\sqrt{2\pi}} e^{-\frac{d^2}{2\pi\sigma_{xy}}} & if \cos\theta > 0 \\ 0 & otherwise \end{cases} \tag{6.3}$$

where $d = \sqrt{(x-x_s)^2+(y-y_s)^2}\sin\theta$ is the projected distance from the odour source. And σ_{xy} is calculated by $\sigma_{xy} = K_s d$ where $K_s \in [0.5, 0.3, 0.2, 0.15, 0.1]$ is the tuning factor determined by the stability of the odour. And θ is the angel between the vector pointing from the position to the source and the wind direction, so can be computed by:

$$\theta = \arccos \frac{(x-x_s)(u\cos\theta_w)+(y-y_s)(u\sin\theta_w)}{\sqrt{(x-x_s)^2+(y-y_s)^2}u} \tag{6.4}$$

6.3.2 Neural Model

We use the simple firing rate to model the neurons in the proposed networks, where the output firing rate C is a sigmoid function of the input I if there is no special note. In the following descriptions and formulas, a subscript is used to represent the layers or name of the neuron while the superscript is used to represent the value at a specific time or with a specific index.

6.3.2.1 Current Heading

The model of the current heading is the same as that in Chapter 3.3.4.1, but only the global compass, (i.e. the activation of I-TB1 neuron) is used here as navigation behaviours we reproduced in this chapter are all assumed using the global compass as the external direction reference.

6.3.2.2 Upwind Direction Encoding

The upwind direction is decoded as the activation of UW neurons copied and shifted from heading neurons (I-TB1), the value of this shifting is determined by the angular difference between the current heading (θ_h) and wind direction (θ_w) encoded by the firing rate of WPN neuron. And the value of WPN neuron is defined as the difference of the antennal deflection encoded by B1 and APN neurons as:

$$C_{WPN} = C_{APN} - C_{B1} = \sin(\theta_w - \theta_h + \pi) - \sin(-(\theta_w - \theta_h + \pi)) \tag{6.5}$$

Then population activation of upwind direction neurons (UW) can be calculated

	$< Thr_{off}$	$> Thr_{off} < Thr_{on}$	$> Thr_{on}$
$< Thr_o$	Random	Random	ON
$> Thr_o$	OFF	ON	ON

Table 6.1: 'Truth table' of the ON and OFF response of the modelled fly odour navigation. The column lists the state of sensed odour concentration while the row indicates the state of the changing of odour concentration.

by:

$$C_{UW} == C^j_{I-TB1}, j = \begin{cases} i + offset & if \quad i + offset \leq 7 \\ i + offset - 7 & otherwise \end{cases} \tag{6.6}$$

6.3.2.3 Fly- ON and OFF Response Triggers Anemotaxis or Chemotaxis

Different navigation strategy will dominate the motor system according to the sensory inputs, i.e., in this chapter, the change of perceived odour concentration. This coordination is modelled as a contextual switching that is very similar with the mechanism with SN1 and SN2 neuron involved in Chapter 5.3.3.2 to define the final output of odour navigation (C_{ON}):

$$C^i_{ON} = \begin{cases} C^i_{chemo} & if \quad OFF\ response \\ C^i_{anemo} & if \quad ON\ response \end{cases} \tag{6.7}$$

And how the sensory information determine the response is shown in Table 6.1, where Random means no reliable sensory input is available, the agent will move forward to a random direction.

OFF Response- Chemotaxis The chemotaxis model is adapted from the previous visual homing model (see Chapter 3.3.4.2) by changing the change of visual familiarity signal from the MBON neuron (ΔC_{MBON}) to the change of the odour concentration to determine the shifting value, thus the desired heading of chemotaxis is:

$$C^i_{chemo} = C^j_{I-TB1}, j = \begin{cases} i + offset & if \quad i + offset \leq 7 \\ i + offset - 7 & otherwise \end{cases} \qquad i = 0, 1, ...7 \tag{6.8}$$

Note that, in Chapter 3.3.4.2, i, j both are integer for the ease of computing, thus, the shifting accuracy is 45°, but here to more accurately model the desired heading and to achieve better performance, the shifting accuracy was set to be 4.5°by interpolating neuron activation of I-TB1 from 8 to 80 then down-sampling to 8 to generate shifted desired heading.

The relationship between the ΔC_o and the $offset$ is shown as following:

$$offset = \begin{cases} 0 & if \quad \Delta C_o < 0 \\ \min(\lfloor k_{chemo} \Delta C_o \rfloor, 3) & otherwise \end{cases} \tag{6.9}$$

Then the desired heading of OH will be fed into the steering circuit (see Chapter 3.3.4.4) to compare with the current heading to generate the motor command.

ON Response- Odour-gated Anemotaxis As shown in Table 6.1, when the ON response is determined, the agent will follow the upwind direction, thus the desired heading input to steering circuit should be the upwind direction encoded by UM neuron ((6.6)):

$$C^i_{anemo} = C^i_{UW} \tag{6.10}$$

6.3.2.4 Ants- integration with PI

The modelling of ants' odour navigation integrated with PI can be regarded as the extension of the fly's odour navigation introduced in Chapter 6.3.2.3 and an application of the unified model of insect navigation presented in Chapter 5. Specifically, the final output of olfactory navigation is determined by the ON and OFF response (see Table 6.1), and then is integrated with PI via RA like that in the optimal integration of PI and VH. Thus the $X1$ in (5.5) should be:

$$X_1^i = C_{PI}^i \qquad i = 0, 1, ...7 \tag{6.11}$$

and $X2$ in (5.5) should be:

$$X_2^i = \begin{cases} k_o CON_o C_{OH}^i & if \quad OFF\ response \\ k_o CON_o C_{anemo}^i & if \quad ON\ response \end{cases} \tag{6.12}$$

Then the output of optimal integration (OI) of the RA acts as the only desired heading input to the steering circuit:

$$\begin{cases} C_{DH}^{0-7} = C_{OI} W_{DH2CPU1L} \\ C_{DH}^{8-15} = C_{OI} W_{DH2CPU1R} \end{cases} \tag{6.13}$$

As only the global compass is needed in this chapter's modelling. Thus the input of current heading will always be the excitation of the I-TB1 neuron:

$$\begin{cases} C_{CH}^{0-7} = C_{I-TB1} \\ C_{CH}^{8-15} = C_{I-TB1} \end{cases} \tag{6.14}$$

The output of the steering circuit (i.e., the summed activation of the left and right CPU1 neurons) is used to generate the turning command in the way that is same as (3.23).

6.3.3 Simulations

In all simulations, at each time step, the simulated agent (walking fly or ant) will sense the odour sensory based on its current location and then update neural activation to generate the desired moving direction and finally move one step to that direction (the same as (3.28) and (3.29) in 3.3.5). Note that compared to the implementation of the motion control in 3.3.5, here to make the motion more realistic, a random wandering component is added in the following way:

$$\theta_M = k_{motor}(\sum_{i=0}^{7} C_{CPU1} - \sum_{i=8}^{15} C_{CPU1})(1 - w_{random}) \pm \pi/4 \times w_{random} \tag{6.15}$$

Table 6.2: The detailed parameters settings for the simulations in this chapter.

		Fly-Chemotaxis		Fly-Anemotaxis	Fly-Integrated	Ant-Integrated
		volcano	Linear			
odour	k	10	10		/	
	τ	0.1	0.1			
	r	6	6			
	q	/	/	10.0	10.0	20
wind	u	no wind		10.0	10.0	10.0
	w_θ			$-\pi/2$	$-\pi/2$	π
model and simulation	Thr_o	/		/	0.001	1.2
	Thr_{on}				0.02	0.5
	Thr_{off}				-0.0002	-0.0002
	k_o				/	2.0
	k_{chemo}	100.0	100.0	/	100.0	100.0
	k_{motor}	1.0	1.0	1.5	1.5	1.0
	S_L	0.02	0.02	0.4	0.4	0.05
	Heading	random	random	random	random	$0-2\pi$

where w_{random} scales the effect of this random wandering, thus even in the simulation of OH, individual agent can have both left and right turn.

The position of odour sources in all simulations are all set to $(0, 0)$, i.e., $x_s = 0, y_s = 0$. Other main parameters are listed in Table 6.2

6.3.3.1 Fly- Chemotaxis

To test the performances of the chemotaxis behaviour, 5 simulated agents with randomly generated heading direction starts from 5 randomly generated locations in the zone of $(-12 < x < 12, -12 < y < 12)$, and then driven by the model for 1500 steps. Then we run this simulation for 4 times in two different odour landscapes ('linear' and 'volcano') to get the results shown in Figure 6.3 and Figure 6.2.

6.3.3.2 Fly- Anemotaxis

To reproduce the behavioural data in [114], the odour was only set on during the second a quarter of total time (e.g, if the agent is set to run 200 steps, then the odour-on time will in 50-100 steps). Four agents with randomly generated heading starts from randomly generated locations in the zone of $(-1.5 < x < 1.5, -13 < y < -5)$, and then guided by the model to run 200 steps. The simulation was conducted for 5 times and the results are shown in Figure 6.5.

6.3.3.3 Fly- Integrated ON and OFF Response

The whole simulation settings are the same as that in the last section except for some model parameters listed in Table 6.2, as this simulation is conducted to verify the integrated model.

6.3.3.4 Ants- Odour Navigation Integrated with PI

To reproduce the behavioural data in [21], we first generate PI memory encoding the home vector with 10m length and $\pi/2$ direction. Then at each release point ($(-1.5, -10)$ and $(1.5, -10)$), we released 10 simulated full-vector (10m-long and pointing to $\pi/2$) ants with different initial headings sampled uniformly from $0 - 2\pi$, see also Table 6.2.

6.4 Conclusion and Discussion

This chapter presents a biology constrained model for interpreting the olfactory navigation behaviours not only in flies but also in ants. This model is simply adapted from the unified model presented in Chapter 5 by changing the sensory input. Simulation results demonstrate that the adapted unified model can reproduce several important characteristics of real animal [315] [114] [21] and thus further suggest that the unified model may be a conserved neural mechanism underpinning multimodal sensory-motor behaviours across insect species. Besides, as the first step to model the wind direction and how the olfactory navigation integrates with PI based on the biological data, testable predictions can be made to provide inspirations for biological studies. For example, ants with ablated CX will fail to use the upwind direction to pinpoint a goal when the attractive odour is perceived.

We further propose the role of the CX in insect navigation is to coordinate cues from multiple guidance systems by continuously doing directional (vector) computations. While the processed sensory information (non-directional) from other brain regions (e.g., MB, LH, ect.) can modulate this coordination in the CX in a way of tuning the weighting of corresponding guidance. This *sensory-processing* $\rightarrow$ *CX* $\rightarrow$

motor pathway may be the fundamental mechanism underlying flexible and complex navigation behaviours. Given the neurobiological data that FB in the CX receives lots of signals from other brain regions, it's likely that with all the desired headings stored in FB, the CX optimally integrates them according to the real-time modulating signal determined by the current sensory experience and then sends this final output to the motor centre.

In the presented model, the modulating signals (odour concentration and the temporal change of odour concentration) injected to the CX are manually provided. But we hypothesise that this signal can be supplied by MB and/or LH given the fact that olfactory processing in insects brain happens in these two brain regions. However, whether the MB and LH compete or cooperate with others to generate such signal still needs investigation. Or they are responsible for different behaviour as the MB for learnt memory while LH exclusively involves in innate behaviours given the recent evidence in vision processing [189]. Although we proposed that multi-guidance coordination happens in the CX, whether the integration of innate and learnt cues also happens in the CX or they are just combined to generate the modulating signal is still unknown. To answer this question, the key point is to distinguish which information is stored in the CX, thus identifying the input arrays to the CX seems to be crucial for the next step to understand the neural basis of insect navigation.

The focus of this chapter is attached to the olfactory navigation, but visual navigation can be easily integrated to the proposed model to make our unified model more completed. Here we will propose one possible way. Since the VH and OH (or chemotaxis) share the same mechanism to generate the desired heading by shifting the current heading according to the temporal change of the sensory information, these two shiftings can be directly summed to obtain a single shifting signal. Following this idea, more sensory cues can be added in to generate a unified shifting signal representing the animal's integrated valence of the current complex surroundings contain varies cues. Then the shifted current heading is integrated with PI and UW by RA. Finally, the RF still acts like the on-route strategy that triggered by enough low visual novelty. Nevertheless, integrating the modulating signal in a winner-take-all way before tuning

the coordination in the CX is also possible. Because directly telling the CX that which sensory cues (here, vision or olfactory) should be relied on also seems to an effective way. Indeed, there are also other possible mechanisms to integrate all the components described in this thesis, assessing which one is more biological realistic depends on more anatomical and physiological data. But the core idea that the CX coordinating multiple guidance according to the corresponding sensory experience encoded by the processing from other brain regions should be reserved.

Chapter 7

General Discussion

7.1 Key Contributions and Future Work

By adopting the computation model as a tool to understand insect navigation behaviours, this dissertation presents a unified model constrained by known anatomical and physiological data to unveil the possible neural mechanisms of insect navigation. Simulation results demonstrate that this model can reproduce the behavioural data observed in real insects and therefore makes the following main contributions to the field (and also answered the question raised in Chapter 1).

- Chapter 3: A frequency encoding based unified model for visual navigation has been developed and can account not only for the visual homing but also route following behaviours. How insects may benefit from frequency encoding (compared with pixel-wise) in extracting the useful information for specific navigation tasks has been discussed.

- Chapter 4: A biology plausible ring attractor model of optimal integrating multiple guidance systems has been built, which provides a possible solution in filling the gap from behaviour to the neural basis concerning cue integration in insect navigation.

- Chapter 5: Computations involved in the proposed unified model are mapped to specific brain regions and neurons based on the known biological data and plausible hypothesis, emphasising that the CX is the coordination centre with

the capacity of directional computing while the MB is the valence calculator sending the non-directional signal to the CX as the weighting to modulate the coordination. An overall figure (see Figure 7.1) was drawn to summarise the hypothesised functional roles played by every neuropil and the information flowing through them.

- Chapter 6: This unified model can also explain the olfactory navigation behaviours in insects thus further demonstrate how useful the *sensory-processing* $\rightarrow$ *CX* $\rightarrow$ *motor* pathway applied in the unified model is for interpreting contextual navigation behaviours.

- This model also provides many testable predictions for neurobiological and behavioural studies which are listed below:

(a) Because the proposed ring attractor network responsible for optimal cue integration is assumed to be in the FB of the CX, there should be some neurons and connections forming this circuit in the FB. That is to say, in the FB, there are neurons with recurrent excitatory connection and uniform/global inhibitory connections. Further, animals will fail to optimally coordinate different guidance systems with the FB blocked.

(b) As the motor command is generated by the mismatch of the current heading and the desired heading via the steering circuit. Like the distinctive activation pattern observed in *Drosophila* [151], there should be another set of neurons activate collectively in a similar way. Furthermore, these two sets of neurons all have connections with the CPU1 neurons.

(c) In the unified model, the output of MBONs modulate the coordination in the CX. Therefore, there must be direction/indirection connections between the lobe of the MB with the FB of the CX. If this connection is ablated, the animals can not do correctly contextual coordination, for example, they can not switch from off-route to on-route strategy.

(d) As memory-based visual navigation is learned in both the MB and the CX, thus lesion on whether the MB and the CX will affect the visual navigation ability. More specifically, the insect loses the ability to approach more visually familiar locations without the MB whilst ablating the CX will disable route learning.

(e) The performance of cue integration will be affected by manually manipulating the weighing of the cues. For instance, like that in [8], [9], if the odour (CO2) spreads more widely (i.e., a wider and stronger distribution of the concentration) to the releasing points in Figure 6.11, the plume following behaviour during homing will happen earlier with the same PI length.

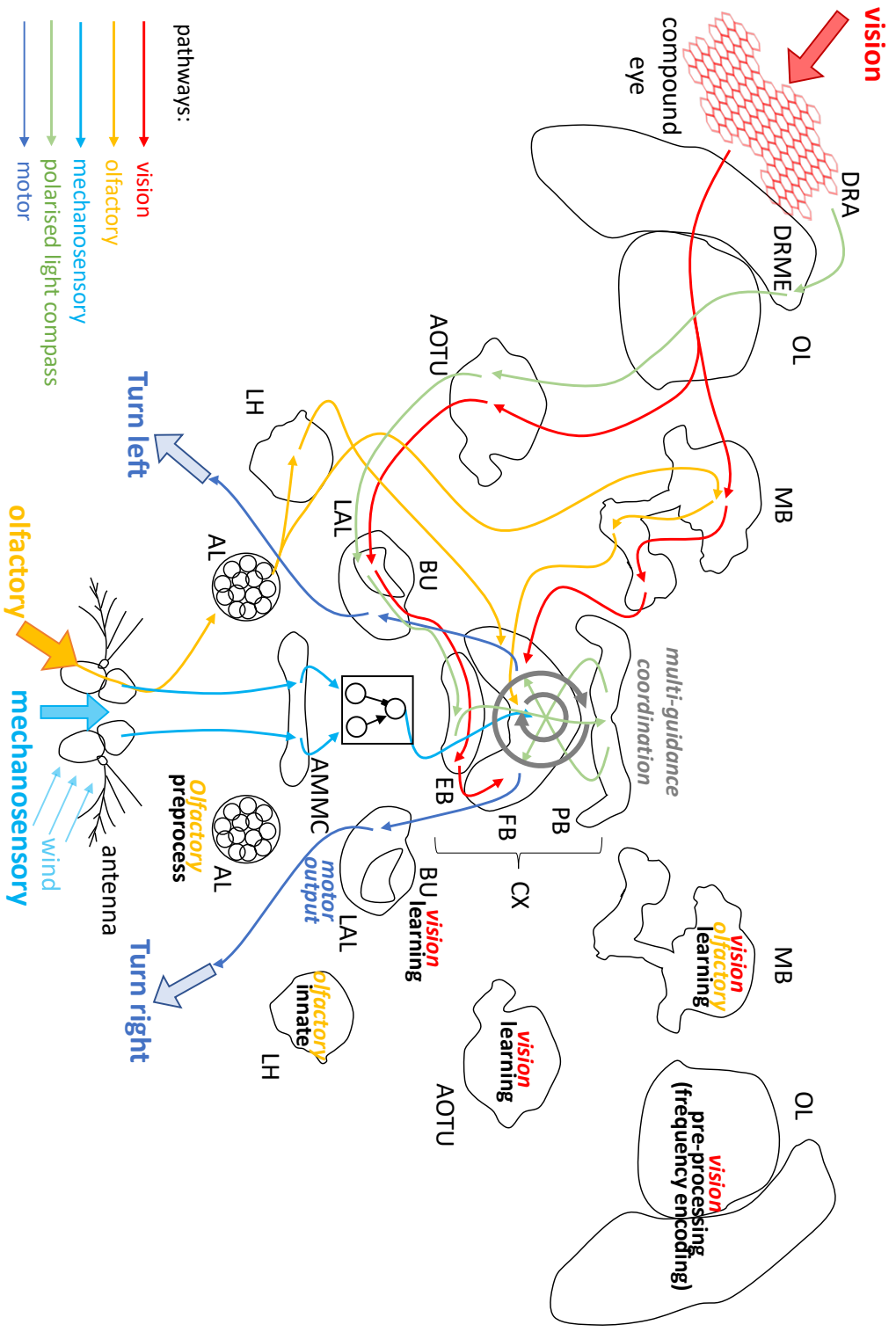

Figure 7.1: **The overall figure summarising the hypothesised functional roles played by every neuropil and the information flowing through them.** Different neural pathways processing different types of sensory information are marked by different colours. The CX's function of multi-guidance coordination are highlighted.

To date, we still fall far short of knowing the whole picture of insect navigation, especially the neural mechanism. From the perspective of computation modelling, based on the proposed unified model, the following researching directions are worth

exploring in the future:

- Like that in Chapter 6, use this model (if possible with some adaptions and adding extra components) to deduce more observed navigational behaviours like navigation when going backwards [306], backtracking [324] and returning to the previous position after being passively displaced by a gust of wind [325], etc. This can be realised by adding new components storing the temporary representation of the currently desired direction in the same format as the PI and VH.

- The whole loop from sensory input to the motor output of insect navigation can be completed by adding the sensory processing (e.g. the polarised-light compass system [271]) and motor control network (e.g. the central pattern generator in the LAL [273]). Moreover, to keep refining the model by updating the computation to be more biological plausible based on new data from biology study. For instance, the current switching circuit can be replaced by neural computation like the synapse plasticity [326].

- As the current simulations are simplified to 2D motion (no pitch and roll involved), but flying insects and even walking insects manoeuvring on uneven terrain will have body tilt. How these may affect the performance of the current visual navigation model is still not clear and needs future investigation. A recent robotic study [311] shown that ant (ground-based insects) inspired visual navigation can be applied to flying robots. Another kind of frequency encoding called Spherical Harmonics method can extend the rotational-invariant property to the 3D domain [249], so the proposed model can still work. These studies provided the possibility to enable the usability of the insect navigation model in 3D motion and further be applied on unmanned aerial vehicle.

- Providing mechanistic interpretation for the understanding of the insect navigation by applying bio-robotic approach [327] [328]. The presented model could be tested on a mobile robot (see an example of robots with panoramic view in Figure 7.2) navigating in a real environment (see the developed platform that can

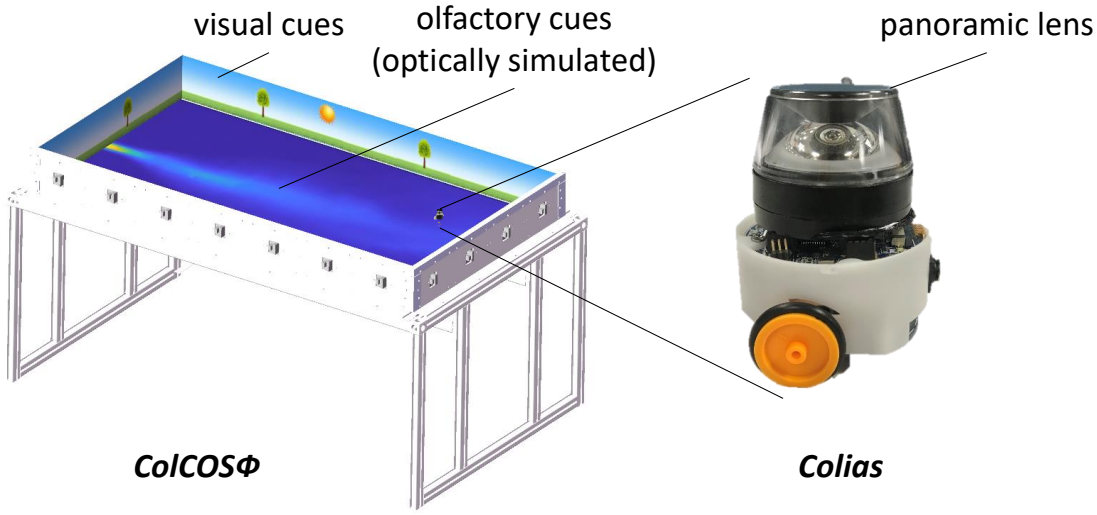

Figure 7.2: **The mobile robot and the platform for future robotic navigation experiments.** Left: The ColCOSΦ platform [22] possess the ability of simultaneously displaying optically simulated olfactory cues on the arena ground and visual cues on the arena wall, therefore is very suitable for undertaking navigation experiments with multiple cues involved. Right: Mobile micro-robot Colias [23] [24] with a panoramic lens mounted.

be used to undertake navigation experiments in Figure 7.2). Validating the model with more noisy and variable sensory inputs could bring more convincing evidence showing the robustness of the model thus explaining why insects evolved to adopt such a mechanism. A quick design of this kind of robotics experiments could be: displaying visual cues on the wall, emulating the olfactory cues on the grounds, and the robot with our model implemented navigates in the arena and test its homing performances.

7.2 Comparison with Mammal Navigation

Unlike the intensive debate on whether there is a 'cognitive map' [236] [237] [238] used by insects during navigation, researchers prefer the idea that mammals use the cognitive map to guide navigation behaviour in a flexible manner [329], [330]. This idea is receiving further supports from neurobiological studies revealing important functional components in the hippocampal and parahippocampal formations (see Figure 7.3 and for a review see [330]): 1) the place cells found by O'Keefe et.al [331] [332] that only fire at specific spatial position; 2) the heading direction cells which fire according to the animal's heading orientation [160] [333] [334]; 3) grid cells that fire in

a regular hexagonal lattice of locations in the exploring environment [335]; 4) border cells which fire when the animal is at the navigational boundaries serves to relate the firing field of grid and place cells to specific features of the environment [336]–[338]. 5) cells in the hippocampus that encode the goal direction and distance [339]. Other evidence also shown the crucial role played by the hippocampus in storing the episodic memory [340] [341] that can be used to retrieve useful memories for navigation such as route following [342]. All these imply the critical function of hippocampal and parahippocampal formation in spatial navigation thus can be regarded as the navigation centre of mammals, the similar role played by the central complex in the midbrain of insects [12], [13], [173]. Neurobiological and computation model studies aiming to unravel the neural basis of mammal navigation have shown how sensory information can be calibrated and integrated to generate a stable and accurate mental representation of the navigating space. For instance, the loop of EC (entorhinal cortex) $\rightarrow$ DG (dentate gyrus) $\rightarrow$ CA3 $\rightarrow$ CA1 $\rightarrow$ EC (see Figure 7.3) can act like a unitary particle filter [343], [344] for place recognition, and how different sub-regions in these two formations contribute to the encoding of the external world (for a review see [345]). This is reminiscent of the sensory information's converging to the central complex in the insect brain to form a combined representation of the animal's surroundings.

Allowing flexible navigation decision under various scenarios, in the mammalian brain, requires a source of sensory valence representing the current context that can not only enable the stimuli-response behaviour but also modulate the goal formation to generate context-dependent behaviours. This function is believed to be located in the striatum [346]–[349] which can be regarded as the analogy of insects' mushroom bodies (see Figure 7.3). From this point of view, the essential fundamental of flexible navigation tends to be the multiple modalities coordination modulated by the spatial memory.

As for the downstream neuron pathway controlling the navigational body movement, the secondary motor cortex (M2, see Figure 7.3) [350] [351] in the mammalian brain is believed to play the main role whilst the primary motor cortex (M1) incorporating the barrel cortex (somatosensory cortex) are more related with the sensory-motor

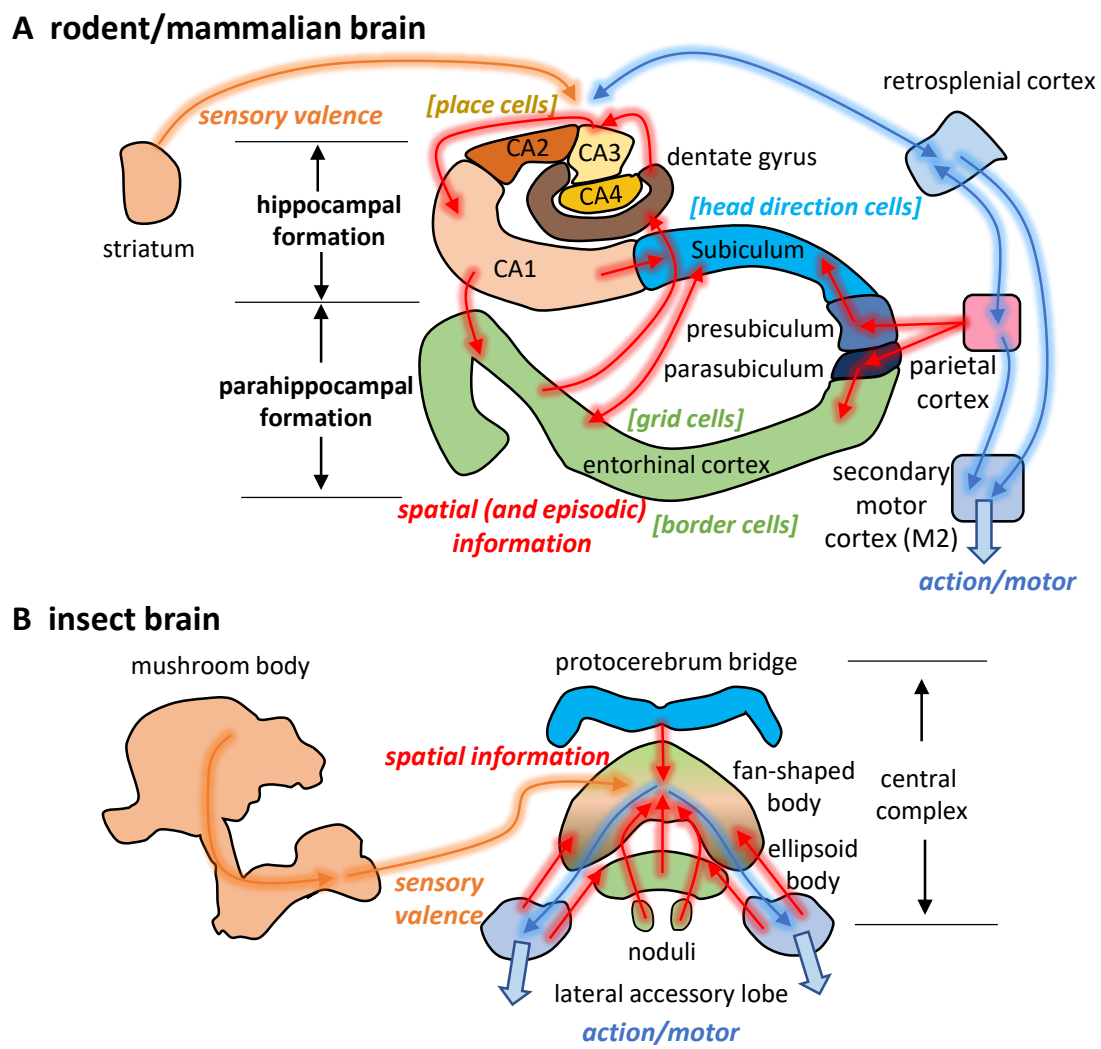

Figure 7.3: **The comparison of the functional brain regions of mammal and insect navigation.** The depicted brain regions with similar function of information processing are marked with colour. The sensory-motor processing loop of spatial information, sensory valence and motor control are coloured by red, orange and blue respectively. (A) The mammal brain. (B) The insect brain.

behaviour especially the whisker-related behaviours [352], [353]. Thus, the secondary motor cortex (M2) could be taken as the analogy of the LAL of an insect to which the output of the integrated navigation decision targets.

To summarise, accurate and flexible navigation in both insects and mammals requires environmental measurement, spatial memory and a coordinating system, although these elementary functions may be implemented in different ways in insects and mammals. Future endeavours are needed to unravel the neural basis of navigation in insects and mammals. Maybe understanding mammal navigation is even harder since it has a much more complex and powerful brain, but inspirations may transfer across studies of these two kinds of species to speed up this research process. For

example, the insect-inspired computation can be applied to explain mammal navigation [354], [355]. Insects and mammals both have heading direction system that encoding the heading by the population activation of specific a set of neurons, implying that there must be something in common in solving navigational tasks even in different living surroundings using various strategies.

7.3 Closing Remarks

We are amazed at the great ability of our brain and want to know how it works. But to date, it is still tremendously difficult to discern the mechanism of the human brain. Starting from a nerve system with much fewer neurons like the larvae could be a solution, however, this biology system lacks rich behaviours to investigate. Fortunately, insects seem to make the optimal trade-off between the scale of the brain and the richness of behaviours, which has motivated this study.

The neural model presented in this work starts from the neural data and ends in explaining behavioural data, aiming to bridge the gap in understanding the mechanism of insect navigation. Although the navigational computations in real insects may not completely the same as that in the proposed model, I hope that by providing bio-plausible solutions, finding out minimum computational requirements and making testable predictions, this work could potentially contribute in a small way to unveil the mechanism of insect navigation and be a small piece of paving stone for future works seeking bio-inspired solutions of robotic navigation.

In recent years, with the aid of rapidly developed techniques, neurobiologists are able to peer the insect brain in a high resolution which will potentially make remarkable progress in this field. Likewise, the increased computational resource and miniaturised integrated circuits allow for the important role played by robotics. We are looking forward to witnessing the exciting progress that will be made in these fields.

Bibliography

[1] F. Bairlein, D. R. Norris, R. Nagel, M. Bulte, C. C. Voigt, J. W. Fox, D. J. Hussell, and H. Schmaljohann, "Cross-hemisphere migration of a 25 g songbird," *Biology letters*, vol. 8, no. 4, pp. 505–507, 2012.

[2] J. B. Stock and M. Baker, "Chemotaxis," in *Encyclopedia of Microbiology*, pp. 71–78, Elsevier Inc., 2009.

[3] E. I. Moser, E. Kropff, and M.-B. Moser, "Place cells, grid cells, and the brain's spatial representation system," *Annu. Rev. Neurosci.*, vol. 31, pp. 69–89, 2008.

[4] S. Heinze, A. Narendra, and A. Cheung, "Principles of insect path integration," *Current Biology*, vol. 28, no. 17, pp. R1043–R1058, 2018.

[5] R. Wehner, "The cataglyphis mahrésienne: 50 years of cataglyphis research at mahrés," *Journal of Comparative Physiology A*, vol. 205, no. 5, pp. 641–659, 2019.

[6] P. Bregy, S. Sommer, and R. Wehner, "Nest-mark orientation versus vector navigation in desert ants," *Journal of Experimental Biology*, vol. 211, no. 12, pp. 1868–1873, 2008.

[7] M. Collett, "How navigational guidance systems are combined in a desert ant," *Current Biology*, vol. 22, no. 10, pp. 927–932, 2012.

[8] A. Wystrach, M. Mangan, and B. Webb, "Optimal cue integration in ants," *Proceedings of the Royal Society B: Biological Sciences*, vol. 282, no. 1816, p. 20151484, 2015.

[9] E. L. Legge, A. Wystrach, M. L. Spetch, and K. Cheng, "Combining sky and earth: desert ants (melophorus bagoti) show weighted integration of celestial and terrestrial cues," *Journal of Experimental Biology*, vol. 217, no. 23, pp. 4159–4166, 2014.

[10] T. Stone, B. Webb, A. Adden, N. B. Weddig, A. Honkanen, R. Templin, W. Wcislo, L. Scimeca, E. Warrant, and S. Heinze, "An anatomically constrained model for path integration in the bee brain," *Current Biology*, vol. 27, no. 20, pp. 3069–3085, 2017.

[11] T. Wolff and G. M. Rubin, "Neuroarchitecture of the drosophila central complex: A catalog of nodulus and asymmetrical body neurons and a revision of the protocerebral bridge catalog," *Journal of Comparative Neurology*, vol. 526, no. 16, pp. 2585–2611, 2018.

[12] S. Heinze, "Unraveling the neural basis of insect navigation," *Current opinion in insect science*, vol. 24, pp. 58–67, 2017.

[13] A. Honkanen, A. Adden, J. da Silva Freitas, and S. Heinze, "The insect central complex and the neural basis of navigational strategies," *Journal of Experimental Biology*, vol. 222, no. Suppl 1, 2019.

[14] B. Cartwright and T. S. Collett, "Landmark learning in bees," *Journal of comparative physiology*, vol. 151, no. 4, pp. 521–543, 1983.

[15] B. Cartwright and T. Collett, "Landmark maps for honeybees," *Biological cybernetics*, vol. 57, no. 1-2, pp. 85–93, 1987.

[16] T. Hoinville and R. Wehner, "Optimal multiguidance integration in insect navigation," *Proceedings of the National Academy of Sciences*, vol. 115, no. 11, pp. 2824–2829, 2018.

[17] P. Ardin, F. Peng, M. Mangan, K. Lagogiannis, and B. Webb, "Using an insect mushroom body circuit to encode route memory in complex natural environments," *PLoS computational biology*, vol. 12, no. 2, p. e1004683, 2016.

[18] A. Wystrach, G. Beugnon, and K. Cheng, "Ants might use different view-matching strategies on and off the route," *Journal of Experimental Biology*, vol. 215, no. 1, pp. 44–55, 2012.

[19] R. Knight, C. E. Piette, H. Page, D. Walters, E. Marozzi, M. Nardini, S. Stringer, and K. J. Jeffery, "Weighted cue integration in the rodent head direction system," *Philosophical Transactions of the Royal Society B: Biological Sciences*, vol. 369, no. 1635, p. 20120512, 2014.

[20] H. J. Page, D. M. Walters, R. Knight, C. E. Piette, K. J. Jeffery, and S. M. Stringer, "A theoretical account of cue averaging in the rodent head direction system," *Philosophical Transactions of the Royal Society B: Biological Sciences*, vol. 369, no. 1635, p. 20130283, 2014.

[21] C. Buehlmann, B. S. Hansson, and M. Knaden, "Path integration controls nest-plume following in desert ants," *Current Biology*, vol. 22, no. 7, pp. 645–649, 2012.

[22] X. Sun, T. Liu, C. Hu, Q. Fu, and S. Yue, "Colcos φ: A multiple pheromone communication system for swarm robotics and social insects research," in *2019 IEEE 4th International Conference on Advanced Robotics and Mechatronics (ICARM)*, pp. 59–66, IEEE, 2019.

[23] F. Arvin, J. Murray, C. Zhang, and S. Yue, "Colias: An autonomous micro robot for swarm robotic applications," *International Journal of Advanced Robotic Systems*, vol. 11, no. 7, p. 113, 2014.

[24] C. Hu, Q. Fu, and S. Yue, "Colias iv: The affordable micro robot platform with bio-inspired vision," in *Annual Conference Towards Autonomous Robotic Systems*, pp. 197–208, Springer, 2018.

[25] H. A. Simon, *Models of my life*. MIT press, 1996.

[26] C. Gallistel and A. E. Cramer, "Computations on metric maps in mammals: getting oriented and choosing a multi-destination route.," *Journal of experimental biology*, vol. 199, no. 1, pp. 211–217, 1996.

[27] B. Webb, "The internal maps of insects," *Journal of Experimental Biology*, vol. 222, no. Suppl 1, 2019.

[28] R. Chavarriaga, T. Strösslin, D. Sheynikhovich, and W. Gerstner, "A computational model of parallel navigation systems in rodents," *Neuroinformatics*, vol. 3, no. 3, pp. 223–241, 2005.

[29] H. Dingle and V. A. Drake, "What is migration?," *Bioscience*, vol. 57, no. 2, pp. 113–121, 2007.

[30] R. Wehner, "Desert ant navigation: how miniature brains solve complex tasks," *Journal of Comparative Physiology A*, vol. 189, no. 8, pp. 579–588, 2003.

[31] M. V. Srinivasan, "Honey bees as a model for vision, perception, and cognition," *Annual review of entomology*, vol. 55, pp. 267–284, 2010.

[32] R. Menzel and M. Giurfa, "Cognitive architecture of a mini-brain: the honeybee," *Trends in cognitive sciences*, vol. 5, no. 2, pp. 62–71, 2001.

[33] C. S. Xu, M. Januszewski, Z. Lu, S.-y. Takemura, K. Hayworth, G. Huang, K. Shinomiya, J. Maitin-Shepard, D. Ackerman, S. Berg, *et al.*, "A connectome of the adult drosophila central brain," *BioRxiv*, 2020.

[34] F. A. Azevedo, L. R. Carvalho, L. T. Grinberg, J. M. Farfel, R. E. Ferretti, R. E. Leite, W. J. Filho, R. Lent, and S. Herculano-Houzel, "Equal numbers of neuronal and nonneuronal cells make the human brain an isometrically scaled-up primate brain," *Journal of Comparative Neurology*, vol. 513, no. 5, pp. 532–541, 2009.

[35] R. Wehner, "On the brink of introducing sensory ecology: Felix santschi (1872–1940)—tabib-en-neml," *Behavioral Ecology and Sociobiology*, vol. 27, no. 4, pp. 295–306, 1990.

[36] R. Wehner, "The architecture of the desert ant's navigational toolkit (hymenoptera: Formicidae)," *Myrmecol News*, vol. 12, no. September, pp. 85–96, 2009.

[37] A. Wystrach and P. Graham, "What can we learn from studies of insect navigation?," *Animal Behaviour*, vol. 84, no. 1, pp. 13–20, 2012.

[38] H. Haberkern and V. Jayaraman, "Studying small brains to understand the building blocks of cognition," *Current Opinion in Neurobiology*, vol. 37, pp. 59–65, 2016.

[39] P. Dayan and L. F. Abbott, *Theoretical neuroscience: computational and mathematical modeling of neural systems*. Computational Neuroscience Series, 2001.

[40] G. W. Brodland, "How computational models can help unlock biological systems," in *Seminars in cell & developmental biology*, vol. 47, pp. 62–73, Elsevier, 2015.

[41] O. C. Zienkiewicz and R. L. Taylor, *The finite element method for solid and structural mechanics*. Elsevier, 2005.

[42] G. W. Brodland, "Computational modeling of cell sorting, tissue engulfment, and related phenomena: A review," *Appl. Mech. Rev.*, vol. 57, no. 1, pp. 47–76, 2004.

[43] T. Wittmann and H. Schwegler, "Path integration—a network model," *Biological Cybernetics*, vol. 73, no. 6, pp. 569–575, 1995.

[44] F. Le Moël, T. Stone, M. Lihoreau, A. Wystrach, and B. Webb, "The central complex as a potential substrate for vector based navigation," *Frontiers in psychology*, vol. 10, p. 690, 2019.

[45] S. Heinze and U. Homberg, "Neuroarchitecture of the central complex of the desert locust: intrinsic and columnar neurons," *Journal of Comparative Neurology*, vol. 511, no. 4, pp. 454–478, 2008.

[46] F. Le Moël and A. Wystrach, "Towards a multi-level understanding in insect navigation," *Current Opinion in Insect Science*, 2020.

[47] J.-H. Fabre, "Souvenirs entomologiques," 1886.

[48] H. Pieron, "Du role du sens musculaire dans l'orientation de quelques espèces de fourmis," *Bull. Inst. Gen. Psychol*, vol. 4, pp. 168–186, 1904.

[49] K. von Frisch, "Die polarisation des himmelslichtes als faktor der orientieren bei den tänzen der bienen," *Experientia*, vol. 5, p. 397, 1949.

[50] A. Narendra, "Homing strategies of the australian desert ant melophorus bagoti ii. interaction of the path integrator with visual cue information," *Journal of Experimental Biology*, vol. 210, no. 10, pp. 1804–1812, 2007.

[51] R. Wehner, M. V. Srinivasan, *et al.*, "Path integration in insects," *The neurobiology of spatial behaviour*, pp. 9–30, 2003.

[52] K. Von Frisch, "The dance language and orientation of bees.," 1967.

[53] M. V. Srinivasan, "Where paths meet and cross: navigation by path integration in the desert ant and the honeybee," *Journal of Comparative Physiology A*, vol. 201, no. 6, pp. 533–546, 2015.

[54] M. Hironaka, S. Nomakuchi, L. Filippi, S. Tojo, H. Horiguchi, and T. Hariyama, "The directional homing behaviour of the subsocial shield bug, parastrachia japonensis (heteroptera: Cydnidae), under different photic conditions," *Zoological science*, vol. 20, no. 4, pp. 423–428, 2003.

[55] M. Hironaka, L. Filippi, S. Nomakuchi, H. Horiguchi, and T. Hariyama, "Hierarchical use of chemical marking and path integration in the homing trip of a subsocial shield bug," *Animal behaviour*, vol. 73, no. 5, pp. 739–745, 2007.

[56] G. Beugnon and R. Campan, "Homing in the field cricket, gryllus campestris," *Journal of insect behavior*, vol. 2, no. 2, pp. 187–198, 1989.

[57] V. Durier and C. Rivault, "Path integration in cockroach larvae, blattella germanica (l.)(insect: Dictyoptera): Direction and distance estimation," *Animal Learning & Behavior*, vol. 27, no. 1, pp. 108–118, 1999.

[58] I. S. Kim and M. H. Dickinson, "Idiothetic path integration in the fruit fly drosophila melanogaster," *Current Biology*, vol. 27, no. 15, pp. 2227–2238, 2017.

[59] S. M. Reppert, H. Zhu, and R. H. White, "Polarized light helps monarch butterflies navigate," *Current Biology*, vol. 14, no. 2, pp. 155–158, 2004.

[60] R. WEHNER and S. STRASSER, "The pol area of the honey bee's eye: behavioural evidence," *Physiological entomology*, vol. 10, no. 3, pp. 337–349, 1985.

[61] D. BRUNNER and T. LABHART, "Behavioural evidence for polarization vision in crickets," *Physiological entomology*, vol. 12, no. 1, pp. 1–10, 1987.

[62] M. Mappes and U. Homberg, "Behavioral analysis of polarization vision in tethered flying locusts," *Journal of Comparative Physiology A*, vol. 190, no. 1, pp. 61–68, 2004.

[63] A. von Philipsborn and T. Labhart, "A behavioural study of polarization vision in the fly, musca domestica," *Journal of Comparative Physiology A*, vol. 167, no. 6, pp. 737–743, 1990.

[64] S. Heinze and S. M. Reppert, "Sun compass integration of skylight cues in migratory monarch butterflies," *Neuron*, vol. 69, no. 2, pp. 345–358, 2011.

[65] B. el Jundi, J. Smolka, E. Baird, M. J. Byrne, and M. Dacke, "Diurnal dung beetles use the intensity gradient and the polarization pattern of the sky for orientation," *Journal of experimental biology*, vol. 217, no. 13, pp. 2422–2429, 2014.

[66] B. El Jundi, K. Pfeiffer, S. Heinze, and U. Homberg, "Integration of polarization and chromatic cues in the insect sky compass," *Journal of Comparative Physiology A*, vol. 200, no. 6, pp. 575–589, 2014.

[67] M. Dacke, E. Baird, M. Byrne, C. H. Scholtz, and E. J. Warrant, "Dung beetles use the milky way for orientation," *Current Biology*, vol. 23, no. 4, pp. 298–300, 2013.

[68] J. J. Foster, B. el Jundi, J. Smolka, L. Khaldy, D.-E. Nilsson, M. J. Byrne, and M. Dacke, "Stellar performance: mechanisms underlying milky way orientation in dung beetles," *Philosophical Transactions of the Royal Society B: Biological Sciences*, vol. 372, no. 1717, p. 20160079, 2017.

[69] M. Dacke, M. J. Byrne, C. H. Scholtz, and E. J. Warrant, "Lunar orientation in a beetle," *Proceedings of the Royal Society of London. Series B: Biological Sciences*, vol. 271, no. 1537, pp. 361–365, 2004.

[70] A. Riveros and R. Srygley, "Do leafcutter ants, atta colombica, orient their path-integrated home vector with a magnetic compass?," *Animal Behaviour*, vol. 75, no. 4, pp. 1273–1281, 2008.

[71] P. A. Guerra, R. J. Gegear, and S. M. Reppert, "A magnetic compass aids monarch butterfly migration," *Nature communications*, vol. 5, no. 1, pp. 1–8, 2014.

[72] P. N. Fleischmann, R. Grob, V. L. Müller, R. Wehner, and W. Rössler, "The geomagnetic field is a compass cue in cataglyphis ant navigation," *Current Biology*, vol. 28, no. 9, pp. 1440–1444, 2018.

[73] P. N. Fleischmann, R. Grob, and W. Rössler, "Magnetoreception in hymenoptera: importance for navigation," *Animal Cognition*, pp. 1–11, 2020.

[74] M. Wittlinger, R. Wehner, and H. Wolf, "The ant odometer: stepping on stilts and stumps," *science*, vol. 312, no. 5782, pp. 1965–1967, 2006.

[75] M. Wittlinger, R. Wehner, and H. Wolf, "The desert ant odometer: a stride integrator that accounts for stride length and walking speed," *Journal of experimental Biology*, vol. 210, no. 2, pp. 198–207, 2007.

[76] H. Esch and J. Burns, "Distance estimation by foraging honeybees," *Journal of Experimental Biology*, vol. 199, no. 1, pp. 155–162, 1996.

[77] M. V. Srinivasan, S. Zhang, M. Altwein, and J. Tautz, "Honeybee navigation: Nature and calibration of the" odometer"," *Science*, vol. 287, no. 5454, pp. 851–853, 2000.

[78] J. S. Kennedy and D. Marsh, "Pheromone-regulated anemotaxis in flying moths," *Science*, vol. 184, no. 4140, pp. 999–1001, 1974.

[79] B. Ronacher and R. Wehner, "Desert ants cataglyphis fortis use self-induced optic flow to measure distances travelled," *Journal of Comparative Physiology A*, vol. 177, no. 1, pp. 21–27, 1995.

[80] S. E. Pfeffer and M. Wittlinger, "Optic flow odometry operates independently of stride integration in carried ants," *Science*, vol. 353, no. 6304, pp. 1155–1157, 2016.

[81] B. Ronacher, K. Gallizzi, S. Wohlgemuth, and R. Wehner, "Lateral optic flow does not influence distance estimation in the desert ant cataglyphis fortis," *Journal of Experimental Biology*, vol. 203, no. 7, pp. 1113–1121, 2000.

[82] S. Sommer and R. Wehner, "Vector navigation in desert ants, cataglyphis fortis: celestial compass cues are essential for the proper use of distance information," *Naturwissenschaften*, vol. 92, no. 10, pp. 468–471, 2005.

[83] M. Dacke and M. V. Srinivasan, "Two odometers in honeybees?," *Journal of Experimental Biology*, vol. 211, no. 20, pp. 3281–3286, 2008.

[84] C. Rivault and V. Durier, "Homing in german cockroaches, blattella germanica (l.)(insecta: Dictyoptera): Multi-channelled orientation cues," *Ethology*, vol. 110, no. 10, pp. 761–777, 2004.

[85] T. A. Ofstad, C. S. Zuker, and M. B. Reiser, "Visual place learning in drosophila melanogaster," *Nature*, vol. 474, no. 7350, pp. 204–207, 2011.

[86] J. Wessnitzer, M. Mangan, and B. Webb, "Place memory in crickets," *Proceedings of the Royal Society B: Biological Sciences*, vol. 275, no. 1637, pp. 915–921, 2008.

[87] M. Collett, L. Chittka, and T. S. Collett, "Spatial memory in insect navigation," *Current Biology*, vol. 23, no. 17, pp. R789–R800, 2013.

[88] T. S. Collett and M. Collett, "Memory use in insect visual navigation," *Nature Reviews Neuroscience*, vol. 3, no. 7, pp. 542–552, 2002.

[89] J. Zeil, "Visual homing: an insect perspective," *Current opinion in neurobiology*, vol. 22, no. 2, pp. 285–293, 2012.

[90] A. M. Anderson, "The influence of pointed regions on the shape preference of honey bees," *Animal Behaviour*, vol. 25, pp. 88–94, 1977.

[91] N. Tinbergen and W. Kruyt, "Über die orientierung des bienenwolfes (philanthus triangulum fabr.)," *Zeitschrift für vergleichende Physiologie*, vol. 25, no. 3, pp. 292–334, 1938.

[92] R. Wehner and F. Räber, "Visual spatial memory in desert ants, cataglyphis bicolor (hymenoptera: Formicidae)," *Experientia*, vol. 35, no. 12, pp. 1569–1571, 1979.

[93] V. Durier, P. Graham, and T. S. Collett, "Switching destinations: memory change in wood ants," *Journal of Experimental Biology*, vol. 207, no. 14, pp. 2401–2408, 2004.

[94] M. Collett, "How desert ants use a visual landmark for guidance along a habitual route," *Proceedings of the National Academy of Sciences*, vol. 107, no. 25, pp. 11638–11643, 2010.

[95] T. Collett and M. Land, "Visual control of flight behaviour in the hoverflysyritta pipiens l.," *Journal of comparative physiology*, vol. 99, no. 1, pp. 1–66, 1975.

[96] W. Junger, "Waterstriders (gerris paludum f.) compensate for drift with a discontinuously working visual position servo," *Journal of Comparative Physiology A*, vol. 169, no. 5, pp. 633–639, 1991.

[97] T. S. Collett, E. Dillmann, A. Giger, and R. Wehner, "Visual landmarks and route following in desert ants," *Journal of Comparative Physiology A*, vol. 170, no. 4, pp. 435–442, 1992.

[98] R. Wehner, B. Michel, and P. Antonsen, "Visual navigation in insects: coupling of egocentric and geocentric information," *Journal of Experimental Biology*, vol. 199, no. 1, pp. 129–140, 1996.

[99] M. Mangan and B. Webb, "Spontaneous formation of multiple routes in individual desert ants (cataglyphis velox)," *Behavioral Ecology*, vol. 23, no. 5, pp. 944–954, 2012.

[100] M. Kohler and R. Wehner, "Idiosyncratic route-based memories in desert ants, melophorus bagoti: how do they interact with path-integration vectors?," *Neurobiology of learning and memory*, vol. 83, no. 1, pp. 1–12, 2005.

[101] R. A. Harris, P. Graham, and T. S. Collett, "Visual cues for the retrieval of landmark memories by navigating wood ants," *Current biology*, vol. 17, no. 2, pp. 93–102, 2007.

[102] D. D. Lent, P. Graham, and T. S. Collett, "Image-matching during ant navigation occurs through saccade-like body turns controlled by learned visual features," *Proceedings of the National Academy of Sciences*, vol. 107, no. 37, pp. 16348–16353, 2010.

[103] D. H. Janzen, "Euglossine bees as long-distance pollinators of tropical plants," *Science*, vol. 171, no. 3967, pp. 203–205, 1971.

[104] P. Ziegler and R. Wehner, "Time-courses of memory decay in vector-based and landmark-based systems of navigation in desert ants, cataglyphis fortis," *Journal of Comparative Physiology A*, vol. 181, no. 1, pp. 13–20, 1997.

[105] M. Gillies, "The role of carbon dioxide in host-finding by mosquitoes (diptera: Culicidae): a review," *Bulletin of Entomological Research*, vol. 70, pp. 525–532, 1980.

[106] B. Hölldobler, E. O. Wilson, *et al.*, *The ants*. Harvard University Press, 1990.

[107] T. J. Czaczkes, C. Grüter, and F. L. Ratnieks, "Trail pheromones: an integrative view of their role in social insect colony organization," *Annual review of entomology*, vol. 60, 2015.

[108] A. Gomez-Marin, G. J. Stephens, and M. Louis, "Active sampling and decision making in drosophila chemotaxis," *Nature communications*, vol. 2, no. 1, pp. 1–10, 2011.

[109] E. Fishilevich, A. I. Domingos, K. Asahina, F. Naef, L. B. Vosshall, and M. Louis, "Chemotaxis behavior mediated by single larval olfactory neurons in drosophila," *Current biology*, vol. 15, no. 23, pp. 2086–2096, 2005.

[110] R. T. Cardé, "Moth navigation along pheromone plumes," *Pheromone communication in moths*, pp. 173–189, 2016.

[111] C. Buehlmann, P. Graham, B. S. Hansson, and M. Knaden, "Desert ants use olfactory scenes for navigation," *Animal Behaviour*, vol. 106, pp. 99–105, 2015.

[112] H. Wolf and R. Wehner, "Pinpointing food sources: olfactory and anemotactic orientation in desert ants, cataglyphis fortis," *Journal of Experimental Biology*, vol. 203, no. 5, pp. 857–868, 2000.

[113] H. Wolf and R. Wehner, "Desert ants compensate for navigation uncertainty," *Journal of Experimental Biology*, vol. 208, no. 22, pp. 4223–4230, 2005.

[114] E. Álvarez-Salvado, A. M. Licata, E. G. Connor, M. K. McHugh, B. M. King, N. Stavropoulos, J. D. Victor, J. P. Crimaldi, and K. I. Nagel, "Elementary sensory-motor transformations underlying olfactory navigation in walking fruit-flies," *Elife*, vol. 7, p. e37815, 2018.

[115] C. Buehlmann, M. Mangan, and P. Graham, "Multimodal interactions in insect navigation," *Animal Cognition*, pp. 1–13, 2020.

[116] R. Wehner and M. V. Srinivasan, "Searching behaviour of desert ants, genuscataglyphis (formicidae, hymenoptera)," *Journal of comparative physiology*, vol. 142, no. 3, pp. 315–338, 1981.

[117] P. Schultheiss, K. Cheng, and A. M. Reynolds, "Searching behavior in social hymenoptera," *Learning and Motivation*, vol. 50, pp. 59–67, 2015.

[118] M. Müller and R. Wehner, "The hidden spiral: systematic search and path integration in desert ants, cataglyphis fortis," *Journal of Comparative Physiology A*, vol. 175, no. 5, pp. 525–530, 1994.

[119] P. Schultheiss and K. Cheng, "Finding the nest: inbound searching behaviour in the australian desert ant, melophorus bagoti," *Animal Behaviour*, vol. 81, no. 5, pp. 1031–1038, 2011.

[120] A. M. Reynolds, A. D. Smith, D. R. Reynolds, N. L. Carreck, and J. L. Osborne, "Honeybees perform optimal scale-free searching flights when attempting to locate a food source," *Journal of Experimental Biology*, vol. 210, no. 21, pp. 3763–3770, 2007.

[121] C. Bühlmann, K. Cheng, and R. Wehner, "Vector-based and landmark-guided navigation in desert ants inhabiting landmark-free and landmark-rich environments," *Journal of Experimental Biology*, vol. 214, no. 17, pp. 2845–2853, 2011.

[122] A. Cheung, L. Hiby, and A. Narendra, "Ant navigation: fractional use of the home vector," *PLoS One*, vol. 7, no. 11, p. e50451, 2012.

[123] A. Narendra, S. Gourmaud, and J. Zeil, "Mapping the navigational knowledge of individually foraging ants, myrmecia croslandi," *Proceedings of the Royal Society B: Biological Sciences*, vol. 280, no. 1765, p. 20130683, 2013.

[124] K. Von Frisch, *Tanzsprache und orientierung der bienen*. Springer-Verlag, 2013.

[125] R. Wehner, T. Hoinville, H. Cruse, and K. Cheng, "Steering intermediate courses: desert ants combine information from various navigational routines," *Journal of Comparative Physiology A*, vol. 202, no. 7, pp. 459–472, 2016.

[126] H. Cruse and R. Wehner, "No need for a cognitive map: decentralized memory for insect navigation," *PLoS Comput Biol*, vol. 7, no. 3, p. e1002009, 2011.

[127] S. Deneve and A. Pouget, "Bayesian multisensory integration and cross-modal spatial links," *Journal of Physiology-Paris*, vol. 98, no. 1-3, pp. 249–258, 2004.

[128] K. Cheng, S. J. Shettleworth, J. Huttenlocher, and J. J. Rieser, "Bayesian integration of spatial information.," *Psychological bulletin*, vol. 133, no. 4, p. 625, 2007.

[129] P. Schultheiss, T. Stannard, S. Pereira, A. M. Reynolds, R. Wehner, and K. Cheng, "Similarities and differences in path integration and search in two species of desert ants inhabiting a visually rich and a visually barren habitat," *Behavioral ecology and sociobiology*, vol. 70, no. 8, pp. 1319–1329, 2016.

[130] K. Steck, B. S. Hansson, and M. Knaden, "Desert ants benefit from combining visual and olfactory landmarks," *Journal of Experimental Biology*, vol. 214, no. 8, pp. 1307–1312, 2011.

[131] T. S. Collett, N. H. de Ibarra, O. Riabinina, and A. Philippides, "Coordinating compass-based and nest-based flight directions during bumblebee learning and return flights," *Journal of Experimental Biology*, vol. 216, no. 6, pp. 1105–1113, 2013.

[132] P. N. Fleischmann, M. Christian, V. L. Müller, W. Rössler, and R. Wehner, "Ontogeny of learning walks and the acquisition of landmark information in desert ants, cataglyphis fortis," *Journal of Experimental Biology*, vol. 219, no. 19, pp. 3137–3145, 2016.

[133] D. M. Vowles, "Interocular transfer, brain lesions, and maze learning in the wood ant, formica rufa," in *Chemistry of learning*, pp. 425–447, Springer, 1967.

[134] M. Mizunami, J. M. Weibrecht, and N. J. Strausfeld, "Mushroom bodies of the cockroach: their participation in place memory," *Journal of Comparative Neurology*, vol. 402, no. 4, pp. 520–537, 1998.

[135] J. Williams, "Anatomical studies of the insect central nervous system: A ground-plan of the midbrain and an introduction to the central complex in the locust, schistocerca gregaria (orthoptera)," *Journal of Zoology*, vol. 176, no. 1, pp. 67–86, 1975.

[136] B. El Jundi, S. Heinze, C. Lenschow, A. Kurylas, T. Rohlfing, and U. Homberg, "The locust standard brain: a 3d standard of the central complex as a platform for neural network analysis," *Frontiers in systems neuroscience*, vol. 3, p. 21, 2010.

[137] U. Hanesch, K.-F. Fischbach, and M. Heisenberg, "Neuronal architecture of the central complex in drosophila melanogaster," *Cell and Tissue Research*, vol. 257, no. 2, pp. 343–366, 1989.

[138] B. el Jundi, E. J. Warrant, K. Pfeiffer, and M. Dacke, "Neuroarchitecture of the dung beetle central complex," *Journal of Comparative Neurology*, vol. 526, no. 16, pp. 2612–2630, 2018.

[139] H. Wei, B. el Jundi, U. Homberg, and M. Stengl, "Implementation of pigment-dispersing factor-immunoreactive neurons in a standardized atlas of the brain of the cockroach leucophaea maderae," *Journal of Comparative Neurology*, vol. 518, no. 20, pp. 4113–4133, 2010.

[140] U. Homberg, "Interneurones of the central complex in the bee brain (apis mellifera, l.)," *Journal of insect physiology*, vol. 31, no. 3, pp. 251–264, 1985.

[141] L. de Vries, K. Pfeiffer, B. Trebels, A. K. Adden, K. Green, E. Warrant, and S. Heinze, "Comparison of navigation-related brain regions in migratory versus non-migratory noctuid moths," *Frontiers in behavioral neuroscience*, vol. 11, p. 158, 2017.

[142] U. Homberg, "Evolution of the central complex in the arthropod brain with respect to the visual system," *Arthropod structure & development*, vol. 37, no. 5, pp. 347–362, 2008.

[143] N. J. Strausfeld, "Brain organization and the origin of insects: an assessment," *Proceedings of the Royal Society B: Biological Sciences*, vol. 276, no. 1664, pp. 1929–1937, 2009.

[144] C.-Y. Lin, C.-C. Chuang, T.-E. Hua, C.-C. Chen, B. J. Dickson, R. J. Greenspan, and A.-S. Chiang, "A comprehensive wiring diagram of the protocerebral bridge for visual information processing in the drosophila brain," *Cell reports*, vol. 3, no. 5, pp. 1739–1753, 2013.

[145] T. Wolff, N. A. Iyer, and G. M. Rubin, "Neuroarchitecture and neuroanatomy of the drosophila central complex: A gal4-based dissection of protocerebral bridge neurons and circuits," *Journal of Comparative Neurology*, vol. 523, no. 7, pp. 997–1037, 2015.

[146] K. Pfeiffer and U. Homberg, "Organization and functional roles of the central complex in the insect brain," *Annual review of entomology*, vol. 59, pp. 165–184, 2014.

[147] D. B. Turner-Evans and V. Jayaraman, "The insect central complex," *Current Biology*, vol. 26, no. 11, pp. R453–R457, 2016.

[148] U. Homberg, S. Heinze, K. Pfeiffer, M. Kinoshita, and B. El Jundi, "Central neural coding of sky polarization in insects," *Philosophical Transactions of the Royal Society B: Biological Sciences*, vol. 366, no. 1565, pp. 680–687, 2011.

[149] S. Heinze, "Polarized-light processing in insect brains: recent insights from the desert locust, the monarch butterfly, the cricket, and the fruit fly," in *Polarized light and polarization vision in animal sciences*, pp. 61–111, Springer, 2014.

[150] S. Heinze and U. Homberg, "Maplike representation of celestial e-vector orientations in the brain of an insect," *Science*, vol. 315, no. 5814, pp. 995–997, 2007.

[151] J. D. Seelig and V. Jayaraman, "Neural dynamics for landmark orientation and angular path integration," *Nature*, vol. 521, no. 7551, pp. 186–191, 2015.

[152] J. Green, A. Adachi, K. K. Shah, J. D. Hirokawa, P. S. Magani, and G. Maimon, "A neural circuit architecture for angular integration in drosophila," *Nature*, vol. 546, no. 7656, pp. 101–106, 2017.

[153] S. S. Kim, H. Rouault, S. Druckmann, and V. Jayaraman, "Ring attractor dynamics in the drosophila central brain," *Science*, vol. 356, no. 6340, pp. 849–853, 2017.

[154] D. Turner-Evans, S. Wegener, H. Rouault, R. Franconville, T. Wolff, J. D. Seelig, S. Druckmann, and V. Jayaraman, "Angular velocity integration in a fly heading circuit," *Elife*, vol. 6, p. e23496, 2017.

[155] S. S. Kim, A. M. Hermundstad, S. Romani, L. Abbott, and V. Jayaraman, "Generation of stable heading representations in diverse visual scenes," *Nature*, vol. 576, no. 7785, pp. 126–131, 2019.

[156] Y. E. Fisher, J. Lu, I. D'Alessandro, and R. I. Wilson, "Sensorimotor experience remaps visual input to a heading-direction network," *Nature*, vol. 576, no. 7785, pp. 121–125, 2019.

[157] I. Pisokas, S. Heinze, and B. Webb, "The head direction circuit of two insect species," *Elife*, vol. 9, p. e53985, 2020.

[158] A. G. Varga and R. E. Ritzmann, "Cellular basis of head direction and contextual cues in the insect brain," *Current Biology*, vol. 26, no. 14, pp. 1816–1828, 2016.

[159] B. el Jundi, E. J. Warrant, M. J. Byrne, L. Khaldy, E. Baird, J. Smolka, and M. Dacke, "Neural coding underlying the cue preference for celestial orientation," *Proceedings of the National Academy of Sciences*, vol. 112, no. 36, pp. 11395–11400, 2015.

[160] J. S. Taube, R. U. Muller, and J. B. Ranck, "Head-direction cells recorded from the postsubiculum in freely moving rats. i. description and quantitative analysis," *Journal of Neuroscience*, vol. 10, no. 2, pp. 420–435, 1990.

[161] J. S. Taube, R. U. Muller, and J. B. Ranck, "Head-direction cells recorded from the postsubiculum in freely moving rats. ii. effects of environmental manipulations," *Journal of Neuroscience*, vol. 10, no. 2, pp. 436–447, 1990.

[162] R. E. Ritzmann, A. L. Ridgel, and A. J. Pollack, "Multi-unit recording of antennal mechanosensitive units in the central complex of the cockroach, blaberus discoidalis," *Journal of Comparative Physiology A*, vol. 194, no. 4, p. 341, 2008.

[163] S. Kuntz, B. Poeck, M. B. Sokolowski, and R. Strauss, "The visual orientation memory of drosophila requires foraging (pkg) upstream of ignorant (rsk2) in ring neurons of the central complex," *Learning & memory*, vol. 19, no. 8, pp. 337–340, 2012.

[164] N. J. Strausfeld and F. Hirth, "Deep homology of arthropod central complex and vertebrate basal ganglia," *Science*, vol. 340, no. 6129, pp. 157–161, 2013.

[165] N. J. Strausfeld, "A brain region in insects that supervises walking," in *Progress in brain research*, vol. 123, pp. 273–284, Elsevier, 1999.

[166] R. Strauss, "The central complex and the genetic dissection of locomotor behaviour," *Current opinion in neurobiology*, vol. 12, no. 6, pp. 633–638, 2002.

[167] T. Triphan, B. Poeck, K. Neuser, and R. Strauss, "Visual targeting of motor actions in climbing drosophila," *Current biology*, vol. 20, no. 7, pp. 663–668, 2010.

[168] C. M. Harley and R. Ritzmann, "Electrolytic lesions within central complex neuropils of the cockroach brain affect negotiation of barriers," *Journal of Experimental Biology*, vol. 213, no. 16, pp. 2851–2864, 2010.

[169] A. L. Ridgel, B. E. Alexander, and R. E. Ritzmann, "Descending control of turning behavior in the cockroach, blaberus discoidalis," *Journal of Comparative Physiology A*, vol. 193, no. 4, pp. 385–402, 2007.

[170] J. A. Bender, A. J. Pollack, and R. E. Ritzmann, "Neural activity in the central complex of the insect brain is linked to locomotor changes," *Current biology*, vol. 20, no. 10, pp. 921–926, 2010.

[171] P. Guo and R. E. Ritzmann, "Neural activity in the central complex of the cockroach brain is linked to turning behaviors," *Journal of Experimental Biology*, vol. 216, no. 6, pp. 992–1002, 2013.

[172] J. P. Martin, P. Guo, L. Mu, C. M. Harley, and R. E. Ritzmann, "Central-complex control of movement in the freely walking cockroach," *Current Biology*, vol. 25, no. 21, pp. 2795–2803, 2015.

[173] B. Webb and A. Wystrach, "Neural mechanisms of insect navigation," *Current opinion in insect science*, vol. 15, pp. 27–39, 2016.

[174] F. Dujardin, "Mémoire sur le système nerveux des insectes," *Ann Sci Nat Zool*, vol. 14, pp. 195–206, 1850.

[175] S. M. Farris and S. Schulmeister, "Parasitoidism, not sociality, is associated with the evolution of elaborate mushroom bodies in the brains of hymenopteran insects," *Proceedings of the Royal Society B: Biological Sciences*, vol. 278, no. 1707, pp. 940–951, 2011.

[176] G. Withers, S. Fahrbach, and G. Robinson, "Effects of experience and juvenile hormone on the organization of the mushroom bodies of honey bees," *Journal of neurobiology*, vol. 26, no. 1, pp. 130–144, 1995.

[177] S. M. Farris, G. E. Robinson, and S. E. Fahrbach, "Experience-and age-related outgrowth of intrinsic neurons in the mushroom bodies of the adult worker honeybee," *Journal of Neuroscience*, vol. 21, no. 16, pp. 6395–6404, 2001.

[178] S. E. Fahrbach, T. Giray, S. M. Farris, and G. E. Robinson, "Expansion of the neuropil of the mushroom bodies in male honey bees is coincident with initiation of flight," *Neuroscience letters*, vol. 236, no. 3, pp. 135–138, 1997.

[179] S. Kühn-Bühlmann and R. Wehner, "Age-dependent and task-related volume changes in the mushroom bodies of visually guided desert ants, cataglyphis bicolor," *Journal of Neurobiology*, vol. 66, no. 6, pp. 511–521, 2006.

[180] W. Gronenberg, S. Heeren, and B. Hölldobler, "Age-dependent and task-related morphological changes in the brain and the mushroom bodies of the ant camponotus floridanus," *Journal of Experimental Biology*, vol. 199, no. 9, pp. 2011–2019, 1996.

[181] S. O'Donnell, N. A. Donlan, and T. A. Jones, "Mushroom body structural change is associated with division of labor in eusocial wasp workers (polybia aequatorialis, hymenoptera: Vespidae)," *Neuroscience letters*, vol. 356, no. 3, pp. 159–162, 2004.

[182] M. Heisenberg, "Mushroom body memoir: from maps to models," *Nature Reviews Neuroscience*, vol. 4, no. 4, pp. 266–275, 2003.

[183] P. Mobbs, "The brain of the honeybee apis mellifera. i. the connections and spatial organization of the mushroom bodies," *Philosophical Transactions of the Royal Society of London. B, Biological Sciences*, vol. 298, no. 1091, pp. 309–354, 1982.

[184] A. C. Paulk and W. Gronenberg, "Higher order visual input to the mushroom bodies in the bee, bombus impatiens," *Arthropod structure & development*, vol. 37, no. 6, pp. 443–458, 2008.

[185] W. Gronenberg, "Subdivisions of hymenopteran mushroom body calyces by their afferent supply," *Journal of Comparative Neurology*, vol. 435, no. 4, pp. 474–489, 2001.

[186] C. Lin and N. J. Strausfeld, "Visual inputs to the mushroom body calyces of the whirligig beetle dineutus sublineatus: modality switching in an insect," *Journal of Comparative Neurology*, vol. 520, no. 12, pp. 2562–2574, 2012.

[187] M. Kinoshita, M. Shimohigasshi, Y. Tominaga, K. Arikawa, and U. Homberg, "Topographically distinct visual and olfactory inputs to the mushroom body in the swallowtail butterfly, papilio xuthus," *Journal of Comparative Neurology*, vol. 523, no. 1, pp. 162–182, 2015.

[188] A. Balkenius, S. Bisch-Knaden, and B. Hansson, "Interaction of visual and odour cues in the mushroom body of the hawkmoth manduca sexta," *Journal of Experimental Biology*, vol. 212, no. 4, pp. 535–541, 2009.

[189] C. Buehlmann, B. Wozniak, R. Goulard, B. Webb, P. Graham, and J. E. Niven, "Mushroom bodies are required for learned visual navigation, but not for innate visual behavior, in ants," *Current Biology*, vol. 30, no. 17, pp. 3438–3443, 2020.

[190] J. F. Kamhi, A. B. Barron, and A. Narendra, "Vertical lobes of the mushroom bodies are essential for view-based navigation in australian myrmecia ants," *Current Biology*, vol. 30, no. 17, pp. 3432–3437, 2020.

[191] S. Heinze, "Visual navigation: Ants lose track without mushroom bodies," *Current Biology*, vol. 30, no. 17, pp. R984–R986, 2020.

[192] Y. Aso, D. Hattori, Y. Yu, R. M. Johnston, N. A. Iyer, T.-T. Ngo, H. Dionne, L. Abbott, R. Axel, H. Tanimoto, *et al.*, "The neuronal architecture of the mushroom body provides a logic for associative learning," *elife*, vol. 3, p. e04577, 2014.

[193] Y. Aso, D. Sitaraman, T. Ichinose, K. R. Kaun, K. Vogt, G. Belliart-Guérin, P.-Y. Plaçais, A. A. Robie, N. Yamagata, C. Schnaitmann, *et al.*, "Mushroom body output neurons encode valence and guide memory-based action selection in drosophila," *Elife*, vol. 3, p. e04580, 2014.

[194] R. Jander, "Die optische richtungsorientierung der roten waldameise (formica ruea l.)," *Zeitschrift für vergleichende Physiologie*, vol. 40, no. 2, pp. 162–238, 1957.

[195] H. Mittelstaedt and M. ML, "Mechanismen der orientierung ohne richtende aussenreize," *Forschr. Zool.*, vol. 21, pp. 46–58, 1973.

[196] M. Müller and R. Wehner, "Path integration in desert ants, cataglyphis fortis," *Proceedings of the National Academy of Sciences*, vol. 85, no. 14, pp. 5287–5290, 1988.

[197] T. Haferlach, J. Wessnitzer, M. Mangan, and B. Webb, "Evolving a neural model of insect path integration," *Adaptive Behavior*, vol. 15, no. 3, pp. 273–287, 2007.

[198] D. Kim and J. C. Hallam, "Neural network approach to path integration for homing navigation," in *From Animals to Animats 6*, pp. 228–235, MIT Press, 2000.

[199] D. Goldschmidt, P. Manoonpong, and S. Dasgupta, "A neurocomputational model of goal-directed navigation in insect-inspired artificial agents," *Frontiers in neurorobotics*, vol. 11, p. 20, 2017.

[200] R. J. Vickerstaff and E. Di Paolo, "Evolving neural models of path integration," *Journal of Experimental Biology*, vol. 208, no. 17, pp. 3349–3366, 2005.

[201] R. Maurer and V. Séguinot, "What is modelling for? a critical review of the models of path integration," *Journal of Theoretical Biology*, vol. 175, no. 4, pp. 457–475, 1995.

[202] R. J. Vickerstaff and A. Cheung, "Which coordinate system for modelling path integration?," *Journal of Theoretical Biology*, vol. 263, no. 2, pp. 242–261, 2010.

[203] A. Cheung and R. Vickerstaff, "Finding the way with a noisy brain," *PLoS Comput Biol*, vol. 6, no. 11, p. e1000992, 2010.

[204] J. Zeil, M. I. Hofmann, and J. S. Chahl, "Catchment areas of panoramic snapshots in outdoor scenes," *JOSA A*, vol. 20, no. 3, pp. 450–469, 2003.

[205] L. Dittmar, W. Stürzl, E. Baird, N. Boeddeker, and M. Egelhaaf, "Goal seeking in honeybees: matching of optic flow snapshots?," *Journal of Experimental Biology*, vol. 213, no. 17, pp. 2913–2923, 2010.

[206] A. Vardy and R. Moller, "Biologically plausible visual homing methods based on optical flow techniques," *Connection Science*, vol. 17, no. 1-2, pp. 47–89, 2005.

[207] M. O. Franz, B. Schölkopf, H. A. Mallot, and H. H. Bülthoff, "Where did i take that snapshot? scene-based homing by image matching," *Biological Cybernetics*, vol. 79, no. 3, pp. 191–202, 1998.

[208] R. Möller, A. Vardy, S. Kreft, and S. Ruwisch, "Visual homing in environments with anisotropic landmark distribution," *Autonomous Robots*, vol. 23, no. 3, pp. 231–245, 2007.

[209] D. Binding and F. Labrosse, "Visual local navigation using warped panoramic images," in *Proceedings of Towards Autonomous Robotic Systems. University of Surrey, Guildford, UK*, pp. 19–26, 2006.

[210] R. Möller and A. Vardy, "Local visual homing by matched-filter descent in image distances," *Biological cybernetics*, vol. 95, no. 5, pp. 413–430, 2006.

[211] W. Stürzl and J. Zeil, "Depth, contrast and view-based homing in outdoor scenes," *Biological cybernetics*, vol. 96, no. 5, pp. 519–531, 2007.

[212] V. V. Hafner, "Adaptive homing—robotic exploration tours," *Adaptive Behavior*, vol. 9, no. 3-4, pp. 131–141, 2001.

[213] R. Möller, D. Lambrinos, T. Roggendorf, R. Pfeifer, and R. Wehner, "Insect strategies of visual homing in mobile robots," in *Proceedings of the Computer Vision and Mobile Robotics Workshop CVMR*, vol. 98, pp. 75–82, Citeseer, 2001.

[214] M. Mangan and B. Webb, "Modelling place memory in crickets," *Biological cybernetics*, vol. 101, no. 4, p. 307, 2009.

[215] T. Stone, M. Mangan, A. Wystrach, and B. Webb, "Rotation invariant visual processing for spatial memory in insects," *Interface focus*, vol. 8, no. 4, p. 20180010, 2018.

[216] D. Nicholson, S. Judd, B. Cartwright, and T. Collett, "Learning walks and landmark guidance in wood ants (formica rufa)," *Journal of Experimental Biology*, vol. 202, no. 13, pp. 1831–1838, 1999.

[217] M. Müller and R. Wehner, "Path integration provides a scaffold for landmark learning in desert ants," *Current Biology*, vol. 20, no. 15, pp. 1368–1371, 2010.

[218] S. Judd and T. Collett, "Multiple stored views and landmark guidance in ants," *Nature*, vol. 392, no. 6677, pp. 710–714, 1998.

[219] L. Smith, A. Philippides, P. Graham, B. Baddeley, and P. Husbands, "Linked local navigation for visual route guidance," *Adaptive Behavior*, vol. 15, no. 3, pp. 257–271, 2007.

[220] B. Baddeley, P. Graham, P. Husbands, and A. Philippides, "A model of ant route navigation driven by scene familiarity," *PLoS Comput Biol*, vol. 8, no. 1, p. e1002336, 2012.

[221] A. Wystrach, M. Mangan, A. Philippides, and P. Graham, "Snapshots in ants? new interpretations of paradigmatic experiments," *Journal of Experimental Biology*, vol. 216, no. 10, pp. 1766–1770, 2013.

[222] P. Graham, A. Philippides, and B. Baddeley, "Animal cognition: multi-modal interactions in ant learning," *Current Biology*, vol. 20, no. 15, pp. R639–R640, 2010.

[223] A. D. Dewar, A. Philippides, and P. Graham, "What is the relationship between visual environment and the form of ant learning-walks? an in silico investigation of insect navigation," *Adaptive Behavior*, vol. 22, no. 3, pp. 163–179, 2014.

[224] J. Müller, M. Nawrot, R. Menzel, and T. Landgraf, "A neural network model for familiarity and context learning during honeybee foraging flights," *Biological cybernetics*, vol. 112, no. 1-2, pp. 113–126, 2018.

[225] J. Wessnitzer, J. M. Young, J. D. Armstrong, and B. Webb, "A model of non-elemental olfactory learning in drosophila," *Journal of computational neuroscience*, vol. 32, no. 2, pp. 197–212, 2012.

[226] K. L. Baker, M. Dickinson, T. M. Findley, D. H. Gire, M. Louis, M. P. Suver, J. V. Verhagen, K. I. Nagel, and M. C. Smear, "Algorithms for olfactory search across species," *Journal of Neuroscience*, vol. 38, no. 44, pp. 9383–9389, 2018.

[227] A. Davies, M. Louis, and B. Webb, "A model of drosophila larva chemotaxis," *PLoS computational biology*, vol. 11, no. 11, p. e1004606, 2015.

[228] A. Wystrach, K. Lagogiannis, and B. Webb, "Continuous lateral oscillations as a core mechanism for taxis in drosophila larvae," *Elife*, vol. 5, p. e15504, 2016.

[229] J. Loveless and B. Webb, "A neuromechanical model of larval chemotaxis," *Integrative and Comparative Biology*, vol. 58, no. 5, pp. 906–914, 2018.

[230] H. Rapp and M. P. Nawrot, "A spiking neural program for sensorimotor control during foraging in flying insects," *Proceedings of the National Academy of Sciences*, vol. 117, no. 45, pp. 28412–28421, 2020.

[231] A. J. Rutkowski, R. D. Quinn, and M. A. Willis, "Three-dimensional characterization of the wind-borne pheromone tracking behavior of male hawkmoths, manduca sexta," *Journal of Comparative Physiology A*, vol. 195, no. 1, pp. 39–54, 2009.

[232] F. van Breugel and M. H. Dickinson, "Plume-tracking behavior of flying drosophila emerges from a set of distinct sensory-motor reflexes," *Current Biology*, vol. 24, no. 3, pp. 274–286, 2014.

[233] K. Steck, D. Veit, R. Grandy, S. B. i Badia, Z. Mathews, P. Verschure, B. S. Hansson, and M. Knaden, "A high-throughput behavioral paradigm for drosophila olfaction-the flywalk," *Scientific reports*, vol. 2, p. 361, 2012.

[234] R. J. Vickerstaff and T. Merkle, "Path integration mediated systematic search: A bayesian model," *Journal of theoretical biology*, vol. 307, pp. 1–19, 2012.

[235] F. Waldner and T. Merkle, "A simple mathematical model using centred loops and random perturbations accurately reconstructs search patterns observed in desert ants," *Journal of Comparative Physiology A*, vol. 204, no. 12, pp. 985–998, 2018.

[236] R. Wehner and R. Menzel, "Do insects have cognitive maps?," *Annual review of neuroscience*, vol. 13, no. 1, pp. 403–414, 1990.

[237] J. F. Cheeseman, C. D. Millar, U. Greggers, K. Lehmann, M. D. Pawley, C. R. Gallistel, G. R. Warman, and R. Menzel, "Way-finding in displaced clock-shifted bees proves bees use a cognitive map," *Proceedings of the National Academy of Sciences*, vol. 111, no. 24, pp. 8949–8954, 2014.

[238] A. Cheung, M. Collett, T. S. Collett, A. Dewar, F. Dyer, P. Graham, M. Mangan, A. Narendra, A. Philippides, W. Stürzl, *et al.*, "Still no convincing evidence for cognitive map use by honeybees," *Proceedings of the National Academy of Sciences*, vol. 111, no. 42, pp. E4396–E4397, 2014.

[239] T. Hoinville, R. Wehner, and H. Cruse, "Learning and retrieval of memory elements in a navigation task," in *Conference on Biomimetic and Biohybrid Systems*, pp. 120–131, Springer, 2012.

[240] W. J. Ma, J. M. Beck, P. E. Latham, and A. Pouget, "Bayesian inference with probabilistic population codes," *Nature neuroscience*, vol. 9, no. 11, pp. 1432–1438, 2006.

[241] M. Collett and T. S. Collett, "How does the insect central complex use mushroom body output for steering?," *Current Biology*, vol. 28, no. 13, pp. R733–R734, 2018.

[242] S. Heinze and K. Pfeiffer, "The insect central complex-from sensory coding to directing movement," *Frontiers in behavioral neuroscience*, vol. 12, p. 156, 2018.

[243] T. Fukushi and R. Wehner, "Navigation in wood ants formica japonica: context dependent use of landmarks," *Journal of Experimental Biology*, vol. 207, no. 19, pp. 3431–3439, 2004.

[244] A. Kodzhabashev and M. Mangan, "Route following without scanning," in *Conference on Biomimetic and Biohybrid Systems*, pp. 199–210, Springer, 2015.

[245] B. Cartwright and T. Collett, "How honey bees use landmarks to guide their return to a food source," *Nature*, vol. 295, no. 5850, pp. 560–564, 1982.

[246] W. Stürzl, J. Zeil, N. Boeddeker, and J. M. Hemmi, "How wasps acquire and use views for homing," *Current Biology*, vol. 26, no. 4, pp. 470–482, 2016.

[247] J. Zeil, A. Kelber, and R. Voss, "Structure and function of learning flights in ground-nesting bees and wasps," *Journal of Experimental Biology*, vol. 199, no. 1, pp. 245–252, 1996.

[248] J. Zeil and P. N. Fleischmann, "The learning walks of ants (hymenoptera: Formicidae)," *Myrmecological News*, vol. 29, 2019.

[249] T. Stone, D. Differt, M. Milford, and B. Webb, "Skyline-based localisation for aggressively manoeuvring robots using uv sensors and spherical harmonics," in *2016 IEEE International Conference on Robotics and Automation (ICRA)*, pp. 5615–5622, IEEE, 2016.

[250] D. B. Turner-Evans, K. Jensen, S. Ali, T. Paterson, A. Sheridan, R. P. Ray, S. Lauritzen, D. Bock, and V. Jayaraman, "The neuroanatomical ultrastructure and function of a biological ring attractor," *bioRxiv*, p. 847152, 2019.

[251] A. J. Cope, C. Sabo, E. Vasilaki, A. B. Barron, and J. A. Marshall, "A computational model of the integration of landmarks and motion in the insect central complex," *PloS one*, vol. 12, no. 2, p. e0172325, 2017.

[252] K. S. Kakaria and B. L. de Bivort, "Ring attractor dynamics emerge from a spiking model of the entire protocerebral bridge," *Frontiers in behavioral neuroscience*, vol. 11, p. 8, 2017.

[253] M. J. Beetz, B. el Jundi, S. Heinze, and U. Homberg, "Topographic organization and possible function of the posterior optic tubercles in the brain of the desert locust schistocerca gregaria," *Journal of Comparative Neurology*, vol. 523, no. 11, pp. 1589–1607, 2015.

[254] J. A. Plath, B. V. Entler, N. H. Kirkerud, U. Schlegel, C. G. Galizia, and A. B. Barron, "Different roles for honey bee mushroom bodies and central complex in visual learning of colored lights in an aversive conditioning assay," *Frontiers in behavioral neuroscience*, vol. 11, p. 98, 2017.

[255] U. Homberg, S. Hofer, K. Pfeiffer, and S. Gebhardt, "Organization and neural connections of the anterior optic tubercle in the brain of the locust, schistocerca gregaria," *Journal of Comparative Neurology*, vol. 462, no. 4, pp. 415–430, 2003.

[256] J. J. Omoto, M. F. Keleş, B.-C. M. Nguyen, C. Bolanos, J. K. Lovick, M. A. Frye, and V. Hartenstein, "Visual input to the drosophila central complex by developmentally and functionally distinct neuronal populations," *Current Biology*, vol. 27, no. 8, pp. 1098–1110, 2017.

[257] L. Timaeus, L. Geid, G. Sancer, M. F. Wernet, and T. Hummel, "Parallel visual pathways with topographic versus non-topographic organization connect the drosophila eyes to the central brain," *bioRxiv*, 2020.

[258] S. Heinze and U. Homberg, "Linking the input to the output: new sets of neurons complement the polarization vision network in the locust central complex," *Journal of Neuroscience*, vol. 29, no. 15, pp. 4911–4921, 2009.

[259] G. Hudson, A. Léger, B. Niss, I. Sebestyén, and J. Vaaben, "Jpeg-1 standard 25 years: past, present, and future reasons for a success," *Journal of Electronic Imaging*, vol. 27, no. 4, p. 040901, 2018.

[260] T. Pajdla and V. Hlaváč, "Zero phase representation of panoramic images for image based localization," in *International Conference on Computer Analysis of Images and Patterns*, pp. 550–557, Springer, 1999.

[261] E. Menegatti, T. Maeda, and H. Ishiguro, "Image-based memory for robot navigation using properties of omnidirectional images," *Robotics and Autonomous Systems*, vol. 47, no. 4, pp. 251–267, 2004.

[262] W. Stürzl and H. A. Mallot, "Efficient visual homing based on fourier transformed panoramic images," *Robotics and Autonomous Systems*, vol. 54, no. 4, pp. 300–313, 2006.

[263] H. Jiang, K. D. Paulsen, U. L. Osterberg, B. W. Pogue, and M. S. Patterson, "Optical image reconstruction using frequency-domain data: simulations and experiments," *JOSA A*, vol. 13, no. 2, pp. 253–266, 1996.

[264] R. C. Gonzalez, R. E. Woods, and S. L. Eddins, *Digital image processing using MATLAB*. Pearson Education India, 2004.

[265] M. R. Teague, "Image analysis via the general theory of moments," *JOSA*, vol. 70, no. 8, pp. 920–930, 1980.

[266] A. Khotanzad and Y. H. Hong, "Invariant image recognition by zernike moments," *IEEE Transactions on pattern analysis and machine intelligence*, vol. 12, no. 5, pp. 489–497, 1990.

[267] G. A. Horridge, "Pattern discrimination by the honeybee: disruption as a cue," *Journal of Comparative Physiology A*, vol. 181, no. 3, pp. 267–277, 1997.

[268] M. Lehrer, "Shape perception in the honeybee: symmetry as a global framework," *International Journal of Plant Sciences*, vol. 160, no. S6, pp. S51–S65, 1999.

[269] D. O'Carroll, "Feature-detecting neurons in dragonflies," *Nature*, vol. 362, no. 6420, p. 541, 1993.

[270] A. James and D. Osorio, "Characterisation of columnar neurons and visual signal processing in the medulla of the locust optic lobe by system identification techniques," *Journal of Comparative Physiology A*, vol. 178, no. 2, pp. 183–199, 1996.

[271] E. Gkanias, B. Risse, M. Mangan, and B. Webb, "From skylight input to behavioural output: a computational model of the insect polarised light compass," *PLoS computational biology*, vol. 15, no. 7, p. e1007123, 2019.

[272] F. Steinbeck, A. Adden, and P. Graham, "Connecting brain to behaviour: a role for general purpose steering circuits in insect orientation?," *Journal of Experimental Biology*, vol. 223, no. 5, 2020.

[273] A. K. Adden, T. C. Stewart, B. Webb, and S. Heinze, "A neural model for insect steering applied to olfaction and path integration," *bioRxiv*, 2020.

[274] B. Ehmer and W. Gronenberg, "Segregation of visual input to the mushroom bodies in the honeybee (apis mellifera)," *Journal of Comparative Neurology*, vol. 451, no. 4, pp. 362–373, 2002.

[275] W. Gronenberg and G. López-Riquelme, "Multisensory convergence in the mushroom bodies of ants and bees," *Acta Biologica Hungarica*, vol. 55, no. 1-4, pp. 31–37, 2004.

[276] S. M. Buchanan, J. S. Kain, and B. L. De Bivort, "Neuronal control of locomotor handedness in drosophila," *Proceedings of the National Academy of Sciences*, vol. 112, no. 21, pp. 6700–6705, 2015.

[277] M. Barth and M. Heisenberg, "Vision affects mushroom bodies and central complex in drosophila melanogaster.," *Learning & Memory*, vol. 4, no. 2, pp. 219–229, 1997.

[278] A. Yilmaz, K. Grübel, J. Spaethe, and W. Rössler, "Distributed plasticity in ant visual pathways following colour learning," *Proceedings of the Royal Society B*, vol. 286, no. 1896, p. 20182813, 2019.

[279] A. C. Paulk, L. Kirszenblat, Y. Zhou, and B. van Swinderen, "Closed-loop behavioral control increases coherence in the fly brain," *Journal of Neuroscience*, vol. 35, no. 28, pp. 10304–10315, 2015.

[280] J. D. Seelig and V. Jayaraman, "Feature detection and orientation tuning in the drosophila central complex," *Nature*, vol. 503, no. 7475, pp. 262–266, 2013.

[281] S. J. Shettleworth, *Cognition, evolution, and behavior*. Oxford university press, 2009.

[282] M. O. Ernst, "A bayesian view on multimodal cue integration," *Human body perception from the inside out*, vol. 131, pp. 105–131, 2006.

[283] H. T. Blair and P. E. Sharp, "Visual and vestibular influences on head-direction cells in the anterior thalamus of the rat.," *Behavioral neuroscience*, vol. 110, no. 4, p. 643, 1996.

[284] K. P. Körding and D. M. Wolpert, "Bayesian integration in sensorimotor learning," *Nature*, vol. 427, no. 6971, pp. 244–247, 2004.

[285] K. P. Kording, "Bayesian statistics: relevant for the brain?," *Current opinion in neurobiology*, vol. 25, pp. 130–133, 2014.

[286] M. O. Ernst and M. S. Banks, "Humans integrate visual and haptic information in a statistically optimal fashion," *Nature*, vol. 415, no. 6870, pp. 429–433, 2002.

[287] M. Kam, X. Zhu, and P. Kalata, "Sensor fusion for mobile robot navigation," *Proceedings of the IEEE*, vol. 85, no. 1, pp. 108–119, 1997.

[288] S. Thrun, W. Burgard, D. Fox, *et al.*, "Probabilistic robotics.[sl]," 2005.

[289] J. Fuentes-Pacheco, J. Ruiz-Ascencio, and J. M. Rendón-Mancha, "Visual simultaneous localization and mapping: a survey," *Artificial intelligence review*, vol. 43, no. 1, pp. 55–81, 2015.

[290] K. Zhang, "Representation of spatial orientation by the intrinsic dynamics of the head-direction cell ensemble: a theory," *Journal of Neuroscience*, vol. 16, no. 6, pp. 2112–2126, 1996.

[291] W. E. Skaggs, J. J. Knierim, H. S. Kudrimoti, and B. L. McNaughton, "A model of the neural basis of the rat's sense of direction," in *Advances in neural information processing systems*, pp. 173–180, 1995.

[292] D. S. Touretzky, "Attractor network models of head direction cells," *Head direction cells and the neural mechanisms of spatial orientation*, pp. 411–432, 2005.

[293] K. J. Jeffery, H. J. Page, and S. M. Stringer, "Optimal cue combination and landmark-stability learning in the head direction system," *The Journal of physiology*, vol. 594, no. 22, pp. 6527–6534, 2016.

[294] R. D. Beer, "On the dynamics of small continuous-time recurrent neural networks," *Adaptive Behavior*, vol. 3, no. 4, pp. 469–509, 1995.

[295] H. J. Page, D. Walters, and S. M. Stringer, "Architectural constraints are a major factor reducing path integration accuracy in the rat head direction cell system," *Frontiers in computational neuroscience*, vol. 9, p. 10, 2015.

[296] U. Homberg, "Flight-correlated activity changes in neurons of the lateral accessory lobes in the brain of the locust schistocerca gregaria," *Journal of comparative physiology A*, vol. 175, no. 5, pp. 597–610, 1994.

[297] A. B. Barron and C. Klein, "What insects can tell us about the origins of consciousness," *Proceedings of the National Academy of Sciences*, vol. 113, no. 18, pp. 4900–4908, 2016.

[298] T. Collett, "Insect navigation en route to the goal: multiple strategies for the use of landmarks," *Journal of Experimental Biology*, vol. 199, no. 1, pp. 227–235, 1996.

[299] J. F. Harrison, J. H. Fewell, T. M. Stiller, and M. D. Breed, "Effects of experience on use of orientation cues in the giant tropical ant.," *Animal behaviour*, 1989.

[300] A. Wystrach, G. Beugnon, and K. Cheng, "Landmarks or panoramas: what do navigating ants attend to for guidance?," *Frontiers in Zoology*, vol. 8, no. 1, pp. 1–11, 2011.

[301] R. Franconville, C. Beron, and V. Jayaraman, "Building a functional connectome of the drosophila central complex," *Elife*, vol. 7, p. e37017, 2018.

[302] B. Ehmer and W. Gronenberg, "Mushroom body volumes and visual interneurons in ants: comparison between sexes and castes," *Journal of Comparative Neurology*, vol. 469, no. 2, pp. 198–213, 2004.

[303] J. Rybak and R. Menzel, "Anatomy of the mushroom bodies in the honey bee brain: the neuronal connections of the alpha-lobe," *Journal of Comparative Neurology*, vol. 334, no. 3, pp. 444–465, 1993.

[304] B. El Jundi, J. J. Foster, L. Khaldy, M. J. Byrne, M. Dacke, and E. Baird, "A snapshot-based mechanism for celestial orientation," *Current biology*, vol. 26, no. 11, pp. 1456–1462, 2016.

[305] S. M. Reppert, P. A. Guerra, and C. Merlin, "Neurobiology of monarch butterfly migration," *Annual review of entomology*, vol. 61, 2016.

[306] S. Schwarz, M. Mangan, J. Zeil, B. Webb, and A. Wystrach, "How ants use vision when homing backward," *Current Biology*, vol. 27, no. 3, pp. 401–407, 2017.

[307] M. Dacke, A. T. Bell, J. J. Foster, E. J. Baird, M. F. Strube-Bloss, M. J. Byrne, and B. el Jundi, "Multimodal cue integration in the dung beetle compass," *Proceedings of the National Academy of Sciences*, p. 201904308, 2019.

[308] M. Collett, T. S. Collett, S. Bisch, and R. Wehner, "Local and global vectors in desert ant navigation," *Nature*, vol. 394, no. 6690, pp. 269–272, 1998.

[309] P. Marin-Plaza, A. Hussein, D. Martin, and A. d. l. Escalera, "Global and local path planning study in a ros-based research platform for autonomous vehicles," *Journal of Advanced Transportation*, vol. 2018, 2018.

[310] R. Kreiser, A. Renner, V. R. Leite, B. Serhan, C. Bartolozzi, A. Glover, and Y. Sandamirskaya, "An on-chip spiking neural network for estimation of the head pose of the icub robot," *Frontiers in Neuroscience*, vol. 14, 2020.

[311] A. Dewar, P. Graham, T. Nowotny, and A. Philippides, "Exploring the robustness of insect-inspired visual navigation for flying robots," in *Artificial Life Conference Proceedings*, pp. 668–677, MIT Press, 2020.

[312] A. Gomez-Marin, B. Duistermars, M. A. Frye, and M. Louis, "Mechanisms of odor-tracking: multiple sensors for enhanced perception and behavior," *Frontiers in cellular neuroscience*, vol. 4, p. 6, 2010.

[313] K. I. Nagel and R. I. Wilson, "Biophysical mechanisms underlying olfactory receptor neuron dynamics," *Nature neuroscience*, vol. 14, no. 2, pp. 208–216, 2011.

[314] A. J. Kim, A. A. Lazar, and Y. B. Slutskiy, "System identification of drosophila olfactory sensory neurons," *Journal of computational neuroscience*, vol. 30, no. 1, pp. 143–161, 2011.

[315] A. Schulze, A. Gomez-Marin, V. G. Rajendran, G. Lott, M. Musy, P. Ahammad, A. Deogade, J. Sharpe, J. Riedl, D. Jarriault, *et al.*, "Dynamical feature extraction at the sensory periphery guides chemotaxis," *Elife*, vol. 4, p. e06694, 2015.

[316] L. Hernandez-Nunez, J. Belina, M. Klein, G. Si, L. Claus, J. R. Carlson, and A. D. Samuel, "Reverse-correlation analysis of navigation dynamics in drosophila larva using optogenetics," *Elife*, vol. 4, p. e06225, 2015.

[317] S.-H. Jung, C. Hueston, and V. Bhandawat, "Odor-identity dependent motor programs underlie behavioral responses to odors," *Elife*, vol. 4, p. e11092, 2015.

[318] J. P. Crimaldi, M. B. Wiley, and J. R. Koseff, "The relationship between mean and instantaneous structure in turbulent passive scalar plumes," *Journal of Turbulence*, vol. 3, no. 14, pp. 1–24, 2002.

[319] J. L. Page, B. D. Dickman, D. R. Webster, and M. J. Weissburg, "Staying the course: chemical signal spatial properties and concentration mediate cross-stream motion in turbulent plumes," *Journal of Experimental Biology*, vol. 214, no. 9, pp. 1513–1522, 2011.

[320] S. Yorozu, A. Wong, B. J. Fischer, H. Dankert, M. J. Kernan, A. Kamikouchi, K. Ito, and D. J. Anderson, "Distinct sensory representations of wind and near-field sound in the drosophila brain," *Nature*, vol. 458, no. 7235, pp. 201–205, 2009.

[321] P. Patella and R. I. Wilson, "Functional maps of mechanosensory features in the drosophila brain," *Current Biology*, vol. 28, no. 8, pp. 1189–1203, 2018.

[322] M. P. Suver, A. M. Matheson, S. Sarkar, M. Damiata, D. Schoppik, and K. I. Nagel, "Encoding of wind direction by central neurons in drosophila," *Neuron*, vol. 102, no. 4, pp. 828–842, 2019.

[323] K. Steck, B. S. Hansson, and M. Knaden, "Smells like home: Desert ants, cataglyphis fortis, use olfactory landmarks to pinpoint the nest," *Frontiers in Zoology*, vol. 6, no. 1, pp. 1–8, 2009.

[324] A. Wystrach, S. Schwarz, A. Baniel, and K. Cheng, "Backtracking behaviour in lost ants: an additional strategy in their navigational toolkit," *Proceedings of the Royal Society B: Biological Sciences*, vol. 280, no. 1769, p. 20131677, 2013.

[325] A. Wystrach and S. Schwarz, "Ants use a predictive mechanism to compensate for passive displacements by wind," *Current Biology*, vol. 23, no. 24, pp. R1083–R1085, 2013.

[326] R. Goulard, C. Buehlmann, J. E. Niven, P. Graham, and B. Webb, "A unified mechanism to support innate and learned use of visual landmark guidance in insects," *bioRxiv*, 2021.

[327] B. Webb, "Can robots make good models of biological behaviour?," *Behavioral and brain sciences*, vol. 24, no. 6, pp. 1033–1050, 2001.

[328] B. Webb, "Robots with insect brains," *Science*, vol. 368, no. 6488, pp. 244–245, 2020.

[329] E. C. Tolman, "Cognitive maps in rats and men.," *Psychological review*, vol. 55, no. 4, p. 189, 1948.

[330] R. A. Epstein, E. Z. Patai, J. B. Julian, and H. J. Spiers, "The cognitive map in humans: spatial navigation and beyond," *Nature neuroscience*, vol. 20, no. 11, p. 1504, 2017.

[331] J. O'Keefe and J. Dostrovsky, "The hippocampus as a spatial map: Preliminary evidence from unit activity in the freely-moving rat.," *Brain research*, 1971.

[332] J. O'keefe and L. Nadel, *The hippocampus as a cognitive map*. Oxford: Clarendon Press, 1978.

[333] J. S. Taube and J. P. Bassett, "Persistent neural activity in head direction cells," *Cerebral Cortex*, vol. 13, no. 11, pp. 1162–1172, 2003.

[334] J. P. Goodridge, P. A. Dudchenko, K. A. Worboys, E. J. Golob, and J. S. Taube, "Cue control and head direction cells.," *Behavioral neuroscience*, vol. 112, no. 4, p. 749, 1998.

[335] T. Hafting, M. Fyhn, S. Molden, M.-B. Moser, and E. I. Moser, "Microstructure of a spatial map in the entorhinal cortex," *Nature*, vol. 436, no. 7052, pp. 801–806, 2005.

[336] T. Solstad, C. N. Boccara, E. Kropff, M.-B. Moser, and E. I. Moser, "Representation of geometric borders in the entorhinal cortex," *Science*, vol. 322, no. 5909, pp. 1865–1868, 2008.

[337] F. Savelli, D. Yoganarasimha, and J. J. Knierim, "Influence of boundary removal on the spatial representations of the medial entorhinal cortex," *Hippocampus*, vol. 18, no. 12, pp. 1270–1282, 2008.

[338] C. Lever, S. Burton, A. Jeewajee, J. O'Keefe, and N. Burgess, "Boundary vector cells in the subiculum of the hippocampal formation," *Journal of Neuroscience*, vol. 29, no. 31, pp. 9771–9777, 2009.

[339] A. Sarel, A. Finkelstein, L. Las, and N. Ulanovsky, "Vectorial representation of spatial goals in the hippocampus of bats," *Science*, vol. 355, no. 6321, pp. 176–180, 2017.

[340] N. Burgess, E. A. Maguire, and J. O'Keefe, "The human hippocampus and spatial and episodic memory," *Neuron*, vol. 35, no. 4, pp. 625–641, 2002.

[341] H. Eichenbaum and N. Fortin, "Episodic memory and the hippocampus: It's about time," *Current directions in psychological science*, vol. 12, no. 2, pp. 53–57, 2003.

[342] T. Hartley, E. A. Maguire, H. J. Spiers, and N. Burgess, "The well-worn route and the path less traveled: distinct neural bases of route following and wayfinding in humans," *Neuron*, vol. 37, no. 5, pp. 877–888, 2003.

[343] C. Fox and T. Prescott, "Hippocampus as unitary coherent particle filter," in *The 2010 International Joint Conference on Neural Networks (IJCNN)*, pp. 1–8, IEEE, 2010.

[344] C. Fox and T. Prescott, "Learning in a unitary coherent hippocampus," in *International Conference on Artificial Neural Networks*, pp. 388–394, Springer, 2010.

[345] N. Van Strien, N. Cappaert, and M. Witter, "The anatomy of memory: an interactive overview of the parahippocampal–hippocampal network," *Nature reviews neuroscience*, vol. 10, no. 4, pp. 272–282, 2009.

[346] W. Schultz, P. Dayan, and P. R. Montague, "A neural substrate of prediction and reward," *Science*, vol. 275, no. 5306, pp. 1593–1599, 1997.

[347] K. Samejima, Y. Ueda, K. Doya, and M. Kimura, "Representation of action-specific reward values in the striatum," *Science*, vol. 310, no. 5752, pp. 1337–1340, 2005.

[348] B. Lau and P. W. Glimcher, "Value representations in the primate striatum during matching behavior," *Neuron*, vol. 58, no. 3, pp. 451–463, 2008.

[349] S. C. Goodroe, J. Starnes, and T. I. Brown, "The complex nature of hippocampal-striatal interactions in spatial navigation," *Frontiers in Human Neuroscience*, vol. 12, p. 250, 2018.

[350] N. Yamawaki, J. Radulovic, and G. M. Shepherd, "A corticocortical circuit directly links retrosplenial cortex to m2 in the mouse," *Journal of Neuroscience*, vol. 36, no. 36, pp. 9365–9374, 2016.

[351] J. M. Olson, J. K. Li, S. E. Montgomery, and D. A. Nitz, "Secondary motor cortex transforms spatial information into planned action during navigation," *Current Biology*, vol. 30, no. 10, pp. 1845–1854, 2020.

[352] C. C. Petersen, "The functional organization of the barrel cortex," *Neuron*, vol. 56, no. 2, pp. 339–355, 2007.

[353] D. Feldmeyer, M. Brecht, F. Helmchen, C. C. Petersen, J. F. Poulet, J. F. Staiger, H. J. Luhmann, and C. Schwarz, "Barrel cortex function," *Progress in neurobiology*, vol. 103, pp. 3–27, 2013.

[354] J. L. Kubie and A. A. Fenton, "Heading-vector navigation based on head-direction cells and path integration," *Hippocampus*, vol. 19, no. 5, pp. 456–479, 2009.

[355] P. Gaussier, J. P. Banquet, N. Cuperlier, M. Quoy, L. Aubin, P.-Y. Jacob, F. Sargolini, E. Save, J. L. Krichmar, and B. Poucet, "Merging information in the entorhinal cortex: what can we learn from robotics experiments and modeling?," *Journal of Experimental Biology*, vol. 222, no. Suppl_1, p. jeb186932, 2019.